ALTERNATIVE ASSEMBLY PATHWAYS OF THE 20S PROTEASOME AND NON-CANONICAL COMPLEXES

by

Dilrajkaur Panfair

A Dissertation

Submitted to the Faculty of Purdue University

In Partial Fulfillment of the Requirements for the degree of

Doctor of Philosophy

Department of Biology

Indianapolis, Indiana

December 2018

THE PURDUE UNIVERSITY GRADUATE SCHOOL
STATEMENT OF COMMITTEE APPROVAL

Dr. Andrew Kusmierczyk
Department of Biology
Dr. Lata Balakrishnan
Department of Biology
Dr. Stephen Randall
Department of Biology
Dr. Eric Rubenstein
Ball State University
Dr. Gregory Anderson
Department of Biology

Approved by:

Dr. Theodore Cummins
Head of the Graduate Program

ACKNOWLEDGMENTS

I am incredibly grateful to my mentor, Andrew Kusmierczyk, for his time, patience, immense support, guidance, and constructive criticism during my graduate studies. He has always inspired me and provided constant motivation. I would also like to acknowledge my thesis committee members; Lata Balakrishnan, Stephen Randall, Eric Rubenstein, and Greg Anderson for providing insightful suggestions that helped to complete this work. I extend sincere gratitude to my friends for creating a friendly environment in the lab and helping me out personally and professionally.

Lastly, I would like to thank my family for their invaluable support: my mother for being my inspiration; my brothers, for pushing me to expand my boundaries; my husband, for encouraging me, providing moral and emotional support, and always believing in me; and last but not the least, my daughter, for raising my potential.

TABLE OF CONTENTS

LIST OF TABLES

LIST OF FIGURES

LIST OF ABBREVATIONS

ARC - AAA ATPase ring-shaped complex

Bpa - bacterial proteasome activator

CC - crosslinkable cysteins

CryoEM – Cryo electron microscopy

CP - core particle

EM – electron microscopy

HbYX - hydrophobic, tyrosine, and amino acid

HGT- horizontal gene transfer

HMWC - high molecular weight complex

Hsp - heat shock protein

ICAR - immobilized cobalt affinity resin

iCP - immunoproteasome

IFNγ - interferon gamma

IP - immunoprecipitation

LM - lysate mixing

MHC-I - major histocompatibility class 1

Mpa - mycobacterium proteasome ATPase

MS - mass spectrometry

PA# - proteasome activator

PAC - proteasome assembly chaperone

PafE - proteasome accessory factor E

PAGE - polyacrylamide gel electrophoresis

PAN - proteasome activating nucleotidase

Pba - proteasome biogenesis-associated

PHP - pre-holoproteasome

PM - protein mixing

POMP - proteasome maturation protein

PPS - pup-proteasome system

PSM - peptide spectral match

Pup - prokaryotic ubiquitin-like protein

REG - regulatory

RP - regulatory particle

SAMP - small archaeal modifier protein

SDS - sodium dodecyl sulphate

Ssa - stress sensitivity subfamily A

TNF - tumor necrotic factor

UbaA - ubiquitin-like activating protein

Ump1 - ubiquitin-mediated proteolysis 1

UPS - ubiquitin proteasome system

WT - wild type

ABSTRACT

Author: Panfair, Dilrajkaur. PhD
Institution: Purdue University
Degree Received: December 2018
Title: Alternative Assembly Pathways of the 20S Proteasome and Non-canonical Complexes
Committee Chair: Lata Balakrishnan

The 20S proteasome, a multi-subunit protease complex, present in all domains of life and some orders of bacteria, is involved in degradation of the majority of cellular proteins. Structurally, it is made of α and β subunits arranged in four heptameric rings, with inner two β-rings sandwiched between outer two α-rings. The 20S proteasome in prokaryotes usually has one type of α and one type of β subunits, whereas eukaryotes have seven distinct types of α and seven distinct types of β subunits. Unlike the highly conserved structure of proteasome, its assembly pathway is different across the domains. In archaea and eukaryotes, proteasome assembly begins with α subunit interactions leading to the α-ring formation. By contrast, bacterial proteasome assembly pathway bypasses the α-ring formation step by initiating assembly through an α and β subunit interaction first. These early interactions are not well understood due to their highly rapid and dynamic nature. This dissertation focused on understanding the early events in proteasome assembly and contributed three significant findings. First, the archaeal proteasome assembly can also begin without formation of α-rings, demonstrating the coexistence of a bacterial-like assembly pathway. Second, a novel assembly intermediate was identified in yeast, and its composition argues for the presence of a similar α-ring independent assembly pathway. Third, the assembly chaperone Pba3-Pba4 prevents the formation of high molecular weight complexes arising from spontaneous and non-productive interactions among the α subunits. These findings provide a broader understanding of proteasome biogenesis and suggest considering proteasome assembly event as a network of interactions rather than a linear pathway. The results also shed light on assembly chaperone's contribution in increasing the efficiency of proteasome assembly by streamlining the productive interactions.

CHAPTER 1. INTRODUCTION TO THE 20S PROTEASOME AND ITS ASSEMBLY

1.1 Ubiquitin Proteasome System (UPS)

Protein synthesis and timely degradation is crucial and tightly regulated processes that ensures proper functioning of the cell. Various kinds of internal and external stressors can often disrupt protein homeostasis which then leads to accumulation of unwanted and misfolded proteins. Such a state is associated with various cancers, neurodegenerative and cardiovascular diseases. In eukaryotes, the ubiquitin-proteasome system (UPS) is responsible for the regulated degradation of the majority of intracellular proteins, including misfolded, or damaged proteins (Varshavsky, 2012).

The UPS contains two main components, the ubiquitin machinery and the 26S proteasome. The ubiquitination machinery functions in the covalent attachment of a small, very highly conserved protein modifier (ubiquitin) to the protein substrate through a cascade of ubiquitination enzymes. A protein tagged with ubiquitin is marked for degradation. The mechanism of ubiquitination is well studied and reviewed elsewhere (Hochstrasser, 1996; Hochstrasser et al., 2008; Komander & Rape, 2012; Kulathu & Komander, 2012). Ubiquitination-like tagging has also been observed in archaea and actinobacteria. The tagged protein substrates are then recognized and degraded by the 26S proteasome. The 26S proteasome is a threonine protease comprising of the 20S proteasome or the core particle (CP) and a 19S regulatory particle (RP). The CP is comprised of 28 proteins arranged in a barrel shaped complex that has the catalytic activity in its central core. The 20S proteasome is also present in archaea, actinomycetes and nirtrospirales orders of bacteria (De Mot, Nagy, & Baumeister, 1998; De Mot, Schoofs, & Nagy, 2007). The entry of substrate into the CP is regulated by activators or regulators that are present across all domains. The 19S regulatory particle is comprised of 19 subunits that are assembled into lid and base subcomplexes. Six of the nine base subunits are AAA ATPase family proteins that form the hexameric ring, and requires ATP to bind either one or both sides of CP. The 19S RP functions in recognizing, unfolding, deubiquitinating and translocating substrate to the central chamber of the CP.

1.2 The 20S Proteasome Structure

The 20S proteasome is coaxially arranged as four heptameric rings with outer α-rings and inner β-rings made from α and β subunits respectively. The structure and arrangement of the proteasome is highly conserved across all domains of life (Fig. 1.1). One major difference lies in the subunit complexity found in higher organisms. Archaeal and bacterial proteasomes usually have one type of α and β subunits (Lin et al., 2006; Lowe et al., 1995; Tamura et al., 1995). Eukaryotes have seven different types of α (α1- α7) and seven different types of β (β1- β7) subunits arranged as α_{1-7} β_{1-7} β_{1-7} α_{1-7} (Groll et al., 1997).

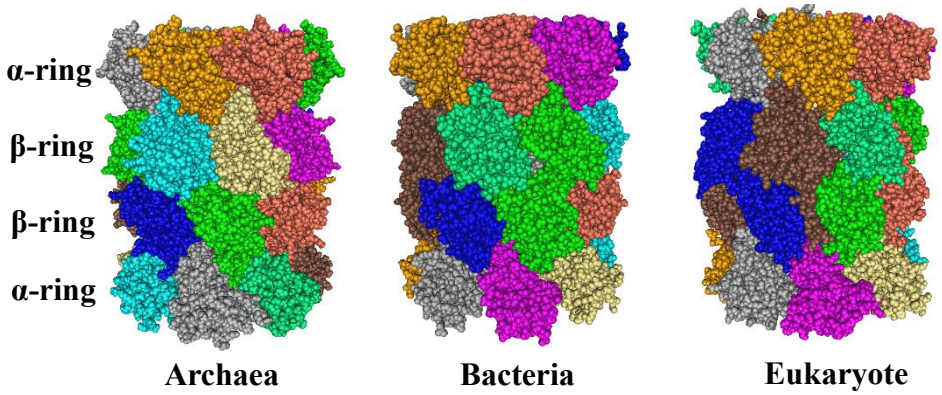

Figure 1.1: The 20S proteasome structure conservation across all domains
Space filling model generated by Cn3D based on the crystal structure of the CP from *Thermoplasma acidophilum* (Archaea), *Rhodococcus erythropolis* (Bacteria) and *Saccharomyces cerevisiae* (Eukaryote). Each proteasome subunit within the same α-ring and β-ring is assigned different color.

All β subunits in the archaeal and bacterial proteasome are catalytically active and preferentially cleave after hydrophobic residues. Among the seven distinct eukaryotic β subunits, β1, β2, and β5 are catalytically active and shows a broader substrate specificity by cleaving after acidic, basic and hydrophobic residues respectively. The active site residues within the surface pocket of β subunits determine its substrate specificity. Interestingly, the CP of *Mycobacterium tuberculosis* has cleavage specificities similar to eukaryotes (acidic, basic and hydrophobic residues) despite having only one type of β subunit (Lin et al., 2006). The crystal structure of *M. tuberculosis* CP revealed their β-subunit active site is unique. It is flanked by hydrophilic residues on one side and hydrophobic residues on the other side, thereby making it a hybrid of eukaryotic

catalytic subunits (Hu et al., 2006). Most β subunits are synthesized with N-terminal propeptides that are proteolytically removed during assembly. Removal of propeptides in the catalytic β subunits exposes its active site threonine (Thr1) residue that makes proteasome active only after its assembly (P. Chen & Hochstrasser, 1996; S. Witt et al., 2006).

1.3 Gating

CryoEM images and crystal structures of the free CP and CP bound to various activators have brought a detailed structural insight of the proteasome (S. Chen et al., 2016; Dambacher, Worden, Herzik, Martin, & Lander, 2016; Forster, Masters, Whitby, Robinson, & Hill, 2005; Groll et al., 1997; Huang, Luan, Wu, & Shi, 2016; Xueming Li et al., 2013; Lowe et al., 1995; Schweitzer et al., 2016; Unno et al., 2002b). The interior of the CP has three chambers, the two antechambers formed between the interface of α-rings and β-rings, and the central catalytic chamber formed between the two β-rings. A narrow opening, called the α-annulus, present at either end of the CP, is the entry site of the substrate. The first 10-15 residues at the N-termini of α subunits extends into the α-annulus to form a gate which remains closed until activated, and thereby prevents untimely entry of substrate into the central catalytic chamber (Groll et al., 2000; Religa, Sprangers, & Kay, 2010).

Binding of activators to the α-ring brings conformational change in the α subunit that leads to opening of the gate (Groll et al., 2000; Hill, Masters, & Whitby, 2002). Deletion of gating residues result in a constitutively "open gate" proteasome conformation that can degrade peptides, unfolded proteins, intrinsically disordered proteins or proteins with disordered regions without binding to the activators (Asher, Reuven, & Shaul, 2006; Asher & Shaul, 2005; Baugh, Viktorova, & Pilipenko, 2009; Choi et al., 2016; Lin et al., 2006). Under the oxidative stress conditions, leading to increased levels of damaged and misfolded proteins, such open gate proteasome might help in their clearance by remaining constantly active. However, in one study, open gated proteasome mutant decreased yeast viability under prolonged stress condition, emphasizing the relevance of an intact gate (Bajorek, Finley, & Glickman, 2003). In eukaryotes, the distinct N-termini residues of all α subunits ($\alpha_{1\text{-}7}$) attain a specific position contributing to a tightly closed gate such that the free CP remains incapable of hydrolysis without activator binding (Groll et al., 1997). Bacterial proteasomes too have fully closed gates despite having only one type of α subunit.

Crystal structure revealed different conformation attained by the same α subunit within the α-ring contributing to a fully closed gate (D. Li, Li, Wang, Pan, & Lin, 2010). By contrast, the archaeal proteasome gate remains in a relatively open state, perhaps due to the disordered nature of gating residues, and these proteasomes show mild activity in the absence of activators (Lowe et al., 1995).

1.4 Activators

Apart from the well-characterized 19S RP, there are also other known activators found in all domains of life. PAN (Proteasome activating nucleotidase) and AMA (archeoglobus and methanogenic archaea) are two CP activators identified in archaea (Wilson, Ou, Aldrich, & Maupin-Furlow, 2000; Zwickl, Ng, Woo, Klenk, & Goldberg, 1999), whereas ARC (AAA ATPase forming ring shaped complexes) and its homolog Mpa (mycobacterial proteasome ATPase) are two activators that have been found in bacteria (Darwin, Ehrt, Gutierrez-Ramos, Weich, & Nathan, 2003; Darwin, Lin, Chen, Li, & Nathan, 2005; Striebel, Hunkeler, Summer, & Weber-Ban, 2010; Wolf et al., 1998). In 19S RP, the AAA ATPase subunits (Rpt1-6) interact with the α-ring of the CP and uses the chemical energy from ATP binding and hydrolysis to unfold and translocate substrate. The interaction is mediated through a conserved three residue C-terminal HbYX (hydrophobic, tyrosine, any amino acid) motif, present in three Rpt subunits, that inserts into an intersubunit surface pocket formed by the α subunits. Another hexameric AAA ATPase, Cdc48, has been shown to bind and activate archaeal and mammalian CP (Barthelme & Sauer, 2012, 2013), suggesting this interaction is significant enough to have an evolutionary conservation. Whether Cdc48: CP forms an alternate type of proteasome that offers specific substrate degradation or may function under certain stress conditions, is yet to be determined.

Certain cofactors lacking the AAA rings can also activate proteasome. These include Blm10 (PA200), 11S in eukaryotes (described in a later section) and Bpa (bacterial proteasome activator) or PafE (proteasome associated factor E) in bacteria (Delley et al., 2014; Jastrab et al., 2015). The seven membered 11S binding to 20S stabilizes the open gate conformation, and it is known to enhance degradation of peptides and partially unfolded proteins, but not of native proteins (Forster et al., 2005; Stadtmueller & Hill, 2011). Bpa is structurally and functionally similar to 11S except it was shown to degrade the fully native protein HspR in the absence of ATP (Bolten et al., 2016; Jastrab et al., 2015).

1.5 Assembly of the 20S Proteasome

Although the 20S proteasome structure is highly conserved across all the domains, the assembly pathway differs among them. While the general assembly steps in archaea and eukaryotes are same, the subunit heterogeneity of eukaryotic proteasome requires their sequential interaction and assistance from assembly chaperones. In this section, assembly pathway and chaperones involved are discussed.

1.5.1 Archaeal Proteasome Assembly

Recombinant expression of archaeal proteasome subunits in *Escherichia coli* helped to understand proteasome biogenesis (Zwickl, Kleinz, & Baumeister, 1994). When archaeal α subunits are expressed *in vitro*, they formed α-rings. The additional H0 helix present in the α subunit, but not in the β subunit, contributes to its self-assembly into rings (Zwickl et al., 1994). Proteasomes formed when both wild-type α and β subunits were coexpressed, but not when the mutant α subunit (α35Δ), lacking 35 amino acid residues from the N-terminal including the H0 helix, was used (Zwickl et al., 1994). These results suggested that the β subunits assemble on the α-rings and that the α-ring formation is the first step of assembly (Fig. 1.2a). The α-ring provides a scaffold for β subunits addition further leading to form an assembly intermediate called the half proteasome. Two of such half proteasomes dimerizes, through opposite β-ring surface interactions, to form a transient intermediate called preholoproteasome (PHP). At this stage, the propeptides of β subunits are autocatalytically removed transforming the PHP intermediate to a mature or catalytically active proteasome (Fig. 1.2a). In this case, the β subunit propeptide is dispensable for assembly. In a recent report, an evidence was provided for the existence of an alternative archaeal proteasome assembly pathway that doesn't begin with α-ring formation (Panfair, Ramamurthy, & Kusmierczyk, 2015). This was demonstrated by showing tendency of α subunit mutants, incapable of forming α-rings, to form proteasomes when coexpressed with β subunits. More details are discussed in chapter 2.

Given that the archaeal α and β subunits can spontaneously assemble to form proteasomes, it was assumed assembly chaperones are not needed. However, two putative assembly chaperones, PbaA and PbaB, that form a heterodimer and contains the C-terminal HbYX motif, similar to their eukaryotic homolog Pba1-Pba2 (described in section 1.5.3.1), were later discovered in

Methanococcus maripaludis (Kusmierczyk, Kunjappu, Kim, & Hochstrasser, 2011). These proteins exclusively interacted with PHP, but not with the mature proteasome. The HbYX motif of PbaA is essential for this binding. Later, homologues of these proteins were also discovered in *Pyrococcus furiosus;* however, they seem to play different roles. Here, *PbaB* not only preferentially binds to mature CP, but can also act as a proteasome activator (Kumoi et al., 2013). Additionally, *P. furiosus* PbaA, despite having a HbYX motif, does not bind to the CP. The crystal structure of this protein showed the C-terminus, containing the HbYX motif, adopted a different orientation, perhaps less suitable for CP binding (Sikdar, Satoh, Kawasaki, & Kato, 2014). The exact roles and relevance of these chaperones are still not very clear.

1.5.2 Bacterial Proteasome Assembly

There is a limited distribution of proteasomes in bacteria, and it is believed they evolutionarily acquired proteasomes from archaea through horizontal gene transfer (HGT) (Volker & Lupas, 2002), yet their assembly pathway seems to differ considerably (Fig. 1.2b). In contrast to archaeal α subunits, *Rhodococcus erythropolis* α subunits could not form α-rings when expressed *in vitro* whereas coexpression of both subunit types resulted in assembly into proteasomes. These results suggested that the bacterial proteasome assembly pathway starts with α/β interactions first that most likely forms a heterodimer which quickly multimerizes to form a half proteasome (Kwon, Nagy, Adams, Baumeister, & Jap, 2004; Zuhl, Seemuller, Golbik, & Baumeister, 1997). This is the first observable assembly intermediate in bacteria. Dimerization of two half proteasomes is followed by formation of PHP and its eventual maturation to CP by autocatalytic β subunit propeptide removal (Fig 1.2b). Our recent report (detailed in chapter 2) showed this seemingly separate bacterial assembly pathway also exists in archaea arguing for a conservation of assembly mechanism across all domains (Panfair et al., 2015).

The crystal structure of bacterial proteasomes revealed a reduced surface contact area between two α subunits (α-α) within an α-ring helping explain their limited capability to form rings on their own. Here, the propeptide of β subunits acts as an internal assembly chaperone by facilitating α-α subunit contact. The exception lies in the propeptide of *M. tuberculosis* in that it is not only dispensable for assembly but also prevents the dimerization of two half proteasome (Lin et al., 2006). The orientation of the propeptide is outward from the β-ring in the half proteasome

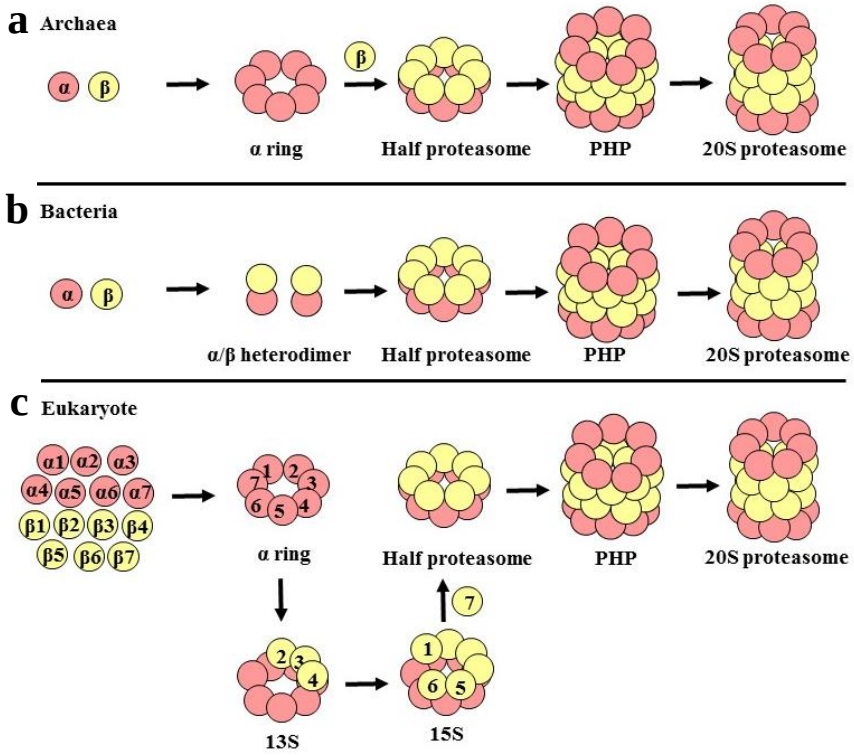

Figure 1.2: Overview of proteasome assembly pathways
Proteasome assembly is mediated by two types of pathways, α-ring dependent and α-ring independent. (a) Archaea follows an α-ring dependent pathway that starts with the formation of α-ring. The β subunits assemble on α-ring to form a half proteasome intermediate. (b) Bacterial proteasome assembly pathway follows an α-ring independent pathway that starts with an α/β heterodimer formation followed by its multimerization to form a half proteasome intermediate. (c) Assembly in eukaryotes is much more complicated requiring assistance of five dedicated assembly chaperones (not shown) and follows an α-ring dependent pathway. The seven distinct α subunits form a heterogenous α-ring ($\alpha_{1\text{-}7}$). Addition of β2, β3, β4 generates a 13S assembly intermediate. Subsequent addition of β1, β5, β6 forms the 15S intermediate. Addition of β7 forms a half proteasome. The pathway follows similar steps in all the domains after half proteasome intermediate that involves dimerization of two half proteasomes leading to the formation of preholoproteasome (PHP) intermediate. This step is quickly coupled with β-subunit propeptide processing leading to maturation of the CP.

intermediate and requires rearrangement during dimerization to attain similar orientation as observed in the PHP of *R. erythropolis* (Hu et al., 2006; D. Li et al., 2010). The propeptide, in this case, may only function in preventing the Thr1 residue from early activation. No assembly chaperones have been identified in bacteria.

1.5.3 Eukaryotic Proteasome Assembly

Assembly in eukaryotes is chaperone-mediated, highly ordered and a regulated process. There are several proteasome isoforms in eukaryotes (discussed in a later section). The order of specific subunit addition and assembly chaperone function slightly varies among different isoforms, and to some extent, among species. In general, the assembly pathway is similar to their archaeal counterparts that starts with the formation of α-rings first (Fig. 1.2c). Assembly chaperone Pba1-Pba2 (PAC1-PAC2) and Pba3-Pba4 (PAC3-PAC4) are known to assist in the α-ring assembly. Onto these rings, β2, β3, β4 subunits are added with the help of assembly chaperone Ump1. The Pba3-Pba4 assembly chaperone dissociates with the entry of these β subunits. This intermediate is called 13S (Hirano et al., 2008). Subsequent addition of β1, β2 and β5 results in forming an intermediate called 15S. Addition of β7 subunit is coupled with half proteasome dimerization that forms the PHP intermediate (Hirano et al., 2008; X. Li, Kusmierczyk, Wong, Emili, & Hochstrasser, 2007; X. Li, Li, Arendt, & Hochstrasser, 2016; Marques, Glanemann, Ramos, & Dohmen, 2007). The β subunit propeptides are removed at this stage, and the assembly chaperone Pba1-Pba2 is likely ejected at this stage. After maturation of proteasome, Ump1 becomes the first proteasome substrate (P. Chen & Hochstrasser, 1996; Nandi, Woodward, Ginsburg, & Monaco, 1997; Schmidtke et al., 1996).

Apart from these five dedicated assembly chaperones, the involvement of a known CP activator, Blm10, is also reported. There is growing evidence of other ancillary proteins directly or indirectly involved in assisting the assembly. Moreover, specific features of α and β subunits itself guide the assembly pathway. More details about assembly chaperones and ancillary proteins are described below.

1.5.3.1 Pba1-Pba2

Pba1 and Pba2 (PAC1 and PAC2 in mammals) stabilize each other by forming a heterodimer (Hirano et al., 2005; Le Tallec et al., 2007; X. Li et al., 2007). Knockdown of PAC1, PAC2 or both resulted in reduced α-ring levels and formed an aberrant complex, likely an α-ring dimer (Hirano et al., 2005). This suggests Pba1 and Pba2 function in α-ring formation and prevent nonspecific interactions of α subunits. While the downregulation of PAC1 and PAC2 leads to reduced cell growth in mammals, *pba1Δ pba2Δ* in yeast did not show any growth defect. However,

when *pba1Δ pba2Δ* is combined with other mutations that reduce proteasome function, strong growth defects are observed. In yeast, Pba1 and Pba2 are associated with several assembly intermediates indicating their multiple roles that expand beyond the α-ring assembly. One of these likely roles is to prevent association of RP to CP assembly intermediates.

Pba1-Pba2 contain conserved C-terminal HbYX motifs, a motif present in most proteasome binders (X. Li et al., 2007). Crosslinking study revealed the Pba1 and Pba2 HbYX motifs insert into the surface pocket formed by proteasome subunit α5-α6 and α6-α7 respectively, this was confirmed in the crystal structure of Pba1-Pba2-20S (Stadtmueller et al., 2012; Tian et al., 2011). As mentioned previously, RP binding to CP is also mediated by HbYX motifs and involves the same surface pocket. However, Pba1-Pba2 has a stronger affinity towards immature CP compared to RP (Wani, Rowland, Ondracek, Deeds, & Roelofs, 2015). Although, in one study, the Pba1-Pba2 was shown to bind mature CP at low salt concentration, the affinity considerably decreases under physiological salt conditions where the affinity of RP for mature CP is higher (Stadtmueller et al., 2012; Wani et al., 2015). Similar affinity bias was observed in the archaeal ortholog of Pba1 and Pba2 towards immature CP (Kusmierczyk et al., 2011). In both cases, the authors hypothesized that processing of β subunit propeptides allosterically alters the binding site of Pba1 and Pba2 in the α-ring, that it no longer favors it's association after the maturation of CP. Additionally, the HbYX motif of Pba2 was shown to be dispensable for binding to mature CP, whereas both HbYX motifs of Pba1-Pba2 are required for binding to immature CP, lending further support for an altered conformation of the α5-α6 surface pocket, binding site of Pba1, after maturation (Wani et al., 2015).

The single particle electron microscopy combined with crosslinked MS based structure of Pba1-Pba2-15S intermediate (containing Pba1, Pba2, Ump1, all α and β subunits except β7) highlighted the detailed orientation and interaction of Pba1-Pba2 in the 15S assembly intermediate (Kock et al., 2015). The structure revealed a much broader α-ring in the 15S intermediate compared to a fully assembled CP. The Pba1-Pba2 orients in the cavity of α-ring making extensive contacts with a majority of α subunits, and these interactions likely stabilizes the α-ring (Kock et al., 2015). The second structure involving Pba1-Pba2-PHP, a state attained after the β7 incorporation and

dimerization of half proteasome, showed Pba1-Pba2 shifted out of the central cavity to the top of α-ring. Such shifting of position might also be one of the contributing factors in the affinity switch.

1.5.3.2 Pba3-Pba4

Pba3 and Pba4 (PAC3 and PAC4 in mammals) also form a heterodimer that stabilizes each other similar to Pba1 and Pba2 (PAC3 and PAC4) and function in α-ring assembly (Hirano et al., 2006; Kusmierczyk, Kunjappu, Funakoshi, & Hochstrasser, 2008) . PAC3 has been shown to bind α2 subunit and certain β subunits (Hirano et al., 2006). *In vitro*, Pba3 and Pba4 strongly associate with the α5 subunit and weakly with α1 and α6 (Kusmierczyk et al., 2008; Le Tallec et al., 2007; Yashiroda et al., 2008).

Unlike Pba1-Pba2, Pba3-Pba4 have only been detected prior to the 13S assembly intermediate suggesting their exclusive role in α-ring formation. These assembly chaperones are structurally similar to α and β subunits (Yashiroda et al., 2008). However, the crystal structure of the ternary complex Pba3-Pba4-α5 revealed that Pba1-Pba2 associates with α subunits differently from the way proteasome subunits interact with each other (Yashiroda et al., 2008). Moreover, the structure revealed that the binding of Pba3-Pba4 to α5 would provide a steric hindrance to β subunits incorporation explaining why Pba3-Pba4 must dissociate early, likely before the arrival of β4 subunit (Hirano et al., 2008).

In yeast, α3 is the only 20S proteasome subunit whose deletion is not lethal. In these cells, a unique isoform of the proteasome is formed, termed the "α4-α4" proteasome, that has an additional copy of α4 subunit in place of α3 subunit. Interestingly, in the absence of Pba3-Pba4, yeast also form the "α4-α4" proteasome, comprising ~20-50% of total proteasome pool (Kusmierczyk et al., 2008; Velichutina, Connerly, Arendt, Li, & Hochstrasser, 2004). Similar appearance of this evolutionarily conserved α4-α4 proteasome was recently shown when assembly chaperone PAC3 and PAC4 are knocked down in mammalian cells (Padmanabhan, Vuong, & Hochstrasser, 2016). These assembly chaperone perhaps assist α3 subunit incorporation between of α2 and α4 subunits (Kusmierczyk et al., 2008). In another study, *pba3Δ* and *pba4Δ* resulted in accumulation of an aberrant (likely assembly incompetent) complex resembling a 13S intermediate that lacked α4 and had twice the level of α2 (Takagi et al., 2014). Overall, it seems that this

assembly chaperone drives the α-ring complex formation by guiding the order of specific α subunits addition within the α-ring. The exact mechanism of how this is achieved is not well understood.

1.5.3.3 Ump1

Ump1, the first assembly chaperone to be discovered, functions from the point of β subunit entry onto α-rings up until the dimerization of two half proteasomes, after which it gets encapsulated within the core and becomes the first substrate of the newly assembled proteasome (Burri et al., 2000; Frentzel, Pesold-Hurt, Seelig, & Kloetzel, 1994; Griffin, Slack, McCluskey, Monaco, & Colbert, 2000; Hirano et al., 2008; X. Li et al., 2007; Ramos, Hockendorff, Johnson, Varshavsky, & Dohmen, 1998; E. Witt et al., 2000). This 16 kDa protein is intrinsically disordered and assist in precise β subunit assembly (Ramos et al., 1998). The mammalian Ump1 (called hUmp1) has been shown to assist β2 subunit entry onto α-rings. Ump1 in yeast is detected at the 13S intermediate state; whether it appears along with β subunit addition, or before, is not known (X. Li et al., 2007). Recent negative stain EM and crosslinking based structure of 15S revealed Ump1 orientation and interaction with proteasome subunits (Kock et al., 2015). More than half of Ump1's C-terminus is looped into the inner chamber of 15S making extensive contact with α and β subunits where it may function in stabilizing incoming β subunits (Howell, Tomko Jr, & Kusmierczyk, 2017). At the later stage of assembly, Ump1 functions to prevent premature dimerization of two half proteasomes (Kusmierczyk et al., 2008; X. Li et al., 2007). The checkpoint function may be attributed to the N-terminus of Ump1 that is observed at the interface of β6 and β7 and ideally oriented to prevent dimerization. Ump1 may also sense entry of β7, the last subunit to be added to form the half proteasome intermediate, after which it reorients towards the inside of the cavity (Budenholzer, Leng Cheng, Li, & Hochstrasser, 2017; Howell et al., 2017).

1.5.3.4 Blm10

Blm10 (PA200 in human) has been shown to be involved in proteasome assembly, maturation, activation, and localization. It is a large dome-shaped protein, with a mass of ~250 kDa, and preferentially binds to CP alone or as a hybrid with RP on the opposite side (Schmidt et al., 2005; Ustrell, Hoffman, Pratt, & Rechsteiner, 2002). Its function is partially redundant with RP in promoting CP activation (Takeuchi, Chen, Hoyt, & Coffino, 2008). Blm10 binds to α-ring

via its single C-terminal HbYX motif that gets inserted into α5-α6 surface pocket (Dange et al., 2011; Sadre-Bazzaz, Whitby, Robinson, Formosa, & Hill, 2010; Schmidt et al., 2005). This binding stimulates gate opening that may involve small peptide degradation in an ATP independent manner (Schmidt et al., 2005; Ustrell, Pratt, Gorbea, & Rechsteiner, 2005). Blm10 is structurally related to importin (nuclear receptor protein) and has been implicated in nuclear import of CP (Weberruss et al., 2013). With regards to CP assembly, Blm10 binds to all the known assembly intermediates (Fehlker, Wendler, Lehmann, & Enenkel, 2003; X. Li et al., 2007). Double deletion of *BLM10* gene and the C-terminal tail of the β7 subunit increased accumulation of proteasome precursors and showed a maturation defect of the β2 subunit propeptide suggesting a role in half proteasome dimerization and CP maturation (Marques et al., 2007).

1.5.3.5 Intrinsic features of α subunits

There exists a high structural similarity between α and β subunit of the proteasome. The variation appears at the N-terminus. While the β subunits N-termini includes a varying length of propeptides that does not form a secondary structure, all the α subunit N-termini have a conserved H0 helix. The H0 helix is one of the primary factors responsible for α-ring formation, the first step of proteasome assembly (Zwickl, Voges, & Baumeister, 1999). Additional factors such as large buried surface area and stabilizing salt bridges between the α subunits also contribute to α-ring formation and stabilization (Kwon et al., 2004; Panfair et al., 2015).

1.5.3.6 Intrinsic features of β subunit in proteasome assembly

Most proteasome β subunits except β3 and β4 are expressed with varying lengths of N-terminal propeptides which are proteolytically removed during maturation of the CP. These propeptides along with C-terminal extensions of specific β subunits, act as intramolecular chaperones ensuring their sequential addition and maturation of CP. The N-terminal propeptide is present in the catalytically active subunits β1, β2, β5, and in non-catalytic subunits β6 and β7. The N-terminal propeptides of the catalytic subunits function in preventing inactivation of the catalytic Thr1 residue via Nα acetylation (Arendt & Hochstrasser, 1999; Jager, Groll, Huber, Wolf, & Heinemeyer, 1999; Schreiner et al., 2008).

In yeast, β5 propeptide also functions in β5 subunit incorporation, and its absence (β5Δpro), is lethal (P. Chen & Hochstrasser, 1996; Howell et al., 2017). When this 75-residue propeptide is expressed separately as an individual polypeptide, it rescues lethality, suggesting propeptide can act as an independent intramolecular chaperone (P. Chen & Hochstrasser, 1996; Jager et al., 1999). Its precise mechanism and whether it attains any specific form is not known. Assembly chaperone *ump1Δ* can also rescue β5Δpro lethality indicating a likely antagonistic role between these two components (Ramos et al., 1998). Functional overlap of β5 propeptide and β7 C-terminal tail exists in assisting dimerization of two half proteasomes (X. Li et al., 2007). The β5 propeptide is also essential for the incorporation of β6 subunit in mammals (Hirano et al., 2008).

The β2 subunit propeptide is essential in mammals and assists in the incorporation of the β3 subunit (Hirano et al., 2008). While the β2 propeptide is not essential for viability in yeast, its deletion causes processing defects of β5 and β7 subunits (P. Chen & Hochstrasser, 1996; Jager et al., 1999). Similar processing defects of the β5 subunit are observed in the absence of the β1 propeptide (P. Chen & Hochstrasser, 1996; Hirano et al., 2008; Jager et al., 1999). The function of the β6 propeptide and Ump1 are linked since Ump1 can rescue the lethal phenotype of β6Δpro (X. Li et al., 2007). The propeptide of β7 is not essential for viability, and its functional role is not clear.

The C-terminal tails of β2 and β7 assist in CP assembly. The β2 C-terminal tail, essential in both yeast and mammals, is necessary for β3 subunit incorporation (Hirano et al., 2008; Ramos, Marques, London, & Dohmen, 2004). This ~ 30 residue tail loops around the adjacent β3 subunit and extends further making contact with the β4 subunit within the same β ring (Groll et al., 1997; Unno et al., 2002b). The β7 C-terminal tail functions in half proteasome dimerization. It does so by inserting its C-terminal tail between β1 and β2 in the opposite β ring, thereby acting as a lynchpin which clamps these rings together (Groll et al., 1997; Unno et al., 2002a). Moreover, this tail also functions in β7 incorporation since its absence increased levels of the 15S intermediate (contains all α and β subunits except β7) (Hirano et al., 2008; X. Li et al., 2007; Marques et al., 2007; Ramos et al., 2004).

1.5.3.7 Other assembly factors

Specific proteins are known to associate with CP subunits and assembly intermediates, but further studies are needed to establish their contribution in CP assembly. Fub1 (function of boundary 1) protein directly interacts with several CP subunits (Hatanaka et al., 2011). When its deletion is combined with CP mutants, growth defects are exacerbated, and in some combinations, results in lethality (Hatanaka et al., 2011; Yashiroda et al., 2015). Hsp70 protein's roles are well established in ubiquitination and substrate delivery to the 26S proteasome (Arndt, Rogon, & Hohfeld, 2007; Huyer et al., 2004; Kettern, Dreiseidler, Tawo, & Hohfeld, 2010; Metzger, Maurer, Dancy, & Michaelis, 2008; Plemper, Bohmler, Bordallo, Sommer, & Wolf, 1997; Shiber & Ravid, 2014). Recently, two Hsp70 group proteins, Ssa1/Ssa2 were shown to interact tightly with early CP assembly intermediates but not with mature CP, a feature commonly found in assembly chaperones (Hammack, Firestone et al. 2017). Their association with α4 complex, an *in vivo* non-canonical complex formed by α4 subunit, suggests a likely role in α-ring formation (L. J. Hammack & A. R. Kusmierczyk, 2017). Other proteins reported to have a link with proteasome assembly pathway are proteins involved in Transmembrane Recognition Complex (TRC) in mammals/Guided Entry of Tail-anchored pathway (GET) in yeast (Akahane, Sahara et al. 2013) and a zygote proteasome assembly chaperone in mouse (Shin, Shimizu et al. 2013).

1.6 Non-canonical Complexes

Certain proteasome α subunits form higher order structures when expressed *in vitro*. Recombinant archaeal α subunit can form single and double α-rings (Groll, Brandstetter, Bartunik, Bourenkow, & Huber, 2003; Panfair et al., 2015; Zwickl et al., 1994). Similarly, *Trypanosoma brucei* α5 can form four heptameric rings structurally similar to 20S (Yao et al., 1999). Recombinant human α7 can also form double α7-rings (Gerards et al., 1997). While the coexpression of α7 with β7 and β1 subunits, the immediate neighbors of the α7 subunit in the adjacent β-ring, still formed α7-rings, coexpression with the α6 subunit, native neighbor of the α7 subunit within the α-ring, formed a complex containing both α6 and α7 subunits (Gerards, de Jong, Bloemendal, & Boelens, 1998; Gerards, de Jong, Boelens, & Bloemendal, 1998; Gerards et al., 1997). Later, it was demonstrated that in the presence of the α6 subunit, a preformed double α7-ring dissociates to form an α6-α7 complex (Ishii et al., 2015). These interactions show the inherent

tendency of α subunits to form non-canonical ring complexes *in vitro*, yet none of these have been observed *in vivo*. While the single α-ring is an on-pathway product, double α-rings are a dead-end complex (Panfair et al., 2015). Perhaps the presence of additional α subunits and assembly chaperones prevent such nonspecific interactions *in vivo*. In support of this, absence of assembly chaperone PAC1 and PAC2 results in accumulation of an aberrant complex, presumably an α-ring dimer, suggesting their role in preventing such off-pathway interaction (Hirano et al., 2005).

Recently, the first evidence of a non-canonical complex formed by α4 subunit in yeast was provided (L. J. Hammack & A. R. Kusmierczyk, 2017). This α4 complex is present in wild-type cells, and its levels increase when the α3 subunit is deleted, suggesting a physiological relevance. Additionally, this complex also contains Ssa1/Ssa2 proteins (members of Hsp70 superfamily), which have recently shown to be associated with proteasome assembly (L. J. Hammack, Firestone, Chang, & Kusmierczyk, 2017). Moreover, crosslinking data suggests similar complex is likely present in mammalian cells, indicating the complex may be evolutionarily conserved (Padmanabhan et al., 2016). A crystal structure and further characterization of this complex might shed some light on its function.

1.7 Alternative Proteasomes

There are several isoforms of proteasome found in eukaryotes, some of which have tissue specific localization whereas others may form more broadly under certain conditions. These variants arise when specific α or β subunit paralogs take the place of their canonical subunit counterparts. These variants assemble differently from the canonical CP and some of them have preference for specific substrates.

1.7.1 α4-α4 Proteasomes

This alternative proteasome has an additional copy of the α4 subunit that takes the place of the α3 subunit. They were first reported in yeast cells lacking the α3 subunit, the only non-essential CP subunit in yeast, and their detection is possible by crosslinking two adjacent α4 subunits in the α-ring (Funakoshi, Li, Velichutina, Hochstrasser, & Kobayashi, 2004). Since the N-terminal tail of the α3 subunit is essential for gating, the absence of α3 indicates α4-α4 proteasome may have open gate conformation (Groll et al., 2000). Yeast cells bearing α4-α4 proteasomes are more

tolerant to heavy metal stress as compared to wild-type cells (Kusmierczyk et al., 2008). Perhaps the open gate conformation might be the contributing factor for enhanced stress tolerance. This isoform is also detected when the assembly chaperone Pba3-Pba4 is deleted (Kusmierczyk et al., 2008). Recently, α4-α4 proteasomes were reported in mammalian cells, and their formation was shown to depend on relative levels of α3, α4 and PAC3-PAC4 (Padmanabhan et al., 2016). Moreover, their stress tolerant property regarding heavy metal tolerance is also evolutionarily conserved suggesting they might have a stress-based induction. Their role and assembly pathway are unclear.

1.7.2 Gonad Specific Proteasome

Testis-specific proteasome, first identified in *Drosophila melanogaster*, contains an alternative α6 subunit (prosalpha6T), which is essential for male fertility (Zhong & Belote, 2007). In mammals, spermatoproteasome were later discovered in testes which contain an alternative α4 subunit called α4S (Qian et al., 2013). There exists ~82-85% of similarity between α4 and α4S; the latter is explicitly expressed in testes (Uechi, Hamazaki, & Murata, 2014).

Spermatoproteasomes preferentially bind to Blm10, and Blm10 is essential for spermatogenesis in mice (Qian et al., 2013). A difference in the sequence of the α4 and α4S subunit, particularly at the outer surface, might be the contributing factor for preferential Blm10 binding (Uechi et al., 2014). These alternative proteasomes are the predominant species in testes. What drives the preferential incorporation of α4S and prosalpha6T, as compared to their canonical counterparts, α4 and α6 respectively, is not known.

1.7.3 Immunoproteasomes

The immunoproteasome replaces catalytically active subunits β1, β2 and β5 with their paralogs β1i, β2i and β5i respectively. These paralogs are induced by interferon gamma (IFNγ) and tumor necrosis factor (TNF) (Akiyama et al., 1994; Tanaka, 1994), and have ~60% identity with their canonical counterparts. The immunoproteasomes have altered functional properties. Specifically, they generate a different peptide population that is optimized for presentation as Major Histocompatibility Class 1 (MHC-1) antigen (Gaczynska, Rock, & Goldberg, 1993). Various subtypes of immunoproteasome, containing different combinations of canonical catalytic

β subunits with their paralogs, have been reported and are hypothesized to result from varying level of IFNγ expression (Guillaume et al., 2010; Klare, Seeger, Janek, Jungblut, & Dahlmann, 2007).

The assembly pathway of immunoproteasomes is different in terms of β subunit incorporation. While in the canonical CP, the first β subunits to add on the α-ring are β2, β3, and β4, in immunoproteasomes it is, β1i and β2i that incorporate first, followed by β3. The β5i is added before the β4 subunit. These changes in the order suggest the β subunit paralogs tend to incorporate more efficiently than their constitutive counterparts. The propeptide of β2i subunit and the mature domain of β5i subunit contribute to their preferential incorporation (Bai et al., 2014; De et al., 2003; Kingsbury, Griffin, & Colbert, 2000).

An IFNγ inducible activator 11S (PA28αβ) binds to immunoproteasomes and is believed to enhance antigen presentation (Dubiel, Pratt, Ferrell, & Rechsteiner, 1992; Realini, Dubiel, Pratt, Ferrell, & Rechsteiner, 1994). The PA28 activator is comprised of α and β subunits that can assemble in three different forms when expressed *in vitro*. PA28α and PA28β form homoheptameric rings of made from α and β subunits respectively, whereas PA28α4β3 forms heteroheptameric rings containing four α and three β subunits (Huber & Groll, 2017; Knowlton et al., 1997; Wilk, Chen, & Magnusson, 2000). Among these three species, PA28α4β3 activator complex is more stable and active, and is likely physiologically relevant (Huber & Groll, 2017). Immunoproteasome can also bind to other activators, 19S RP and Blm10, either alone or as a hybrid with PA28 (Cascio, Call, Petre, Walz, & Goldberg, 2002; Hendil, Khan, & Tanaka, 1998; Tanahashi et al., 2000). This combinatorial binding enhances the epitope diversity for antigen presentation (Cascio et al., 2002; Hendil et al., 1998). A homologue of PA28αβ, PA28γ, present throughout metazoan but not in yeast and plants, can also bind to immunoproteasomes (Masson, Andersson, Petersen, & Young, 2001). Its functional role is not very clear.

1.7.4 Thymoproteasome

The thymoproteasomes are similar to immunoproteasomes except the β5i is substituted by a thymus specific β5t subunit. The order of β5t incorporation is identical to β5i in immunoproteasome, but unlike the mature domain of β5i, here, the propeptide of β5t promotes its

preferential incorporation to form thymoproteasome (Bai et al., 2014). This proteasome isoform is involved in the positive selection of $CD8^+$ T cells (Murata, Takahama, & Tanaka, 2008). A recent computational analysis of the human genome revealed a high polymorphism in the sequence of β5t subunit and suggested the variation may lead to individual's susceptibility to autoimmunity (Nitta et al., 2017).

1.8 Proteasome in Cancer Therapeutics

The proteasome mediates degradation of various proteins involved in diverse cellular processes such as cell cycle progression, differentiation, apoptosis, DNA damage repair (Ciechanover, 2005; Ciechanover & Schwartz, 2004; Finley, Ulrich, Sommer, & Kaiser, 2012; Hochstrasser, 1996). Consequently, alterations in proteasome activity are associated with several diseases. In previous studies on understanding catalytic activity of the proteasome, its inhibition lead to unwanted accumulation of regulatory proteins that triggered apoptosis (Adams, 2004; Vinitsky, Cardozo, Sepp-Lorenzino, Michaud, & Orlowski, 1994). This sensitivity towards apoptosis appeared greater in certain cancer cell lines and even in some solid tumors (Imajoh-Ohmi et al., 1995; Orlowski & Kuhn, 2008; Shinohara et al., 1996). This sensitization enabled the use of proteasome inhibitors as a new therapeutic approach for treatment of certain cancers.

1.8.1 Proteasome Inhibitors

Most proteasome inhibitors are peptide like compounds containing an electrophilic head comprised of either a boronic acid, β-lactone, or an epoxyketone, that occupies the active site Thr1 residue. Protein degradation rates are majorly affected by inhibition of the chymotrypsin like activity of the β5 subunit (Jung, Catalgol, & Grune, 2009). Bortezomib (Velcade, Millennium Pharmaceuticals), a reversible boronate inhibitor targeting β5 subunit activity, was the first proteasome inhibitor approved by the FDA in 2003 for the treatment of multiple myeloma (Kane, Farrell, Sridhara, & Pazdur, 2006). It was later approved for the treatment of mantle cell lymphoma and showed efficacy for non-small cell lung cancer and pancreatic cancer (Frankland-Searby & Bhaumik, 2012). Treatment with bortezomib, however, develops resistance and shows adverse side effects including cardiac and pulmonary disorders, peripheral neuropathy, gastrointestinal problems and pain (Frankland-Searby & Bhaumik, 2012). Current investigations are focused on its combinatorial use with other chemotherapeutic agents for improving resistance and toxicity.

Carfilzomib (Kyprolis, Proteolix Inc.), an irreversible epoxyketone family proteasome inhibitor, with a broader therapeutic range was approved by the FDA in 2012 and showed an improved efficacy on bortezomib failed multiple myeloma patients (Kuhn et al., 2007; Moreau, 2014). Ixazomib (Millenium Pharmaceuticals) is the second-generation peptide boronate inhibitor approved by the FDA in 2015 (Crawford, Walker, & Irvine, 2011; Kupperman et al., 2010). This is the first orally available proteasome inhibitor; however, its half-life is shorter than bortezomib (Teicher & Tomaszewski, 2015).

Numerous studies have shown upregulation of immunoproteasome or increased expression of their catalytic subunits in autoinflammatory and autoimmune diseases, neurological disorders, and in certain types of cancers including prostate cancer, multiple myeloma, lung cancer and others (Basler, Kirk, & Groettrup, 2013; Kaur & Batra, 2016). Selective inhibition of immunoproteasome is the recent focus of therapy since most proteasome inhibitors could not differentiate between the catalytic subunits of constitutive proteasomes (β1, β2 and β5) and immunoproteasomes (β1i, β2i and β5i) (Cromm & Crews, 2017). Perhaps this could be one of the reasons for numerous side effects of proteasome inhibitor therapies. Recent crystal structure of murine constitutive proteasome and immunoproteasome highlighted structural differences between the active site of β5 and β5i subunit which is helping to design specific immunoproteasome inhibitors (Huber et al., 2012). One such inhibitor, KZR-616 (Kezar lifesciences) specifically targets β5i subunit, and it is under phase I clinical trial for the treatment of certain inflammatory and autoimmune diseases (Cromm & Crews, 2017).

1.8.2 Proteasome Assembly Inhibition

Upon malignant transformation of cells, with a consequent increase in metabolic and protein synthesis rates, there occurs a disruption in protein homeostasis. Among other mechanisms, certain cancer cells are heavily dependent on the increase in proteasome activity to help them survive this proteotoxic stress. Such increased proteasome activity does not entirely rely upon increasing the expression of proteasome subunit, but also involves an increase in the proteasome assembly (Hanssum et al., 2014; Levin, Minis, Lalazar, Rodriguez, & Steller, 2018). The evidence is building up linking the increase in proteasome assembly to tumorigenesis and developing resistance towards treatment with proteasome inhibitors in certain cancers.

A microRNA miR-101 is a potent tumor suppressor that targets a CP assembly chaperone POMP (mammalian Ump1) by reducing its expression (Zhang et al., 2015). Downregulation of POMP disrupts proteasome assembly and thereby makes miR-101 an endogenous proteasome inhibitor (Zhang et al., 2015). Interestingly, miR-101 is downregulated in a variety of cancers correlating uncontrolled proteasome assembly with disease progression (Varambally et al., 2008). Moreover, overexpression of POMP induced resistance in bortezomib sensitive tumor cells whereas, in another study, its inhibition re-sensitized bortezomib-resistant cells suggesting a link between increased proteasome assembly with the development of drug resistance (B. Li et al., 2015; Zhang et al., 2015). A recent study reported an increase in the association of 19S RP to 20S CP without a change in the individual subunit levels in tumor cells of gut epithelium, correlating enhanced 26S assembly to cancer (Levin et al., 2018). This increase in 26S assembly rate was shown to be achieved by reducing and eventual silencing the expression of a proteasome assembly inhibitor protein, PSMD5, during tumor progression. Intriguingly, in a separate study, suppression of PSMD5 was also linked to bortezomib resistance suggesting the involvement of enhanced 26S proteasome assembly in developing bortezomib resistance (Levin et al., 2018). Another study showed cooperation of a RP assembly chaperone NRF2 with a mutant p53 protein in cancer cells leading to activation of proteasome genes and resulted in resistance to proteasome inhibitor carfilzomib (Walerych et al., 2016).

Thus, in addition to directly target proteasome activity, inhibiting proteasome assembly, either alone or in combination with the proteasome inhibitors, could offer a more effective therapeutic strategy. Despite having an elaborate structural and functional insights into the proteasome, its process of assembly is not completely understood. An in-depth understanding of proteasome assembly could provide a better insight into its regulation and may offer new approaches for its inhibition. Moreover, there are differences in the regulation and assembly pathways of proteasome isoforms. Such differences could be exploited to target assembly of specific isoform.

The highly dynamic nature of the CP assembly, especially at the very early stages, poses one of the challenges in elucidating the mechanism of early interactions. This dissertation focuses on investigating early events in the assembly of the 20S proteasome. In the following chapter, the

evidence is provided for an alternative α-ring independent pathway of the archaeal proteasome. Chapter 3 presents evidence for a novel early assembly intermediate in yeast, sub-13S, that contains a subset of α and β subunits, and likely originates from an α-ring independent pathway. Chapter 4 demonstrates the ability of eukaryotic α subunits to form high molecular weight complexes (HMWC) whose formation is prevented by assembly chaperone Pba3 and Pba4. The data herein contribute to a better understanding of 20S proteasome biogenesis and suggest that, rather than being a strictly linear process, assembly can likely occur through multiple pathways that are interconnected through common intermediates.

CHAPTER 2. ALTERNATE PROTEASOME ASSEMBLY PATHWAY

Chapter 2 along with Appendix A were originally published in Scientific Reports.

Panfair, D., Ramamurthy, A., & Kusmierczyk, A. R. (2015). Alpha-ring Independent Assembly of the 20S Proteasome. *Scientific reports, 5*.

2.1 Abstract

Archaeal proteasomes share many features with their eukaryotic counterparts and serve as important models for assembly. Proteasomes are also found in certain bacterial lineages, yet their assembly mechanism is thought to be fundamentally different. Here, α-ring formation was investigated using recombinant proteasomes from the archaeon *Methanococcus maripaludis*. Through an engineered disulfide cross-linking strategy, the results demonstrate that double α-rings are structurally analogous to half-proteasomes and can form independently of single α-ring. More importantly, the targeted mutagenesis results show that single α-rings are not required for the efficient assembly of 20S proteasomes. The data supports updating the currently held "α-ring first" view of assembly, initially proposed in studies of archaeal proteasomes, and present a way to reconcile the seemingly separate bacterial assembly mechanism with the rest of the proteasome realm. The results suggest that a common assembly network underpins the absolutely conserved architecture of proteasomes across all domains of life.

2.2 Introduction

Most intracellular proteins end their existence at the proteasome, a large multifunctional protease complex found in all domains of life. Proteasomes share a common architecture of a central protease capped by one or more regulatory complexes (J. Maupin-Furlow, 2012). The regulatory complexes differ in composition, from the hexameric ring-shaped AAA ATPases such as PAN in archaea (Benaroudj & Goldberg, 2000; Wilson et al., 2000) and MpA/ARC in bacteria, to the ~19 subunit Regulatory Particle of eukaryotes (RP, also called PA700 or 19S proteasome) (Glickman et al., 1998; Lander et al., 2012). By contrast, the central protease, called the 20S proteasome or core particle (CP), has an absolutely conserved quaternary structure (Groll et al., 1997; Hu et al., 2006; Lowe et al., 1995; Unno et al., 2002b). The CP consists of four stacked

heptameric rings. Structurally related subunits, α and β, comprise the outer and inner rings, respectively. Only β subunits are proteolytically active; they are synthesized as proprotein precursors and undergo autocatalytic activation to expose the N-terminal threonine nucleophile (P. Chen & Hochstrasser, 1995, 1996; Frentzel et al., 1994). Eukaryotic CP rings contain 7 unique α and β subunits, while those of archaea and bacteria usually consist of one or two types of subunit each. Although ubiquitous in archaea and eukaryotes, only a small subset of bacteria possess 20S proteasomes, possibly owing to a lateral gene transfer from archaea (Volker & Lupas, 2002).

Assembly of the proteasome, and of the 20S CP in particular, has garnered considerable attention recently reviewed in (Kunjappu & Hochstrasser, 2013; Saeki & Tanaka, 2012; Tomko & Hochstrasser, 2013). The general consensus posits that α subunits form rings first which act as a platform for the subsequent entry of β subunits (Hirano et al., 2008; Zwickl et al., 1994). Incorporation of the β subunits leads to the formation of a double-ring structure, the half-proteasome, which quickly dimerizes to form the 20S CP. A cadre of dedicated chaperones assists in CP assembly in eukaryotes (Hirano et al., 2006; Hirano et al., 2005; Kusmierczyk & Hochstrasser, 2008; Le Tallec et al., 2007; X. Li et al., 2007; Ramos et al., 1998; Yashiroda et al., 2008) and a subset of these chaperones may be conserved in archaea (Kusmierczyk et al., 2011). Despite differences in complexity, the assembly of archaeal and eukaryotic CP shares the same mechanism. Consequently, archaea have served as an important model for eukaryotic CP assembly (Frankenberg, Hsu, Yakota, Kim, & Clark, 2001; Groll et al., 2003; Zwickl et al., 1994). By contrast, the bacterial CP assembles via a different mechanism involving the formation of αβ heterodimers and their subsequent assembly into half-proteasomes (Kwon et al., 2004; Sharon, Witt, Glasmacher, Baumeister, & Robinson, 2007; Zuhl, Seemuller, et al., 1997).

Since early events in CP assembly, including those leading to the formation of α-rings, are not completely understood, this step was explored in more detail using recombinantly produced archaeal α subunits as a model. The results show that the currently held α-ring first view of CP assembly should be updated to include an alternate, parallel assembly pathway highly reminiscent of bacterial CP assembly. Our findings demonstrate that the common CP architecture across all domains of life is underpinned by common mechanisms of assembly, further underscoring the shared evolutionary origin of this important complex.

2.3 Materials and Methods

2.3.1 Creation of Plasmids and Mutant Constructs

Plasmids used in this study are listed in Supplementary Table 1 in Appendix A. DNA fragments encoding archaeal α and β subunits were cloned by PCR from *Methanococcus maripaludis* S2 genomic DNA kindly provided by John Leigh (University of Washington). Where indicated, primers were designed to incorporate C-terminal hexahistidine tags (his-tag). DNAs were subcloned into pET42 vector for expression in bacteria. Construction of polycistronic expression plasmids enabling the coexpression of archaeal α and β subunits was carried out as described (Kusmierczyk et al., 2011). Mutagenesis was carried out by PCR using the Quickchange method and kit (Stratagene). Automated DNA sequencing was used to verify all constructs.

2.3.2 Protein Expression and Isolation from Bacteria

Plasmid transformation into *Escherichia coli* BL21 cells, subsequent induction of protein synthesis by IPTG, and harvesting of the cultures were performed as described (Kusmierczyk et al., 2008; Kusmierczyk et al., 2011). Frozen cell pellets were thawed on ice and resuspended in 0.6 ml of Buffer A (50 mM HEPES-NaOH, pH 7.5, 0.3 M NaCl, and 5 mM $MgCl_2$ supplemented with 2 mM Pefabloc, 0.3 mg ml^{-1} lysozyme, 10 µg ml^{-1} DNase I and 0.1% (v/v) Triton X-100. The suspensions were lysed by shaking at 30 °C for 30 min. The resulting total crude lysate was centrifuged at 10,000 × *g* for 10 min at room temperature to separate soluble and insoluble material. The soluble material was applied to 50 µl of equilibrated immobilized cobalt affinity resin (ICAR) (Talon resin; Clontech), incubated for 1 hour and centrifuged at 700 × *g* for 5 min. The resin beads were washed 2 times with 1 ml of Buffer A, 2 times with 1 ml of Buffer B (Buffer A supplemented with 5 mM imidazole), and 1 time with 1 ml of Buffer C (Buffer A supplemented with 10 mM imidazole). Each wash step was carried out with gentle rocking for 5 mins at 4 °C, followed by centrifugation at 700 × *g* for 5 mins to pellet the resin. His-tagged proteins were eluted in 600 µl of Buffer E (Buffer A supplemented with 200 mM imidazole). Following purification, protein samples were desalted by serial centrifugation as described (Kusmierczyk et al., 2011). Prior to gel electrophoresis or size exclusion chromatography, protein concentrations were measured using the BCA Assay (ThermoScientific). For lysate mixing experiments, total crude lysates of desired samples were mixed and incubated at 37 °C with slow shaking for 30 mins. Following incubation,

mixed total crude lysates were separated into soluble and insoluble fractions as described above and subjected to protein purification by ICAR.

2.3.3 Polyacrylamide Gel Electrophoresis

Equal amounts of protein (10 µg or 20 µg) were mixed with 5× nondenaturing sample buffer (0.5 M Tris-HCl, pH 8.8, 50% (v/v) glycerol, traces of bromophenol blue). Samples were subjected to analysis by nondenaturing gel electrophoresis as described (Kusmierczyk et al., 2008; Kusmierczyk et al., 2011) except 4-15% gradient and 5-10% gradient gels were used as indicated in the Figure legends. All gels were lab poured except for the 4-15% gradient gels which were precast Mini-PROTEAN TGX gels (BioRad). Aliquots of native high molecular weight marker mix for nondenaturing gel electrophoresis (GE Healthcare) were mixed with 5× nondenaturing sample buffer and loaded along with the protein samples. The electrophoretic run was carried out at 55 V and 4 °C until the dye front ran off the gel. Where indicated, following electrophoresis, nondenaturing gels were subjected to substrate overlay assay using the fluorogenic substrate Suc-LLVY-AMC (Enzo) to visualize the peptidase activity of the proteasome on a UV transilluminator (Kusmierczyk et al., 2011) and then stained with GelCode blue (ThermoScientific). Aliquots of samples analyzed by nondenaturing gel electrophoresis were mixed with 5× SDS sample buffer and separated on 12% SDS-PAGE as indicated in the Figure legends.

2.3.4 Cross-linking Analysis

For experiments utilizing engineered cysteine mutant α subunits, no cross-linking and/or oxidizing agents were added to the samples to induce disulfide formation. Experimental conditions during expression, lysis, and ICAR purification were sufficiently oxidizing to allow disulfide bonds to form. Purified proteins (20 µg) were analyzed by nondenaturing PAGE as described above. Bands of interest were excised from the gel, cut into small pieces, and incubated overnight at 4 °C in 1× SDS sample buffer without DTT in order to allow proteins to elute. The supernatants containing the eluted proteins were analyzed by 12% SDS-PAGE under non-reducing conditions and stained with the Pierce Silver Stain Kit (ThermoScientific). Where indicated, DTT was added back to some aliquots prior to electrophoresis.

2.3.5 Size Exclusion Chromatography

Wild-type and mutant α subunits (780 µg) were loaded on to a HiPrep Sephacryl S-300 HR column (GE Healthcare) coupled to an AKTA Prime Plus chromatography system (GE Healthcare). Elution profiles were analyzed using Prime View evaluation software. The column was equilibrated with Buffer D (25 mM Tris-HCl, pH 7, 150 mM NaCl), the flow rate was 0.8 ml min^{-1}, and 3 ml fractions were collected. Calibration of the column was carried out using 360 µg of each of six molecular weight standards (Serva). Aliquots (15 µl) of sizing column fractions were mixed with 5× SDS sample buffer and analyzed by 12% SDS-PAGE followed by staining with GelCode blue. In addition, aliquots (50 µl) of sizing column fractions were mixed with 5× nondenaturing sample buffer and analyzed by nondenaturing 4-15% gradient precast gels followed by staining with Imperial Stain (ThermoScientific) or Pierce Silver Stain Kit (ThermoScientific). In experiments requiring the pooling of sizing column fractions, the indicated fractions were combined and concentrated down to a volume of 0.6 ml using Pierce Protein Concentrators, 9K (ThermoScientific). These pooled and concentrated fractions were then mixed with crude lysates of BL21 cells expressing untagged archaeal β subunits. Proteins were repurified by ICAR and analyzed by native PAGE and substrate-overlay assay as described above.

2.4 Results

2.4.1 Archaeal α-rings

Recombinant archaeal α subunits form single (Groll et al., 2003) or double (Zwickl et al., 1994) rings. To investigate early events of α subunit assembly, C-terminally hexahistidine-tagged (his-tagged) α subunits (α-his) from the archaeaon *Methanococcus maripaludis* S2 were expressed in *Escherichia coli*. The α-his protein was purified by immobilized-cobalt affinity resin (ICAR) and analyzed by native PAGE. Two main bands were observed: a prominent lower band near the 232 kDa size standard and a weaker upper band near the 440 kDa size standard (Fig. 2.1a, lane 1). Size exclusion chromatography confirmed that these two bands represented distinct species; the two elution peaks overlapped in fractions 17-20 (Fig. 2.1b). A smaller third peak was observed in fractions 25-28 most likely representing free α-his subunits (expected M_r 29.5 kDa); referred as "non-ring" (nonR) to account for the possibility that some dimers might be present. The lower and

upper bands on native PAGE were tentatively assigned to be single α-rings (SR; expected M_r 206 kDa) and double α-rings (DR; expected M_r 413 kDa), respectively.

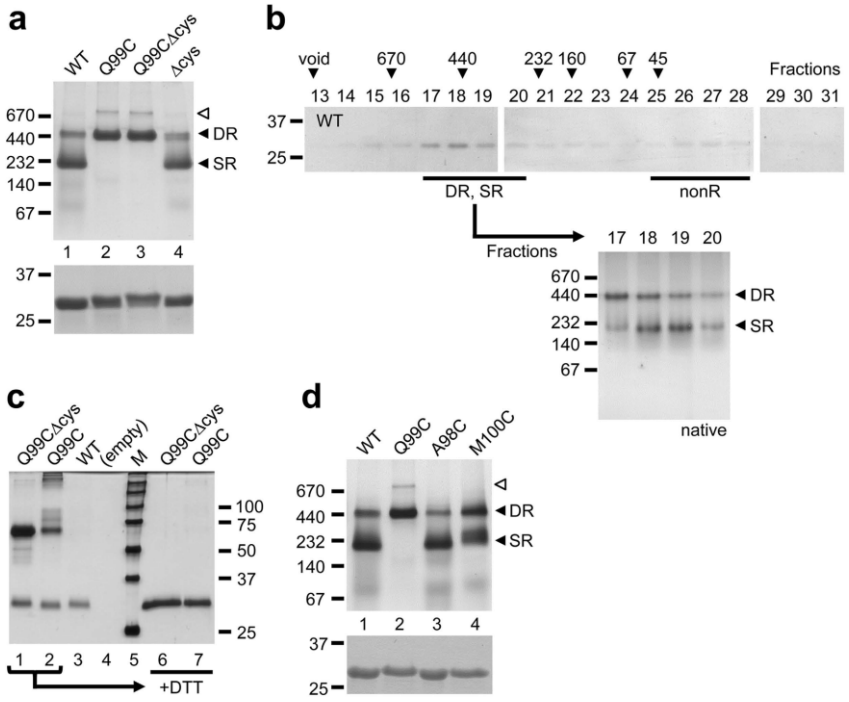

Figure 2.1: Structural similarity between double α-rings and half-proteasomes
(a) Recombinant wild-type (WT) and mutant archaeal α-his subunits (20 µg) were analyzed by nondenaturing 4–15% gradient gel (top panel). Equal protein loading was verified by 12% SDS-PAGE (bottom panel). Proteins visualized by GelCode blue. Black arrowheads denote double α-ring (DR) and single α-ring (SR) species. White arrowhead denotes a gel-induced higher order species. The position of several molecular size standards (in kDa) is indicated in each panel. (b) Wild-type α-his protein (780 µg) subjected to size exclusion chromatography on a Sephacryl S-300 column. Indicated fractions were analyzed by three 12% SDS-PAGE gels stained with GelCode blue (top panels). Black arrowheads indicate the column void volume and the elution peaks of molecular size standards (in kDa). Aliquots from the major peak (fractions 17–20) were analyzed on a nondenaturing 5–10% gradient gel stained with silver (bottom panel, "native"). Black arrowheads denote SR and DR species. The position of several molecular size standards (in kDa) is indicated. (c) The Q99C mutation results in cross-linked α-rings. Bands corresponding to several DR species were excised from the native gel in a. Proteins within the bands were eluted, analyzed by 12% SDS-PAGE under non-reducing (lanes 1–3), or reducing (lanes 6,7), conditions, and visualized by silver staining. M, molecular size standards (size in kDa indicated at right). (d) Q99C is ideally placed to enable cross-linking of α-rings. Recombinant wild-type (WT) and mutant archaeal α-his subunits were purified and analyzed as described in (a).

Some eukaryotic α-subunits also assemble into DR when expressed in bacteria (Gerards, de Jong, Bloemendal, et al., 1998; Gerards et al., 1997). The significance of DR formation is not known, and no high-resolution data describes their structure. Cryoelectron microscopy (cryoEM) analysis reveals that the two α-rings are offset by ~25° relative to each other (Zwickl et al., 1994). An identical offset exists between α-rings and β-rings within each half of the CP, contributing to the saw-tooth interdigitation of the subunits (Lowe et al., 1995) mediated mainly by contact between respective H1 helices (Sup Fig. 1). Since α and β subunits are structurally related (Lowe et al., 1995), one can hypothesize that a DR and an αβ ring pair (i.e. a half-proteasome) exhibit a similar quaternary structure. To test this, a cross-linking strategy was adopted: if DR and half-proteasomes are structurally analogous, it should be possible to cross-link two α subunits with a suitably placed cysteine residue in the H1 helix.

A glutamine at position 99 of the *M. maripaludis* α-subunit may be well positioned for an engineered disulfide cross-link (Sup Fig. 1). Three α subunit mutants were generated by site directed mutagenesis: a mutant containing an engineered H1 helix cysteine in addition to the three endogenous cysteines (Q99C); a mutant containing the H1 helix cysteine but with no endogenous cysteines (Q99CΔcys); and a mutant with no endogenous cysteines (Δcys). These α-his subunit mutants were expressed in *E. coli*, purified them by ICAR, and analyzed them by native PAGE (Fig. 2.1a, lanes 2-4). Unlike wild-type α subunits, the Q99C and the Q99CΔcys mutants exhibited no SR band but a prominent DR band instead. An even slower-migrating band (Fig. 2.1d, white arrowhead) was a gel-induced higher order species (Sup Fig. 2). The transition to DR as the major species was absent in the Δcys mutant.

These results were consistent with Q99C-dependent cross-linking of α subunits locking two α-rings together, causing SR to convert to DR. To confirm this, the DR bands were excised from the wild-type, Q99C, and Q99CΔcys samples, eluted the proteins within, and subjected them to SDS-PAGE under non-reducing conditions (Fig. 2.1c, lanes 1-3). The wild-type sample exhibited only a band at ~30 kDa, corresponding to an α subunit monomer. The Q99C and the Q99CΔcys samples exhibited the monomer band and a new ~60 kDa band, consistent with an α subunit dimer, which disappeared under reducing conditions (Fig. 2.1c, lanes 6,7). The lack of endogenous cysteines in the Q99CΔcys mutant means that only the desired cross-links are

observed, consistent with the higher intensity of the ~60 kDa band in the Q99CΔcys sample versus the Q99C sample. The cross-linking efficiency was not 100% in either mutant (Fig. 2.1c), yet the SR to DR shift on native PAGE was complete in both (Fig. 2.1a). This is explained by only one cross-linked pair of α subunits being needed to lock the two α-rings in a DR. Placing the cross-linkable cysteine even one residue away from position 99 eliminated (A98C), or greatly reduced (M100C), the transition from SR to DR (Fig. 2.1d). The data conclude that the Q99C mutation can cross-link two α-subunits in opposite rings together, effectively locking the DR, because the α-rings interact via precisely aligned H1 helices. This is a strong evidence that our tentative assignment of the lower (SR) and upper (DR) bands on native PAGE was correct and, more importantly, supports the hypothesis that DR are structurally analogous to half-proteasomes.

2.4.2 Charged Residues and α-ring Assembly

In the current view of CP assembly, α-subunits assemble into single rings (SR) first. Double rings (DR) presumably arise from preformed SR and exist in equilibrium with them; our cross-linking results are consistent with this view. Interactions between H0 helices, present in α but not β subunits, help stabilize the formation of α-rings (Zwickl et al., 1994). Site directed mutagenesis was used to investigate what other factors influence ring stability. Based on available structures (Groll et al., 2003; Lowe et al., 1995), highly conserved charged residues at α subunit interfaces within the same ring were targeted (Sup Fig. 3). Those that were close to highly conserved residues of opposite charge on an adjacent subunit might form stabilizing salt bridges; if so, mutating them would destabilize α-rings, interfering with their formation. Two mutant α-his subunits were expressed in *E. coli* (K59E and R88D), purified them by ICAR, and analyzed them by native PAGE.

In both mutants, the SR band was replaced with a much faster migrating species, consistent with these two mutations having a destabilizing effect on α-ring formation (Fig. 2.2a). This faster migrating species most likely represents free α subunits but, as above, referred as nonR to allow for the possibility of some dimers. For the R88D mutant, the nonR species was the only readily-observed species, arguing that this mutation had a profound effect on ring formation. By contrast, the K59E mutant exhibited a weak band migrating near the DR of the wild-type. This band was surmised as a DR whose mobility on native PAGE was slightly different because the mutation

affected the mass-to-charge ratio of the protein. Size exclusion chromatography verified the native PAGE results (Fig. 2.2 b, c and Sup Fig. 4). The K59E mutant protein exhibited two peaks, a major peak in fractions 25-28 (nonR) and a minor peak in fractions 17-19 (DR). The R88D mutant protein exhibited only the major peak in fractions 25-28 (nonR). In conclusion, perturbing conserved charged residues at the intra-ring α subunit interface interferes with the assembly of SR, but not necessarily DR, and that the R88 residue has a much bigger effect on ring stability.

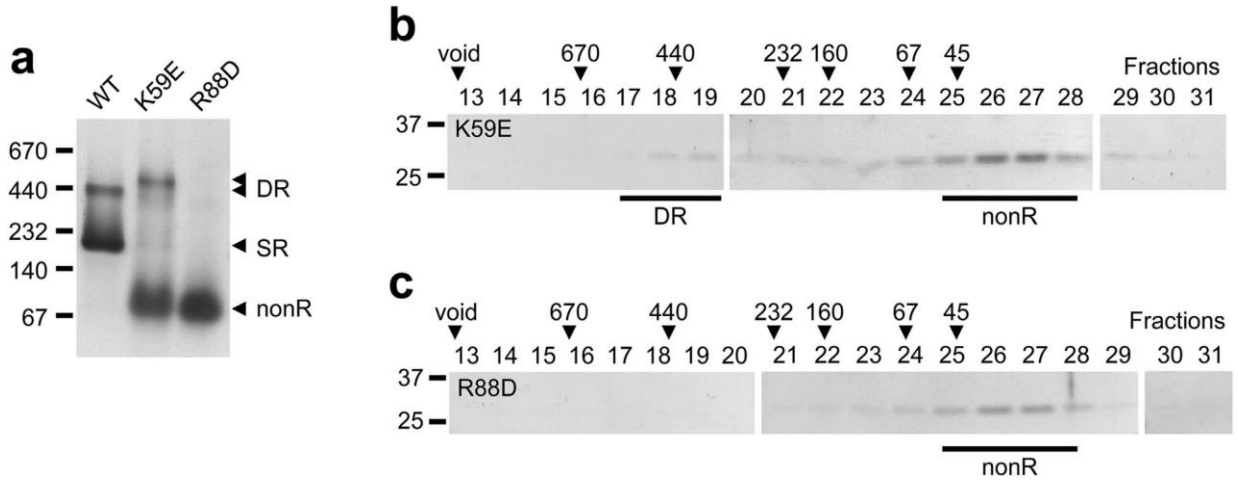

Figure 2.2: Conserved charged residues at α-α subunit interface contribute to α-ring stability Recombinant wild-type (WT) and mutant archaeal α-his subunits were purified by immobilized cobalt affinity resin (ICAR) and 10 µg of protein from each sample eluate was analyzed on a nondenaturing 4–15% gradient gel stained with GelCode blue (a). Double α-ring (DR), single α-ring (SR), and non-ring (nonR) species are denoted with black arrowheads; nonR denotes α subunits that have not assembled into any ring and consist mostly of free α subunits. The position of several molecular size standards (in kDa) is indicated. (b, c) The purified mutant proteins (780 µg) were subjected to size exclusion chromatography on a Sephacryl S-300 column and 3 mL fractions were collected. Aliquots (50 µl) of the indicated fractions were analyzed by three 12% SDS-PAGE gels and stained with GelCode blue. Black lines delineate the position of the DR and nonR peaks. The locations of the column void volume and the elution peaks of the indicated molecular size standards (in kDa) are indicated with black arrowheads.

2.4.3 α-ring Independent 20S Assembly

The SR is considered to be an obligatory assembly intermediate in archaea and eukaryotes while a DR is thought to be an assembly-incompetent complex (Hirano et al., 2005). Since both mutants appeared unable to form any detectable SR (K59E did form some DR), it was expected

they would be incapable of proteasome formation. To determine if this was the case, *M. maripaludis* α-his and β subunits were expressed in bacteria (Kusmierczyk et al., 2008), purified them by ICAR and analyzed them by native PAGE (Fig. 2.3).

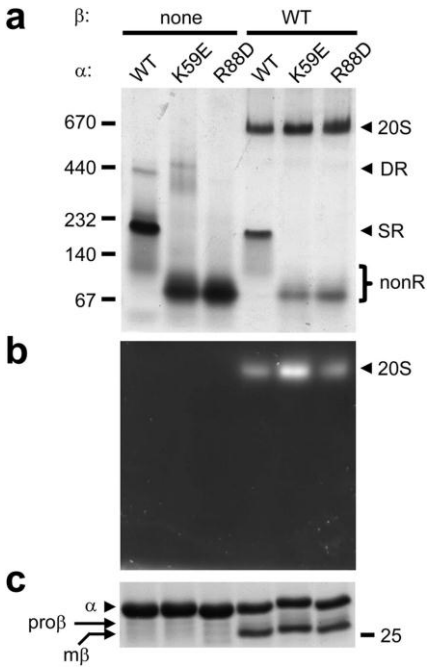

Figure 2.3: Mutant α subunits form functional 20S proteasomes
(a,b) Wild-type (WT) and mutant archaeal α-his subunits were expressed in *E. coli* either individually, or coexpressed with wild-type archaeal β subunits. The recombinant proteins were purified by immobilized cobalt affinity resin (ICAR) and 10 µg of protein from each sample eluate was electrophoresed on a nondenaturing 5–-10% gradient gel. Immediately prior to GelCode blue staining (a), the polyacrylamide gel was overlaid with buffer solution containing the fluorogenic peptide substrate Suc-LLVY-AMC to detect peptidase activity (b). Black arrowheads denote the positions of assembled 20S core particle (20S), double α-ring (DR) and single α-ring (SR). The position of α subunit species that do not assemble into any ring (nonR), and are mostly free α subunits, is shown with a bracket. The migration of several molecular size standards (in kDa) is indicated. (c) Aliquots of the ICAR-purified proteins from a were also analyzed by 12% SDS-PAGE stained with GelCode blue. Migration of the 25-kDa molecular size standard is indicated.

Coexpression of wild-type α and β subunits resulted in a prominent species near the 670 kDa size standard (Fig. 2.3a). This band has been earlier shown to be a functional 20S (Kusmierczyk et al., 2011) and it exhibited peptidase activity in an in-gel assay (Fig. 2.3b). Some SR, and a small amount of nonR, was also observed in the wild-type sample but no DR band was present. Unexpectedly, coexpression of both K59E and R88D mutants with wild-type β subunits

also resulted in catalytically active bands near the 670 kDa size standard; small amounts of nonR species were observed in each mutant as well. SDS-PAGE analysis revealed both α and primarily mature β subunits in all 3 proteolytically active samples (Fig. 2.3c). The results conclude that the mutant α subunits formed functional proteasomes.

Next, an important control experiment was carried out. Protein assembly is cooperative and strongly concentration dependent (Williamson, 2008). Mutant α subunits appeared incapable of forming SR (Fig. 2.2, lanes 1-3), but this conclusion is based on *in vitro* experiments where the purified protein is at much lower concentrations. By contrast, excluded volume effects inside bacteria result in much higher effective protein concentrations (Zimmerman & Trach, 1991). Therefore, one cannot rule out that these higher concentrations during coexpression could promote just enough SR assembly from mutant α subunits to allow β subunits to bind and form CP. To overcome this uncertainty, α-his and untagged β subunits were separately expressed in bacteria and performed lysate mixing prior to purification by ICAR. Since the mutant α subunits do not appear to form SR under the decreased protein concentrations post-lysis (Fig. 2.2), this eliminated the concentration concerns. The purified proteins were analyzed by native PAGE and, in all cases, functional proteasomes were formed (Fig. 2.4a). In conclusion, formation of SR is not required for assembly of functional proteasomes.

Interestingly, lysate mixing produced a number of changes. First, the DR species reappeared in the wild-type sample. Second, while the coexpressed samples contained mostly fully mature β subunits (mβ), the lysate mixing samples all contained higher levels of immature (proβ) β subunits (Fig. 2.4b). This argued for much less efficient assembly during lysate mixing relative to coexpression likely because the lower protein concentrations in lysates result in decreased assembly rates. Third, a prominent new band migrating between the 670 and 440 kDa size standards appeared in all three samples; it was slightly more abundant in the two mutants. This band was already faintly present in the mutant samples during coexpression, but it was more

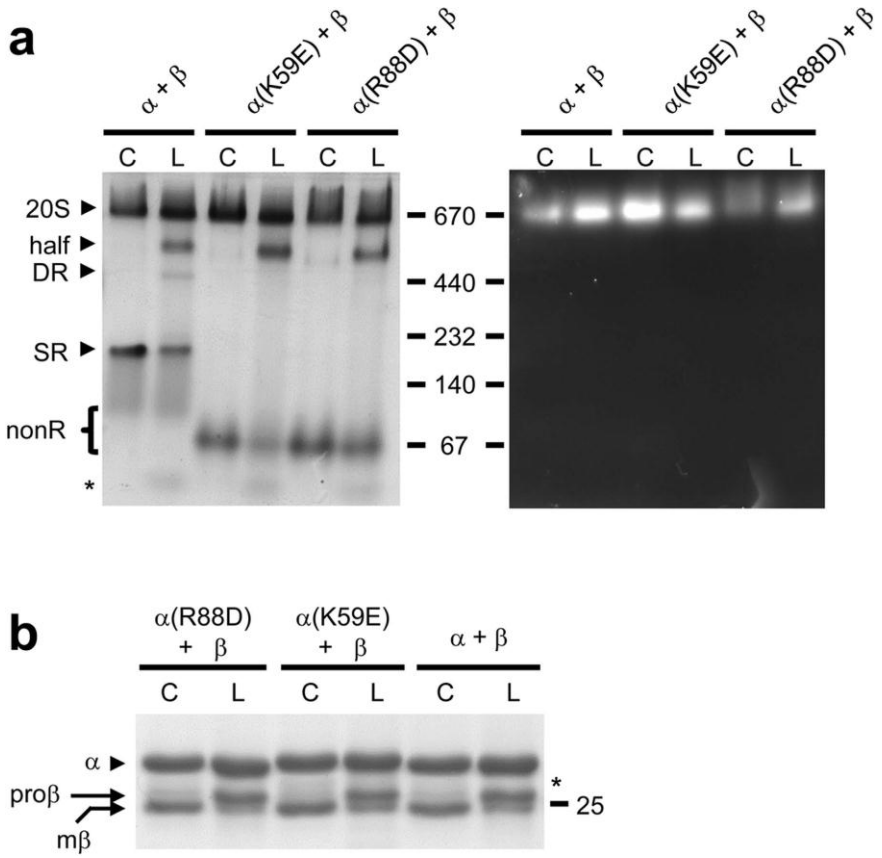

Figure 2.4: Proteasome assembly assayed by coexpression and lysate mixing
(a) For coexpression (C), wild-type (WT) or mutant α-his subunits were coexpressed with wild-type β subunits in *E. coli* and the proteins purified by immobilized cobalt affinity resin (ICAR). For lysate mixing (L), proteasome assembly was initiated by mixing equal volumes of lysates from cells separately expressing the indicated α-his and β subunits, and proteins were purified by ICAR. Purified proteins (10 μg) from each sample eluate were electrophoresed on a nondenaturing 5–10% gradient gel. Immediately prior to GelCode staining (left panel), the gel was overlaid with buffer solution containing the fluorogenic peptide substrate Suc-LLVY-AMC to detect peptidase activity (right panel). Black arrowheads denote the assembled 20S core particle (20S), putative half-proteasome (half), double α-ring (DR) and single α-ring (SR). The position of α subunit species that do not assemble into any ring (nonR), and are mostly free α subunits, is shown with a bracket. The migration of several molecular size standards (in kDa) is indicated. (b) Decreased processing of β subunit propeptides during lysate mixing. Aliquots of the ICAR-purified proteins from a were analyzed by 12% SDS-PAGE stained with GelCode blue. Black arrowhead denotes migration of α-his subunit and arrows indicate position of fully mature (mβ) and immature (proβ) β subunits. The migration of the 25-kDa molecular size standard is shown. Asterisk denotes the migration of a truncated α-his subunit resulting from non-specific proteolysis post lysis; its migration is also apparent on native PAGE in (a).

prominent during lysate mixing. It was tentatively assigned as half-proteasome (Fig. 2.4a, half) since excision of this band, and elution of the proteins within, revealed comparable levels of α and β subunits (not shown) yet it had no peptidase activity in the in-gel assay (Fig. 2.4a, right panel).

2.4.4 Bacterial-like Assembly Features

How functional proteasomes can form independently of SR could be explained if α and β subunits combined directly to form half-proteasomes. This would imply that archaeal CP assembly can proceed along a pathway similar to bacterial CP assembly (Zuhl, Tamura, et al., 1997). That mutant α subunits can form half-proteasomes without forming SR or DR was suggested by lysate mixing experiments (Fig. 2.4a, half). Additional data was needed to confirm the identity of this putative half-proteasome and demonstrate that it is an on-pathway intermediate. In the archaeal CP, a highly conserved β subunit arginine (R166 in *M. maripaludis*) in one β-ring is well positioned to form stabilizing salt bridges with conserved acidic residues on the opposing β-ring (Sup Fig. 3 and (Lowe et al., 1995)). This residue was mutated to a tryptophan (R166W), reasoning that this should disrupt half-proteasome dimerization and hence CP assembly. Consequently, levels of the half-proteasome precursor should accumulate while levels of the 20S CP product should decrease, consistent with a precursor-product relationship. Lysates expressing wild-type or mutant α-his subunits were mixed with lysates expressing full length wild-type or mutant β subunits. The mixtures were purified by ICAR and the purified proteins analyzed by native PAGE and in-gel substrate overlay assay.

As before, mixing wild-type α and wild-type β subunits resulted in functional proteasomes; DR, SR, nonR and half species were also present (Fig. 2.5a, b, lane 1). Mixing wild-type α with mutant β (R166W) subunits resulted in the same banding pattern except the 20S species was greatly reduced and the half species was increased (Fig. 2.5a, lanes 1 versus 6). The change in the relative intensities of the 20S and half species (lane 1 versus lane 6) implies a precursor-product relationship for these two bands. The results conclude that the R166W mutation disrupts assembly at the half-proteasome stage and that our tentative assignment of the half species as a half-proteasome was correct.

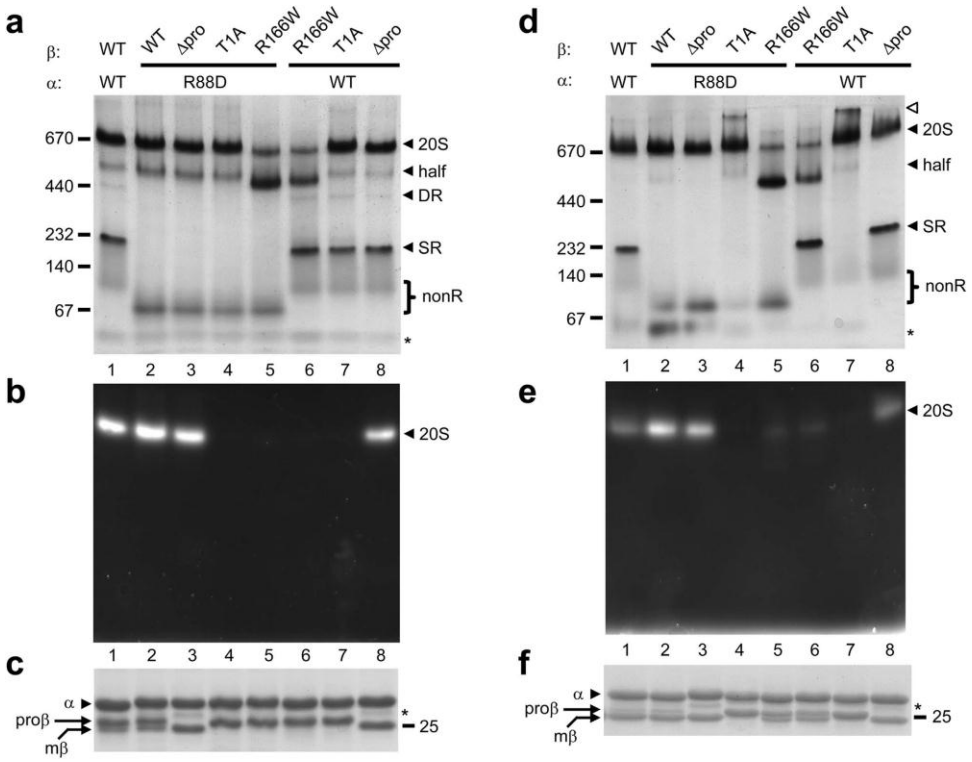

Figure 2.5: Bacterial-like features of archaeal 20S proteasome assembly
(a-c) Lysate mixing. Proteasome assembly was initiated by mixing equal volumes of lysates from cells separately expressing the indicated α-his and β subunits, and proteins were purified by ICAR. (d-f) Coexpression. Wild-type (WT) or mutant α-his subunits were coexpressed with wild-type β subunits in *E. coli* and the proteins purified by immobilized cobalt affinity resin (ICAR). Purified proteins (10 µg) from each sample eluate were electrophoresed on a nondenaturing 5–10% gradient gel. Immediately prior to staining with GelCode blue (a, d) the native gels were overlaid with buffer solution containing the fluorogenic peptide substrate Suc-LLVY-AMC to detect peptidase activity (b,e). Black arrowheads denote the assembled 20S core particle (20S), half-proteasome (half), double α-ring (DR) and single α-ring (SR). The position of α subunit species that do not assemble into any ring (nonR), and are mostly free α subunits, is shown with a bracket. White arrowhead denotes a gel-induced higher order species. The migration of several molecular size standards (in kDa) is indicated. (c, f) Aliquots of the ICAR-purified proteins from a and d were also analyzed by 12% SDS-PAGE stained with GelCode blue. Black arrowhead denotes migration of α-his subunit and arrows indicate position of fully mature (mβ) and immature (proβ) β subunits. The migration of the 25-kDa molecular size standard is shown. Asterisk denotes a truncated α-his subunit resulting from non-specific proteolysis post lysis; its migration is also apparent on native PAGE in a and d.

When α (R88D) was combined with wild-type β subunits, functional proteasomes were again observed (lane 2). NonR and half species were also present, and the half species was slightly more abundant in the α (R88D) sample than in the wild-type α sample (Fig. 2.5a, lane 2 versus 1). Finally, when α (R88D) was combined with β (R166W), the same decrease in the 20S species and

the same increase in the half species was observed (Fig. 2.5a, lane 2 versus lane 5). These results conclude that the same precursor-product relationship was being observed and that the half species in the α (R88D) mutant samples was also an on-pathway half proteasome.

There was no peptidase activity in any sample employing the R166W mutant (Fig. 2.5b) and this correlated with a lack of fully mature β subunits (Fig. 2.5c). This is also consistent with the R166W mutation disrupting assembly at the half-proteasome stage, thereby reducing the likelihood of assembly of mature 20S. The slight migration differences of the half-proteasome bands between the various samples (Fig. 2.5a, lanes 1, 2, 5, 6) was attributed to both mutations (R88D and R166W) being capable of altering the mass-to-charge ratios of this complex relative to wild-type. As might be expected, the degree of accumulation of the half-proteasome was greatest in the double mutant and least in the wild-type sample. The degree of half-proteasome accumulation in the various mutants is summarized as: [α (R88D) β (R166W)] > [α β (R166W)] > [α (R88D) β] > [α β]. When repeated the entire R166W analysis described above (Fig. 2.5a-c) using subunit coexpression, as opposed to lysate mixing, an essentially identical results were obtained (Fig. 2.5d-f). The major difference was that coexpression, but not lysate mixing, resulted in some 20S activity in the R166W samples (compare corresponding lanes 5 and 6). This was likely due to more efficient maturation during coexpression, evidenced by increased levels of the mature β (mβ) subunit (Fig. 2.5c, f).

Prior to this study, one aspect of assembly where archaeal and bacterial CP were similar was in the role of the β subunit propeptide: neither required it (Lin et al., 2006; Zwickl et al., 1994) though it greatly improved assembly efficiency in some bacteria (Zuhl, Seemuller, et al., 1997). To determine the role of the β subunit propeptide when archaeal α subunits were incapable of forming rings, the β subunit mutants lacking the propeptide (Δpro), and ones incapable of cleaving their propeptide due to an active site mutation (T1A) (Kusmierczyk et al., 2011) were employed. Functional proteasomes were obtained in both lysate mixing (Fig. 2.5a-c) and coexpression (Fig. 2.5d-f) experiments employing β (Δpro), indicating that the propeptide is not required for assembly. Fully assembled, albeit inactive, 20S species were also obtained in both lysate mixing and coexpression experiments employing β (T1A), indicating that a permanently present propeptide does not prevent assembly. The data conclude that even when α subunits cannot form

rings, archaeal and bacterial CP assembly remain similar with regards to the role of the β subunit propeptide (see Supplementary Note, appendix A). Two minor differences between lysate mixing and coexpression results, which do not affect this conclusion, are noted in the text that accompanies Supplementary Figure 5. This supplementary Figure also demonstrates that results obtained with the α (K59E) mutant were identical to those described for α (R88D) in Figure 2.5.

2.4.5 Assembly-competent Species

The data so far suggest that archaeal α subunits can form proteasomes along an SR-independent pathway, reminiscent of bacterial 20S assembly. It was needed to show that the free/unassembled α subunits served as the starting point for this alternative pathway. To this end, wild-type and mutant α-his subunits were purified by ICAR and fractionated them by size exclusion chromatography as before (Figs. 2.1b and 2.2b). The fractions 17-19 were combined into pool 1, corresponding to "ringed species". As seen in Figure 2.1b, the sizing column cannot cleanly separate SR from DR, hence the "ringed species" pool from wild-type subunits contains both SR and DR. Fractions 25-28 were compiled into pool 2, corresponding to nonR species (mostly free α subunits). The pooled samples were concentrated, mixed with equal volumes of bacterial lysates containing untagged wild-type β subunits, and repurified by ICAR. The repurified samples were analyzed by native PAGE (Fig. 2.6 and Sup Fig. 6).

In the wild-type sample, pool 1 contained the expected SR and DR bands and gave rise to functional CP (lane 1). Pool 2 also gave rise to functional CP (lane 2), consistent with the idea that nonR species (mostly free αsubunits) can serve as starting material for assembly. There was more CP formed from pool 1 because wild-type α subunits exist primarily as SR and DR (Fig. 2.1) so this pool contained more α subunits to begin with. The small amount of DR in pool 2 likely formed from free α subunits during sample concentration. The α(K59E) subunits can also form some DR (Fig. 2.2 and Sup Fig. 4) and pool 1 from the α (K59E) mutant sample exhibited a DR band. However, there was very little assembled CP generated from this pool (Fig. 2.6 lane 6) suggesting that DR is a poor substrate for CP formation. DR have been proposed to be dead-end complexes (Hirano et al., 2005). The barely-perceptible amount of 20S species formed from this pool could be due to some DR dissociating into assembly competent nonR. A barely-perceptible amount of

20S species was also observed from pool 1 of the α (R88D) mutant (lane 4); a likely reason for this is presented in Supplementary Figure 7.

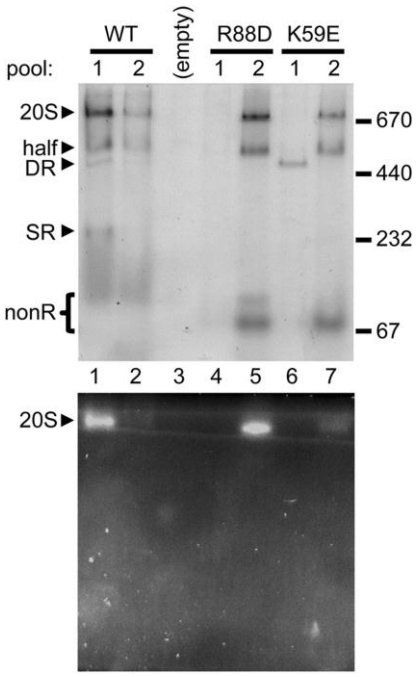

Figure 2.6: Ring independent assembly of archaeal 20S proteasomes
Recombinant wild-type (WT) and mutant archaeal α-his subunits were purified by immobilized cobalt affinity resin (ICAR). The purified proteins (780 μg) were fractionated by size exclusion chromatography on a Sephacryl S-300 column exactly as described in Figures 2.1b and 2.2b, c. For each of the three α-his samples, fractions 17–19 were combined and concentrated (pool 1; ringed species), and fractions 25–28 were combined and concentrated (pool 2; nonR species). The three pool 1 and three pool 2 samples were mixed with equal volumes of lysate from *E. coli* expressing wild-type archaeal β subunits. The proteins were repurified by ICAR and equal volumes of each eluate were electrophoresed on a nondenaturing 5–10% gradient gel. Immediately prior to GelCode staining (top panel), the polyacrylamide gel was overlaid with buffer solution containing the fluorogenic peptide substrate Suc-LLVY-AMC to detect peptidase activity (bottom panel). Black arrowheads denote the positions of assembled 20S core particle (20S), half-proteasome (half), double α-ring (DR) and single α-ring (SR). The position of α subunit species that do not assemble into any ring (nonR), and are mostly free α subunits, is shown with a bracket. The migration of several molecular size standards (in kDa) is indicated.

Unlike wild-type α subunits, both mutant α subunits existed primarily as nonR species (Fig.s. 2.2, 2.3). When these nonR species were used as the starting material for assembly (i.e. pool 2), functional proteasomes formed readily (Fig. 2.6 lanes 5 and 7). This strongly argues that free α subunits can serve as starting material for SR-independent assembly of CP. Interestingly,

all the pools which readily gave rise to functional CP also gave rise to the half-proteasome (lanes 1, 2, 5, 7). This was consistent with results showing that the half-proteasome is an on-pathway intermediate in both SR-dependent and SR-independent pathways (Fig. 2.5).

Bacterial 20S proteasomes most likely assemble via αβ heterodimers (Kwon et al., 2004; Sharon et al., 2007; Zuhl, Seemuller, et al., 1997). To determine if the SR-independent assembly of archaeal 20S proteasomes also involved the formation of αβ heterodimers, a time course experiments was designed. These experiments, based on the mixing of separately purified α-his and β-his subunits, demonstrated that assembly was rapid (Sup Fig. 8). The results did not show any novel bands on nondenaturing gels that would be consistent with αβ heterodimer formation. This could be due to αβ heterodimers being a transient species, which assembles quickly into half-proteasomes, or to αβ heterodimers not being stable enough to survive electrophoresis, or both. As an alternate approach, lysates expressing wild-type or mutant α-his subunits were mixed with lysates expressing untagged full length wild-type or mutant β subunit. The mixtures were purified by ICAR and the purified proteins fractionated by size exclusion chromatography (Sup Fig. 9).

When wild-type α-his subunits were mixed with wild-type untagged β subunits, a prominent peak of α and β subunits in fractions 15-18 was observed. This peak corresponded to assembled proteasomes and half-proteasomes. The excess of α-his subunits over β subunits in these fractions was due to the presence of DR and some SR, since the Sephacryl S-300 column cannot reliably separate these species (Fig. 2.1b and not shown). Some free β subunits eluted in fractions 32 to 34, consistent with what was observed for purified α-his subunits (Sup Fig. 8). A small amount of β subunits was also found coeluting with α-his subunits in fractions 25 to 30. This region contains the nonR α subunit species (Fig. 2.1b) and is consistent with where an αβ heterodimer (predicted M_r, 53.1 kDa) might be expected to elute. When mutant α-his subunits (K59E) were mixed with wild-type untagged β subunits, a peak in fractions 15-18, corresponding to assembled proteasomes, was again observed. Here, the levels of α-his and β subunits were approximately equal because the K59E mutant forms very little DR (and no SR). Interestingly, more β subunits were now coeluting with the mutant α-his in factions 25 to 30 (Sup Fig. 9). The K59E mutation generates more nonR species (Fig. 2.2c). Hence, increased levels of β-subunits in these fractions could be due to more αβ heterodimer formation from the free α subunits in the nonR species,

because the SR-dependent assembly pathway is not available to the K59E mutant. Finally, the analysis was repeated with the α-his (K59E) mutant but employed a β subunit mutant (K29E) that is expected to weaken β-β subunit interactions within a β-ring (Sup Fig. 9). This β mutant should impair the SR-independent assembly pathway, which is the only assembly pathway operating in the α(K59E) mutant. If the SR-independent pathway involves the formation of αβ heterodimers, even more β subunits should accumulate in fractions 25 to 30 due to the accumulation of these precursors. This is exactly what was observed (Sup Fig. 9). Taken together, our results are consistent with the existence of archaeal αβ heterodimers. However, the possibility of heterotrimers ($\alpha_2\beta$ or $\alpha\beta_2$) cannot be excluded given the resolving capacity of the size exclusion column (see also Supplementary Note).

2.5 Discussion

Until now, two separate narratives described the assembly of the 20S proteasome. In one, bacterial α subunits do not form rings but likely form heterodimers with β subunits that assemble into half-proteasomes which then dimerize to form the 20S proteasome (Kwon et al., 2004; Sharon et al., 2007; Zuhl, Seemuller, et al., 1997). In the other, archaeal and eukaryotic α subunits form α-rings first; these template βsubunit incorporation until a half-proteasome is formed, which then dimerizes (Hirano et al., 2008; Zwickl et al., 1994). Here the results suggest that this dichotomy might not be necessary. Archaeal proteasomes can assemble along a pathway independent of α-ring formation, reminiscent of bacterial 20S assembly (Fig. 2.7).

The α-ring first view of proteasome assembly arose from observations demonstrating that archaeal and eukaryotic α subunits form rings on their own (Gerards, de Jong, Bloemendal, et al., 1998; J. A. Maupin-Furlow, Aldrich, & Ferry, 1998; Yao et al., 1999; Zwickl et al., 1994). Stability of α-rings is partly due to extensive inter-subunit interactions mediated by α subunit H0 helices. Lacking the N-terminal extensions that contain H0 helices, β subunits cannot form rings by themselves and depend on α-rings to guide their assembly (Hirano et al., 2008; Lowe et al., 1995; Zwickl et al., 1994). Many of these studies relied on bacterial expression of proteasome subunits. This continues to be a valuable approach because one can generate subunits in isolation, in combination with other subunits, and as both wild-type and mutant versions, without the need to worry about interference from endogenous 20S, which *E. coli* lacks. Using recombinant α subunits

from the archaeon *M. maripaludis*, which form single (SR) and double (DR) α-rings (Fig. 2.1), the data show that highly conserved charged residues at the α-α subunit interface are important for α-ring stability, likely through the formation of stabilizing salt-bridges. The K59E and R88D α subunit mutants do not form any detectable SR (Fig. 2.2) yet both efficiently assemble into functional 20S proteasomes (Fig. 2.3, 2.4) via a pathway that involves direct formation of half-proteasomes (Fig. 2.5, 2.6), probably from αβ heterodimers (Sup Fig. 9).

Assembly of recombinant α subunits into DR had been documented (Gerards, de Jong, Bloemendal, et al., 1998; Zwickl et al., 1994). The implicit assumption was that DR arose from SR, yet this was never explored. Here it was shown that the α (K59E) mutant, which does not form any detectable SR, is able to generate some DR (Fig. 2.2). This suggests that DR can form independently of SR. The significance of this observation is made clear by our cross-linking data showing that DR are structurally analogous to half-proteasomes; both types of double rings interact via H1 α helices (Fig. 2.1, Sup Fig. 1, and (Lowe et al., 1995). This quaternary structure for DR was foreshadowed by cryoEM analysis (Lowe et al., 1995; Zwickl et al., 1994) but our study presents the first biochemical confirmation of this arrangement. To form DR without first forming SR, α subunits need to pair *in trans* (i.e. using the H1-helix-based surfaces used to hold two α-rings together). Since α and β subunits share the same structure, and interact via H1 helices, this *trans* pairing would be analogous to the formation of αβ heterodimers that give rise to half-proteasomes in bacteria (Sharon et al., 2007) and probably now in archaea. The structural similarities between DR and half-proteasomes, which this study confirms, suggest that direct α-subunit-to-DR assembly mimics the direct α-subunit-to-half-proteasome assembly, with both occurring independently of SR. Yet these similarities remained elusive, until now.

As the direct precursor to 20S CP, the half-proteasome is an important intermediate in CP assembly. Having more than one pathway to reach the half-proteasome could be advantageous in case one is compromised.

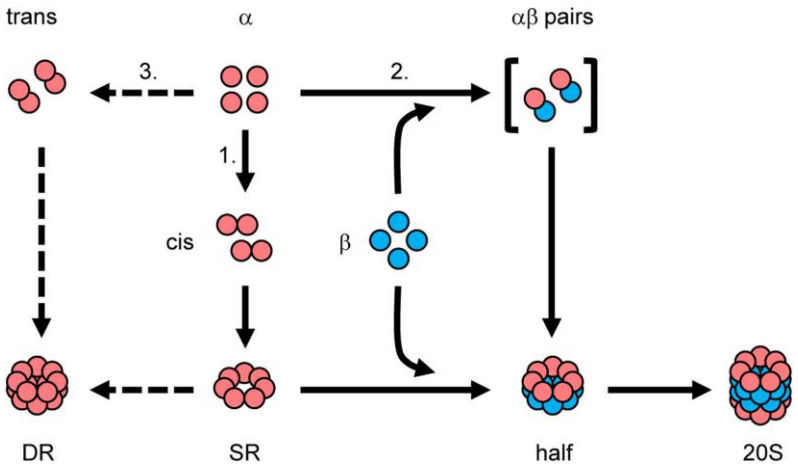

Figure 2.7: Assembly network for the archaeal 20S proteasome
Three assembly pathways are available to α subunits. The α subunits can interact with each other in cis (pathway 1) leading to the formation of an α-ring (SR). The SR acts as a template for β subunit entry until a half-proteasome (half) is formed, which dimerizes to give rise to the core particle (20S). This pathway is followed by archaeal and eukaryotic α subunits. The α subunits can interact with βsubunits to form the half-proteasome directly (pathway 2) and independently of SR. Here, the bracket denotes αβ heterodimers as the most likely precursor to half-proteasomes. Pathway 2 is highly reminiscent of bacterial 20S assembly. It is not known if eukaryotic α subunits can follow an SR-independent route. The α subunits can interact with each other in trans mediated by contacts between H1 helices (pathway 3) in a manner that would be entirely analogous to the formation of αβ heterodimers. This leads to the formation of a double α-ring (DR) that is structurally analogous to a half-proteasome. This pathway can be followed by archaeal and eukaryotic α subunits. DR can also form directly from SR. Regardless of how it arises, the DR is an assembly-incompetent species. Its formation is an example of an off-pathway process (dashed lines) that competes with on-pathway reactions (solid lines) leading to functional 20S.

The idea of alternative pathways for proteasome assembly is supported by studies which showed that paralogous β subunits in mammalian immune cells are incorporated in a different order than their constitutive counterparts (Griffin et al., 1998; Groettrup, Standera, Stohwasser, & Kloetzel, 1997; Kingsbury et al., 2000); that deletion of an assembly factor in yeast results in simultaneous production of both normal CP and alternate versions in which a second copy of α4 replaces the endogenous copy of α3 (Kusmierczyk et al., 2008); and that the 19S regulatory particle can assemble via pathways dependent on (Hendil et al., 2009; Lee, Moon, Yoon, & Yoon, 2012; Park et al., 2009; Yu et al., 2015), and independent of (Thompson, Hakala, & DeMartino, 2009), a pre-existing 20S proteasome. Consequently, the concept of a single linear assembly "pathway" for the proteasome should perhaps be updated to an assembly "network" consisting of several

pathways leading to the formation of this complex. There are ~33 different proteins that make up the eukaryotic proteasome. In addition to productive pathways leading to its formation, there will also be unproductive pathways giving rise to assembly-incompetent (i.e. dead-end) complexes. The DR may be one such complex. DR and various DR-like species have been postulated to be dead-end complexes in eukaryotes *in vivo* (Hirano et al., 2005; Takagi et al., 2014; Yashiroda et al., 2008). Archaeal proteasomes are compositionally simpler, but the data show here that archaeal DR are poor substrates for CP formation (Fig. 2.6) and thus likely candidates for dead-end complexes.

If multiple assembly pathways are possible, determining the extent to which each pathway is populated *in vivo*, and how unproductive pathways leading to dead-end complexes are avoided, remains to be determined. Kinetics and thermodynamics governing subunit association are important; pairings that occur quickly and/or produce stable intermediate complexes will be favored (Williamson, 2008). According to the updated assembly model (Fig. 2.7), α subunits can assemble with each other *in cis*, leading to the formation of SR, or with β subunits, leading to the half-proteasome, or with each other *in trans*, leading to the unproductive DR. The DR formation was observed under lysate mixing but not coexpression. This argues that the pathway leading α subunits to DR can be suppressed if conditions ensure that the SR and/or half-proteasome pathways occur faster. This is not the case during lysate mixing which artificially creates a low subunit concentration condition that slows assembly and thus allows the DR pathway to become populated. Besides kinetics and thermodynamics, dedicated assembly factors (Hirano et al., 2005; Takagi et al., 2014; Yashiroda et al., 2008) and post translational modifications (Humbard, Zhou, & Maupin-Furlow, 2009) will be shown to play increasingly important roles in shepherding assembling subunits onto productive pathways, and away from non-productive ones.

Our data do not question the importance of the SR to archaeal 20S assembly, as demonstrated by others (J. A. Maupin-Furlow et al., 1998; Zwickl et al., 1994). Nor do our data establish the extent to which SR-dependent and SR-independent assembly occurs *in vivo*. However, our findings that archaeal 20S proteasomes can assemble along an SR-independent pathway, reminiscent of bacterial 20S assembly, suggest a path toward a clearer understanding of proteasome evolution. Unlike eukaryotes and archaea, the proteasome has a limited distribution in

bacteria; it has been argued that a horizontal gene transfer (HGT) from archaea endowed these limited lineages with proteasomes (Volker & Lupas, 2002). Under the current dichotomy of assembly, one is forced to argue that bacterial 20S proteasomes must have lost their ability to assemble like archaeal proteasomes (SR-dependent pathway) and gained an entirely new assembly mechanism (SR-independent pathway) soon after HGT from the archaeal donor. Our results suggest that this ancestral archaeal donor assembled its 20S along both SR-dependent and SR-independent pathways, as its descendant *M. maripaludis* can today (at least *in vitro*). Therefore, the bacteria that received the proteasome from this donor would only need to lose the SR-dependent pathway while retaining the SR-independent pathway; no gain of function change is required. This is a more parsimonious explanation for the evolution of bacterial proteasome assembly. This explanation is also supported by structural data showing less surface area buried between α subunits, a likely reason for unstable bacterial α-ring (Hu et al., 2006; Kwon et al., 2004). The conserved CP architecture across all domains of life contradicts the expected common assembly mechanisms, which this data now suggest are conserved across evolutionary time. It will now be interesting to determine if eukaryotic 20S proteasomes also retain an SR-independent assembly pathway.

CHAPTER 3. A NOVEL ASSEMBLY INTERMEDIATE "SUB-13S"

3.1 Abstract

The eukaryotic 20S proteasome is composed of seven distinct α-type and β-type subunits that assemble into four heteroheptameric rings in an $\alpha_{1-7}\beta_{1-7}\beta_{1-7}\alpha_{1-7}$ arrangement. These subunits assemble in an ordered and efficient manner requiring the assistance of assembly chaperones. Assembly begins with α subunit interactions that form an α-ring first which acts as a base for the sequential addition of β subunits. The rapid rate of a α subunit interaction poses a challenge to study a-ring formation step. Neither the order of α subunit interaction is known, nor these rings have been formally observed in yeast. The earliest known assembly intermediate is a 13S complex that contains all the α subunits plus the β2, β3 and β4 subunits. Here, identity of a complex, named as "sub-13S" that contains α1, α2, α3, α4, β2, β3, and β4 subunits, as a novel assembly intermediate is investigated in *Saccharomycetes cerevisiae* is investigated. Its existence becomes more apparent when proteasome assembly is slowed down. More importantly, the protein mixing experiment demonstrates that sub-13S is an assembly competent species that can convert into 13S intermediate when the remaining subunits, α5, α6, and α7, and assembly chaperone Pba3-Pba4 are provided. Lack of a complete α-ring in the sub-13S intermediate argues its origin from an α-ring independent proteasome assembly pathway that may coexist with the canonical α-ring dependent pathway.

3.2 Introduction

The proteasome, a part of ubiquitin proteasome system (UPS), is a multiprotein complex that plays a major role in degradation of proteins. The 26S proteasome is composed of two major complexes, the proteolytic core particle (CP) or 20S proteasome, and the regulatory particle (RP). The proteins targeted for degradation are usually tagged by ubiquitin. The RP is responsible for recognition, deubiqutination, unfolding of ubiquitinated substrates and directing them into the proteolytic CP for degradation (Tomko & Hochstrasser, 2013). The CP is arranged as a barrel of four coaxially stacked heptameric rings with outer rings composed of α-type subunits and the inner rings composed of β-type subunits. The β subunits are expressed with N-terminal propeptides that mask the catalytic N-terminal threonine residue. These propeptide are autocatalytically removed during assembly making the β subunits catalytically active only after CP is fully assembled (P.

Chen & Hochstrasser, 1996; Groll et al., 1997; S. Witt et al., 2006). The CP, found in all three domains of life (archaea, eukaryota, actinomycetes and nitrospirales lineages of bacteria), is compositionally simpler in prokaryotes having only one or two type of α and β subunits, whereas in eukaryotes, there are seven different types of α (α1- α7) and seven different types of β (β1- β7) subunits with β1, β2 and β5 bearing the catalytic function (Groll et al., 1997; Lin et al., 2006; Lowe et al., 1995; Tamura et al., 1995).

Eukaryotic proteasome assembly is a rapid, highly efficient, and ordered process that requires sequential addition of subunits and assistance of assembly chaperones (Howell et al., 2017; Kunjappu & Hochstrasser, 2013). Assembly begins with α subunits assembling into an α-ring first aided by assembly chaperones Pba1-Pba2 and Pba3-Pba4 (Hirano et al., 2005; Hirano et al., 2008; Kusmierczyk & Hochstrasser, 2008; Le Tallec et al., 2007; X. Li et al., 2007; Yashiroda et al., 2008). This α-ring serves as a template for subsequent addition of β subunits (Frentzel et al., 1994; Nandi et al., 1997). The β2, β3, and β4 are first β subunits added on the α-ring with the assistance of assembly chaperone Ump1. This step is accompanied by the dissociation of Pba3-Pba4, forming an intermediate called 13S (Hirano et al., 2008; Kock et al., 2015; Ramos et al., 1998). This is the smallest assembly intermediate observed in yeast. Subsequent entry of β5, β6 and β1 forms the 15S intermediate. β7 is the last subunit to be added onto the α-ring to form a half proteasome intermediate that quickly dimerize to form an immature CP intermediate referred to as the preholoproteasome (PHP) (X. Li et al., 2007; Marques et al., 2007).The proteolytic removal of β subunit's propeptides occurs at this stage and transforms the PHP to mature CP (P. Chen & Hochstrasser, 1995; Heinemeyer, Fischer, Krimmer, Stachon, & Wolf, 1997). The assembly chaperone Ump1 is encapsulated during assembly, becoming the first proteasome substrate, and the assembly chaperone Pba1-Pba2 dissociates after the maturation process.

Due to the rapid nature of proteasome biogenesis, not much information is known about the early events that involves α-ring assembly. Based on the detection of α-rings in mammals (Hirano et al., 2005) and the inherent tendency of archaeal and certain eukaryotic α subunit, but not β subunits, to spontaneously assemble into rings when expressed *in vitro* (Gerards et al., 1997; Yao et al., 1999; Zwickl et al., 1994), the assembly pathway in eukaryotes and archaea is considered α-ring dependent. Bacterial proteasome assembly was considered an exception in

which the α subunits interact with the β subunits first, possibly forming α/β heterodimers that multimerize to form half proteasomes (D. Li et al., 2010; Sharon et al., 2007; Zuhl, Seemuller, et al., 1997). Recent demonstration of an α-ring independent assembly pathway in archaea allowed to offer a plausible hypothesis about the origin of the seemingly different assembly pathway in bacteria (Panfair et al., 2015). Recent reports from our lab mentioned a novel species, referred to as "sub-13S", that lacks a full α-ring and contains subset of β subunits along with Ssa1/Ssa2 proteins (L. J. Hammack et al., 2017; Lindsay J. Hammack & Andrew R. Kusmierczyk, 2017). Here, further characterization, including the possibility of this complex to be an assembly intermediate, is investigated. Perturbation in the formation of the 13S intermediate increased the accumulation of the sub-13S complex suggesting their product precursor relationship. Moreover, when providing the missing subunits, maturation of sub-13S complex into a 13S like complex demonstrated the assembly competency of the sub-13S species. These results provide evidence for sub-13S as a novel assembly intermediate, smaller than the 13S intermediate.

3.3 Materials and Methods

3.3.1 Yeast Strains and Media

All yeast manipulations were carried out according to standard protocols (C. Guthrie, 1991). Strains used in this study are listed in Supplementary Table 2 in Appendix B. Dilution series experiments were carried out as described (Kusmierczyk et al., 2008). For biochemical analyses, one-liter yeast cultures were grown in YPD at 30 °C to mid-log phase. Yeast cells were harvested by centrifugation at 3000 x *g* for 10 minutes and the pellets washed with 40 ml of H_2O prior to storage at –80 °C.

3.3.2 Yeast lysis and Flag purification

The lysis of yeast pellets and subsequent Flag purification was carried out as described (L. J. Hammack et al., 2017). The elution of proteins was slightly modified for the samples used for depletion, lysate mixing and purified protein mixing experiments. Briefly, the purified proteins were eluted in 450 µl of 5 µg/µl flag peptide (Sigma) in Tris-buffered saline (TBS), for 30 minutes at 4 °C. The eluted proteins were collected by transferring the resin mixture to a Pierce Micro-spin column (ThermoScientific) and centrifuging at 10,000 × *g* for 3 minutes. Samples were concentrated to a final volume of 200 µl by centrifugation using Vivaspin 500 columns

(Vivascience) with a molecular weight cut-off of 10 kDa. Depletion experiment was carried out as described (L. J. Hammack & A. R. Kusmierczyk, 2017) with the following modifications. The Flag eluate (450ul) was applied to 100 µl of cobalt resin (TALON resin; Clontech) for 1h at 4 °C with gentle rocking. The flow through from the first round of ICAR depletion was subjected to a second round of ICAR depletion using a fresh 100 µl aliquot of resin. The flow through from the second round of ICAR depletion was concentrated to a final volume of 100 µl using Vivaspin 500 columns (Vivascience) with a molecular weight cut-off of 10 kDa. Native sample buffer (0.5 M Tris-HCl pH 8.8, 50% (v/v) glycerol, traces of bromophenol blue) and 5X denaturing buffer (0.3 M Tris-HCl pH 6.8, 600 mM dithiothreitol (DTT), 10% (w/v) SDS, 50% (v/v) glycerol and traces of bromophenol blue) were added to purified protein aliquots to final 1X concentration for Native and SDS Page analysis respectively.

3.3.3 Bacterial Protein Expression and Purification

Bacterial expression plasmids, including those enabling polycistronic gene expression from a single mRNA, were generated as described (Kusmierczyk et al., 2008) and listed in Supplementary Table 3 in Appendix B. Proteins were expressed as described in (Kusmierczyk et al., 2008) with some modifications. After transformation of plasmid into BL21 cells, single colonies were inoculated in 6 ml of LB medium supplemented with ampicillin. After 6 hours of growth at 37 °C with shaking, the primary culture was diluted to an OD_{600} of 0.2 in 200ml of LB with ampicillin and reincubated at 37 °C for 40 minutes. The cultures were then transferred to 30 °C and incubated for another 30 mins before adding 1 mM IPTG to induce protein expression. After 14 hours of induction, the culture was split into 50 ml aliquots and pelleted by centrifugation for 10 mins at 13000 rpm. The pellets were stored in -80°C. Frozen pellet lysis and immobilized cobalt affinity resin (ICAR) purification were carried out as described in (Panfair & Kusmierczyk, 2016) with two changes. The pellets were lysed in 1ml of lysis buffer and for the total, soluble and pellet fraction analysis by denaturing gels, the lysates were diluted to 50% in lysis buffer and 5 µl of samples were loaded.

3.3.4 Lysate Mixing and Purified Protein Mixing

For lysate mixing experiments, soluble bacterial lysates of desired samples were mixed with soluble yeast lysate and incubated at 30 °C with slow shaking for 30 min. Similarly, wild-type yeast lysates were mixed with *doa5-1* mutant yeast lysate and incubated at 30 °C for 30 mins. Following incubation, mixed lysates were subjected to Flag purification as described previously. For purified protein mixing, ICAR purified proteins from bacterial lysates of desired sample recombinantly expressing yeast proteins of desired samples were mixed with Flag purified proteins from the yeast *doa5-1* mutant at 1:4 and 1:5 ratios.

3.3.5 Electrophoresis

Samples were subjected to SDS-PAGE and native PAGE as previously described (Kusmierczyk et al., 2011) except 4–15% non-denaturing polyacrylamide gradient gels, 5% , as well 12% SDS-PAGE gels were used as indicated. For all gels, the migration of molecular size standards is indicated to the left of each gel image in the Figures. The 4–15 % gradient gels were precast Mini-PROTEAN TGX (Bio-Rad) while all others were poured in lab. Non-denaturing gradient gels were run at 60 V for 11 hours at 4 °C, 5% non-denaturing gels were run at 55V for 3.5 hours. The native gels were stained with Imperial Protein Stain (ThermoScientific). Loading control samples were run on reducing 12% SDS-PAGE. All SDS-PAGE gels were stained with GelCode blue (ThermoScientific).

3.3.6 Mass Spectrometry Analysis

Gel slices were submitted to the Indiana University School of Medicine Proteomics Core Facility (IUSM-PCF) on a fee-for-service basis. Protein contents of the gel slices were identified by LC-MS/MS as described in (L. J. Hammack & A. R. Kusmierczyk, 2017). Additional tables are presented in the supplementary information.

3.4 Results

3.4.1 Recapitulating Appearance of the Sub-13S Complex

Two separate reports from our lab mentioned a novel complex that appears when certain *S. cerevisiae* proteasome subunits were tagged (L. J. Hammack et al., 2017; Lindsay J. Hammack & Andrew R. Kusmierczyk, 2017). Both complexes are likely the same in that they comprise

proteasome subunits α1, α2, α3, α4, β2, β3, β4. Additional proteins belonging to Hsp70 proteins family such as Ssa1/a2 and assembly chaperone Ump1 are also present. It is not clear whether assembly chaperone Pba1-Pba2 is component of the sub-13S complex. The complex is termed as sub-13S because it lacks just three α subunits (α5, α6, and α7) compared to the 13S intermediate. Here, further characterization of this complex is carried out. The characterization began with recapitulating its appearance by tagging different proteasome subunits. For this, proteasome subunits α2, α4, α5, and β4 were either Flag tagged (F) or hexahistidine and Flag tagged (HF). Before purifying proteins from these strains, it needed to be determined if tagging the proteasome subunits does not cause any growth defect. Temperature sensitive growth assays of these strains were carried out by doing a dilution series. Serially diluted yeast cells from these strains were spotted on YPD plates and incubated at 30 °C and 37 °C for 3 days. There were no clear growth defects in the tagged strains as compared to the wild type, suggesting the tags were well tolerated and did not significantly perturb proteasome function (Fig. 3.1a, top). However, yeast has a robust feedback mechanism, mediated by the Rpn4 transcription factor, which upregulates proteasome levels whenever proteasome function is compromised. Consequently, mild defects in proteasome function can escape detection and become apparent only when combined with a deletion of the *RPN4* gene (Le Tallec et al., 2007). When the tagged subunit alleles were generated in a *rpn4Δ* background, again, no obvious growth defects or temperature sensitivity was observed (Fig. 3.1a bottom). This lack of a phenotype increased our confidence that the tagged proteasome subunits do not cause any notable functional deficiency.

Continuing with reproducing the appearance of sub-13S complex, mid-scale cultures (1L) from the indicated yeast strains were then grown, and lysates prepared were subjected to Flag purification followed by native PAGE analysis. As expected, the most abundant species in all the purified proteins samples was the CP (Fig. 3.1b). Bands migrating slower than the CP are usually CP-bound Blm10 species (Lehmann, Jechow, & Enenkel, 2008). In addition to the most abundant 20S CP band, one faster migrating band, most likely a common assembly intermediate, appeared in all the samples (Fig. 3.1b, band 1, 3, 4 and 5). Mass spectrometry (MS) analysis revealed these bands are likely a mixture of 13S/15S intermediates (Sup Fig. 10). Band 1 has been identified as 13S in the previous study (Lindsay J. Hammack & Andrew R. Kusmierczyk, 2017). An additional faster migrating band appeared when α4 subunit is Flag tagged (Fig. 3.1b, band 2). This species is

identified as sub-13S in the previous study (L. J. Hammack et al., 2017)**.** MS analysis of this band showed relative abundances of the expected subunits (Sup Fig. 10) suggesting the complex is sub-13S.

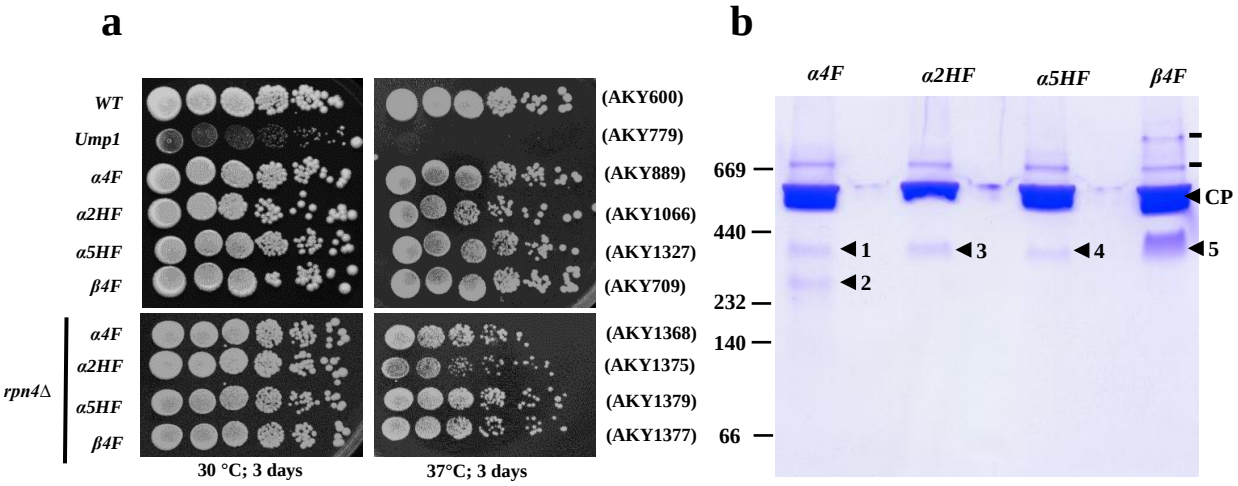

Figure 3.1: Analysis of yeast strains with tags on different subunits
(a) Dilution series of indicated yeast strains grown at 30 °C and 37 °C. (b) Flag purified proteins from the indicated yeast strains were analyzed by native 4-15% gradient PAGE. (-) Denotes CP-bound Blm10 complex. Species indicated are based on relative molecular weight and previous mass spectrometry (MS) analysis. Unique species and other intermediate bands were excised for MS analysis to confirm identity. Figure 3.1b is derived and modified from (L. Hammack, 2017).

The sub-13S complex uniquely appeared only in purifications of α4F strain. Since this complex does not contain α5 subunit, its absence in purification of α5HF strain was expected. But one questions why, despite the presence of β4 and α2 subunit in sub-13S complex, it did not appear in purifications from α2HF and β4F strains (Fig. 3.1b, lane 2 and 4). One possibility is that even though the epitope tagging of the α4 subunit does not lead to discernible growth defects, even in the context of an *RPN4* deletion, assembly could be slightly perturbed. And this effect may slow down some assembly step(s) just enough to enable the appearance of novel complexes, such as sub-13S, without causing a significant growth defect.

3.4.2 Induction of the Sub-13S Complex

The composition and selective appearance of sub-13S, likely due to assembly slow down, suggest two possibilities related to its identity. Either sub-13S is an assembly intermediate existing

before the 13S intermediate, or it is an aberrant complex. To investigate the possibility of sub-13S as an assembly intermediate, a strategy was employed to further impair assembly of the 13S intermediate in the α4F strain. The difference between 13S and sub-13S concerning proteasome subunit composition is the absence of α5, α6 and α7 subunits in the latter. If incorporation of either of the missing subunits (α5, α6, and α7) is impaired, then the rate of formation of the 13S intermediate would decrease. This slow down should lead to an increase in the accumulation (and appearance) of the precursor intermediate, i.e., sub-13S.

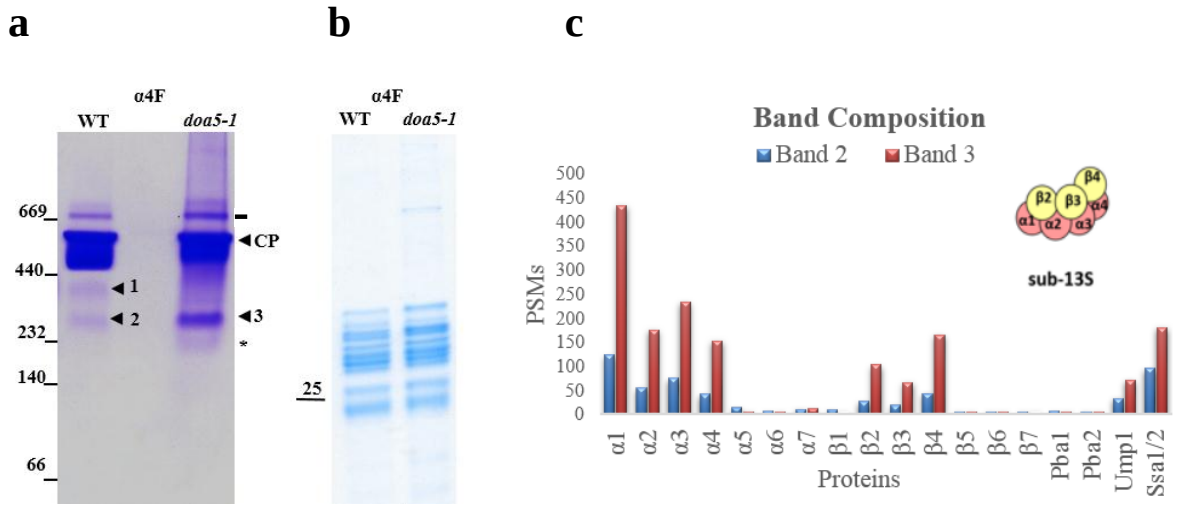

Figure 3.2: Induction of the sub-13S complex with *doa5-1*
(a) Equal amounts (30 µg) of Flag purified protein (α4F) were analyzed by native PAGE followed by imperial blue staining. Species of interest are indicated by arrowheads. Asterisk denotes an additional very faint band appearing in lane 2. (-) Denotes CP-bound Blm10 complex. (b) shows equal protein loading (5µg) from (a) on 12% SDS PAGE, stained with GelCode blue. (c) Comparison of peptide spectral matches (PSMs) generated by MS analysis of band 2 and band 3. These bands are similar to band 2 and band 3 from (a) except they are excised from a different gel shown in Sup. Fig 11a. Red indicates PSMs of band 3 and blue indicates PSMs of band 2.

To this end, we crossed a *doa5-1* mutant strain with the α4F strain to generate a *doa5-1* α4F strain. The *doa5-1* is an α5 subunit mutant that causes an amino acid change from Gly to Asp at position 49 (P. Chen & Hochstrasser, 1995). This Gly residue is normally buried within the hydrophobic core, and its change to a charged Asp residue may affect the folding of α5 perhaps impairing its ability to reach the native state. This, in turn, should slow the rate at which α5 is incorporated during assembly.

Flag purified proteasomes from α4F and α4F *doa5-1* strains were then analyzed on native PAGE (Fig. 3.2a). In both samples, CP was the dominant species, and in the α4F sample, two species migrating faster than CP were again observed (Fig 3.2a). Bands were excised from a repeat of this experiment analyzed on a separate gel shown in Sup. Fig 11. MS analysis showed the higher of the two bands is again a 13S intermediate (Sup Fig. 12, band 1) while the lower band is sub-13S complex (Sup Fig. 12 band 2). Interestingly, in the *doa5-1* α4F sample, a band migrating at the position of the 13S intermediate was no longer present. Instead, this position on the gel was more smeared, suggesting assembly of 13S was likely perturbed. Consistent with this, a prominent band migrating at the position of sub-13S was observed (band 3). Indeed, band 3 showed PSMs for α1, α2, α3, α4, β2, β3, β4, Ump1, Ssa1/2 consistent with the composition of the sub-13S complex (Sup Fig. 12). Additional Hsp70 group proteins Sse1/2 were also detected. Band 2 and band 3 have similar composition and migration on native PAGE suggesting both of these complexes are the same, i.e., sub-13S (Fig. 3.2a, c). Because band 3 is more prominent here, the MS data has a higher signal to noise ratio, and clearly shows a strikingly higher PSMs for proteins present within the complex (Fig. 3.2c). The PSMs of additional proteins that showed up in band 2 did not increase in band 3 further supporting those proteins are not the component of the sub-13S complex (Fig. 3.2c). The PSMs of assembly chaperone Pba1-Pba2 also did not increase in band 3 as compared to band 2 suggesting this chaperone is not present in the complex.

If interpretation of the nature of sub-13S species in the *doa5-1* α4F strain is correct, then the same genetic manipulation should slowdown 13S assembly and induce accumulation of the sub-13S species in the strains that did not previously showed sub-13S, i.e. β4F and α2HF. Among these strains, the α2HF strain was chosen, with no specific preference, to incorporate the genetic manipulation. To this end, the *doa5-1* mutation was introduced in α2HF strain via mating and dissection. Flag purified proteins from both α2HF and α2HF *doa5-1* strains were analyzed by native PAGE. In the latter strain, as expected, a newly formed faster-migrating band appeared (Sup Fig. 11b, lane 2, band 6). MS analysis confirmed the composition of this band is similar to sub-13S complex (Sup Fig. 12). The increase in the appearance of the sub-13S complex in both the strains confirms its direct association with the 13S intermediate. The correlation between decreasing levels of 13S being accompanied by the increasing levels of sub-13S hints at a

precursor-product relationship between these two species and suggests that sub-13S species is more likely an assembly intermediate.

An additional very faint band (band 7) appeared migrating faster than the sub-13S band (Sup Fig. 11b). MS analysis showed the composition of this species is similar to sub-13S except there are relatively higher PSMs for Hsp70 group proteins (Sup Fig. 12 band 7). This species was provisionally called as pre-sub-13S. The migration profile of a band labeled as an asterisk in Fig. 3.2a, lane 2, is similar to pre-sub-13S, suggesting both of these complexes could be similar.

3.4.3 Sub-13S is Not a Gel Artifact

Based on the compositional similarity between 13S and sub-13S with the later lacking three proteasome subunits, one could wonder if dissociation of 13S, perhaps due to electrophoretic conditions during native PAGE, results in the appearance of the sub-13S complex. To eliminate the possibility of sub-13S being a gel artifact, a depletion strategy was employed (diagrammed in Sup Fig. 13) to isolate sub-13S species from the 13S intermediate before native PAGE. For this, an α4F α5HF strain was generated. When proteins are flag purified, by virtue of the α4F subunit, the eluates should contain (and does contain) both the 13S intermediate and the sub-13S species (Sup Fig. 12, lane 3). However, if the Flag-purified eluate is subjected to depletion by passing it over the cobalt resin beads (ICAR) prior to native PAGE, all the α5-containing species, including the 13S intermediate, will bind to the resin (due to the hexahistidine tag on α5). As a result, the depleted sample, now lacking the 13S intermediate, should also lack sub-13S complex, if the latter arose due to dissociation of 13S during electrophoresis.

Nevertheless, even after depletion, a band migrating at the position of sub-13S species was observed (Sup Fig. 14a, lane 6) suggesting the complex did not result from dissociation of 13S after native PAGE. The depletion procedure dilutes and reduces the protein amount leading to the faint appearance of the likely sub-13S band. A larger scale culture and concentrating the depleted sample enhanced the appearance of this band (Fig. 3.3 lane 3, band 1) whose migration is similar to sub-13S. Usually, the high abundance of the 20S CP as compared to assembly intermediates results in some amount of CP retention in the depleted sample (L. J. Hammack et al., 2017). Due

to the additional concentration step involved and higher protein loads, the CP retained even higher in the depleted sample (Fig. 3.3).

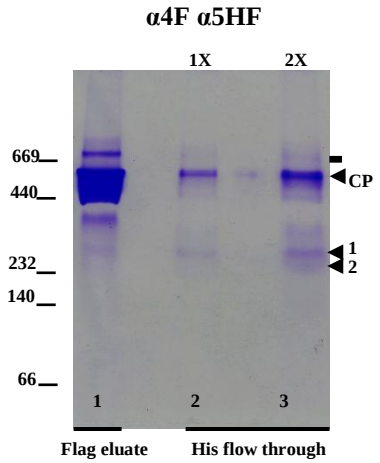

Figure 3.3: Depletion analysis shows presence of sub-13S species in WT yeast strain
Flag purified proteins (flag eluates) of indicated yeast strain was subjected to two rounds of depletion by ICAR to remove his-tagged proteins. Aliquots of the flag eluate and His flow through from the second ICAR round were analyzed on the native PAGE gel. Lane 3 is loaded 1.5x times lane 2. Arrowheads denote CP and other bands of interest. (-) denotes CP-bound Blm10 complex.

As in the *doa5-1* mutant strains, another band (more like a smear) was visible below the sub-13S species in the depleted and only in higher protein loading lane (Fig. 3.3 lane 3 pre-sub-13S) (Fig. 3.2). MS analysis of the band revealed its composition is similar to the previously mentioned pre-sub-13S band (Sup Fig. 15 and Sup Fig 12, band 7).

3.4.4 Sub-13S is an Assembly Competent Species

The data, so far, have demonstrated that sub-13S species appearance can be induced by slowing down assembly. We now sought data to verify the precursor-product relationship between sub-13S and 13S demonstrating that sub-13S is an on pathway intermediate. If sub-13S is a precursor to 13S, then by providing the missing subunits (i.e. α5, α6 and α7), sub-13S should convert into 13S, and this can be viewed as a band shift on native PAGE. To this end, untagged wild-type yeast lysate was mixed with the *doa5-1* α4F lysate for 30 mins at 30 °C followed by Flag purification. The wild type copy of α5 from the wild-type yeast strain should complement the *doa5-1* defect and convert the putative precursor (sub-13S) to the product (13S). Unfortunately, the expected gel shift (Sup Fig. 16) was not observed probably because in the wild-type yeast

lysate, most of the proteasome subunits are in the fully assembled state and very little exist as free subunits.

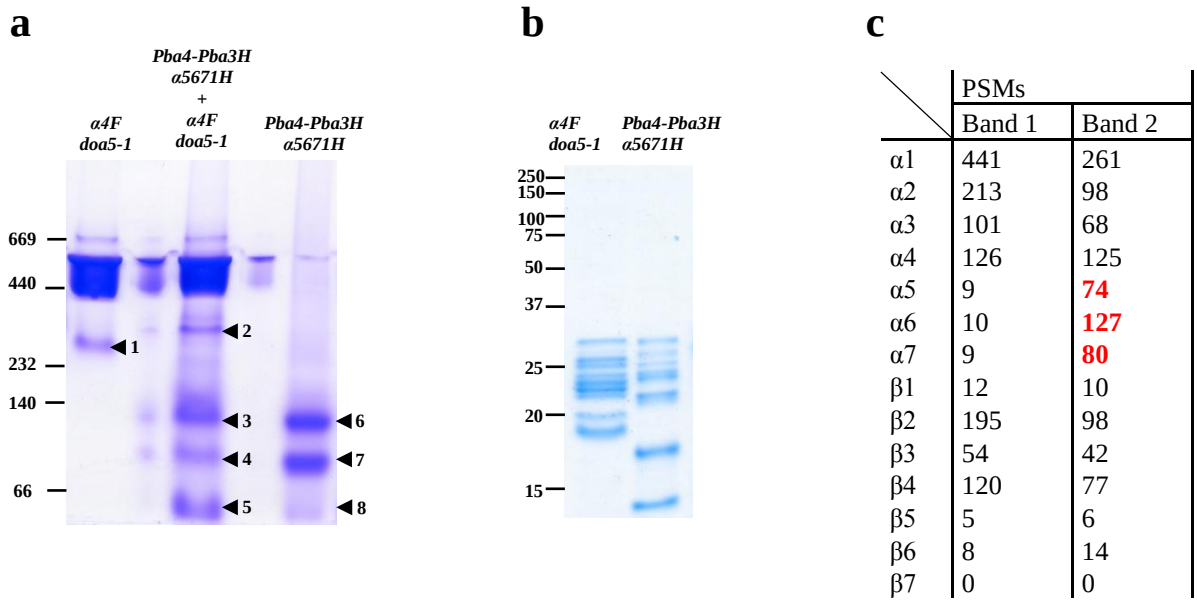

c

	PSMs	
	Band 1	Band 2
α1	441	261
α2	213	98
α3	101	68
α4	126	125
α5	9	**74**
α6	10	**127**
α7	9	**80**
β1	12	10
β2	195	98
β3	54	42
β4	120	77
β5	5	6
β6	8	14
β7	0	0

Figure 3.4: Sub-13S is an assembly competent species
(a) Flag purified proteins from a yeast mutant α4F doa5-1 (40µg) were mixed ICAR purified proteins from E. coli lysate expressing Pba4 Pba3H α5α6α7α1 (8µg) at a ratio of 5:1. Samples were incubated at 30 °C for 30 minutes and analyzed by native PAGE followed by imperial blue staining. Lane 1 and lane 3 are input lanes. Bands of interest are labeled with an arrowhead. (b) Shows the loading control of the input lanes from (a) analyzed by 12% SDS PAGE followed by GelCode blue staining. Lane 1 shows CP subunits. The migration of several molecular size standards (in kDa) is indicated on the left. (c) Contents of indicated bands excised from (a) were analyzed by LC-MS/MS. The table indicates the total count of PSMs for peptides derived from individual proteins. Proteins with a significant increase in PSMs in band 2 as compared to band 1 are highlighted in red.

To overcome this issue, recombinantly expressed proteasome subunits in *E. coli* were chosen as a source of free subunits. Coexpression of α5, α6, and α7 subunits results in partially soluble proteins (Sup Fig. 17a), but these proteins may not be properly folded as the soluble material sticks to the resin (Kusmierczyk et al., 2008). Addition of α1 to an operon containing α5, α6, and α7 results in a high molecular weight complex that is likely a dead-end product (see chapter 4). Proteasome assembly chaperone Pba3-Pba4 binds strongly to α5 and weakly to α1 and have been shown to play an exclusive role in α-ring assembly. When Pba4-Pba3H (his tagged Pba3) is coexpressed with α5, α6, and α7, and α1 subunit, the expressed α subunits were soluble (Sup Fig. 17b) and did not form HMWC (see chapter 4). When the lysates were subjected to ICAR

purification, the bound material mainly contained α5, α6, and α7 along with Pba3-Pba4 (Sup Fig. 17b lane E, also Fig. 4.2b lane 5).

Flag purified proteins from the *doa5-1* α4F sample were mixed with the ICAR purified proteins from *E. coli* expressing Pba4-Pba3Hα5α6α7α1 for 30 mins at 30 °C. Native PAGE analysis showed the expected sub-13S complex in the *doa5-1* α4F strain (Fig. 3.4 lane 1, band 1) and faster migrating complexes likely multimers of Pba3-Pba4 and α5, α6, α7, and α1 in Pba4-Pba3Hα5α6α7α1 sample (Fig. 3.4 lane 3). Protein mixing of these two samples resulted in complete disappearance of the sub-13S band and the appearance of a new slower migrating band (Fig. 3.4 lane 2, band 2). MS analysis of the band showed an abundance of all the α subunits in addition to the β2, β3, and β4, a composition consistent with the 13S intermediate (Fig. 3.4c). A detailed composition including additional proteins is shown in Sup Fig. 18. These results showed successful incorporation of α5, α6 and α7 in the newer complex demonstrating its assembly competency. Few PSMs of Pba3-Pba4, not usually present in the 13S intermediate, also appeared in the newly formed species, suggesting this chaperone's involvement in conversion of sub-13S to highly ordered species (Sup Fig. 18). Moreover, its presence also means the newly formed complex is not completely transformed into 13S suggesting likely involvement of other proteins for its dissociation. Another possibility is perhaps the conformation of the newly formed complex is different from the 13S intermediate in a way that it no longer poses the expected steric hindrance between Pba3-Pba4 complex and the β subunits (Yashiroda et al., 2008).

The faster migrating bands in lane 2 and lane 3 (band 3-8) are sub-complexes containing Pba3, Pba4, α5, α6, α7, α1 in different stoichiometries (Fig. 3.4a and Sup Fig. 18). Among these bands, Pba3-Pba4-α5 has been previously well characterized (Yashiroda et al., 2008). Association of α5, α6, α7, and α1 with Pba3-Pba4 prevents non-specific interactions among the subunits (see chapter 4). There is also another faint band present right above the shifted band. When the ratio of Pba3Hα5α6α7α1 in protein mixing with *doa5-1* mutant was increased, this additional faint band became more prominent (Sup Fig. 19a). MS analysis revealed of both band 2 and band 3 are similar (Sup Fig. 19b, band 3). Perhaps these two newly formed species have different conformation or stoichiometry.

3.5 Discussion

The results herein provide evidence for a novel assembly intermediate, sub-13S, comprising of proteasome subunits α_{1-4}, β_{2-4}, as well as certain members of Hsp70 family proteins. The canonical proteasome assembly pathway is known to start with the formation of an α-ring followed by β subunit incorporation. The absence of a complete α-ring with the presence of a subset of β subunits in this novel species argues for the existence of an α-ring independent assembly pathway in yeast. This complex was first described in a previous report (L. J. Hammack et al., 2017). Here, its existence as an assembly intermediate was investigated. To reproduce the appearance of sub-13S in other strains, different proteasome subunits were epitope tagged for protein purification. These tagged subunits did not exhibit growth defects on their own or in the absence of *RPN4* gene (Fig. 3.1a). Native PAGE analysis showed the sub-13S species appeared only when the α4 subunit was tagged, but not when α2 or β4 were tagged, despite their presence in the complex (Fig. 3.1b). It is possible that tagging of α4 subunit, while not resulting in visible growth defects, could perturb the assembly just enough to accumulate sub-13S. Consistent with this, in the previous report, sub-13S appeared when both β4 and β5 subunits were tagged, but not when only β4 was tagged (L. J. Hammack et al., 2017). The additional tag on the β5 subunit, just like the tag on the α4 subunit, might have slowed assembly down sufficiently to allow sub-13S to accumulate.

An α5 subunit mutant, *doa5-1*, enabled further slow down of the assembly that resulted in increased levels of sub-13S when combined with a2HF and a4 Flag strains (Fig. 3.2a and Sup Fig. 11). The mutant likely delays the folding of α5 subunit into the native state, and thereby its incorporation into nascent CP. This mutant directly affected the formation of 13S intermediate as evident from the disappearance (or smeary appearance) of the 13S intermediate band in the mutant lane (Fig. 3.2a and Sup Fig. 11). The correlation between the disappearance of 13S and the appearance of sub-13S suggest a product precursor relationship between the two complexes.

Since sub-13S is closely related to 13S intermediate based on its composition, one could argue that tagging of specific subunit perhaps makes 13S intermediate unstable, leading to its dissociation into sub-13S likely during (or after) lysis or electrophoresis. The depletion strategy demonstrated sub-13S complex does not result from 13S dissociation during electrophoresis (Fig.

3.3, Sup Fig. 13-15). It is worth to mention that the order in which a protein complex disassociates *in vitro* is usually in reverse of the order they assemble. Therefore, even if some amount of sub-13S arises due to dissociation of 13S intermediate, this could still be consistent with sub-13S being a precursor to the 13S intermediate.

The last piece of evidence provided by protein mixing experiment demonstrated that sub-13S is an assembly competent complex. It involved mixing the recombinantly expressed missing subunits (α5, α6, and α7) with the purified sub-13S complex that resulted in complete disappearance of sub-13S complex and appearance of a slower migrating complex (13S intermediate) that contained α5, α6 and α7 subunits (Fig. 3.4, Sup Fig. 19). The missing subunits required coexpression with the assembly chaperone Pba3-Pba4 and α1 subunit to attain better solubility and prevention of non-specific interaction among the expressed subunits. Since Pba3-Pba4 are not normally present in the 13S intermediate, its appearance in the slowly migrating complex suggests other proteins might be needed for dissociation of this chaperone. One likely candidate could be assembly chaperone Pba1-Pba2. Their binding might influence the orientation of the proteasome subunits in the 13S intermediate that could induce dissociation of Pba3-Pba4. It is likely that Pba3-Pba4 have an additional role in the conversion of sub-13S to 13S, but the exact mechanism remains to be determined.

The data provided strong evidence of a bona-fide novel assembly intermediate, sub-13S. The absence of a complete α-ring and presence of β subunits in this intermediate suggest its origin is likely from an alternative proteasome assembly pathway that does not begin with the α-ring formation. This pathway could very well coexist with the canonical α-ring dependent assembly pathway. The existence of a similar α-ring independent pathway was demonstrated in archaea arguing the multiple assembly pathway theme is likely conserved. This is another evidence, a first in eukaryotes, supporting the need to update the linear proteasome assembly pathway into an assembly network which is connected through common assembly intermediates.

It is worthwhile to mention that an additional band “pre-sub-13S” appeared in both wild-type and *doa5-1* mutant strains and migrated faster than the sub-13S intermediate (Sup. Fig. 11b and Fig 3.3). Compared to sub-13S, this complex has an abundance of the Hsp70 group proteins

and has additional members of the group including Ssb1/2, Sse1/2, and Ssc1. This complex could be another novel species likely to be an assembly intermediate precursor to sub-13S, but this hypothesis remains to be determined. Association of Ssa1/Ssa2 with proteasome assembly intermediates and a newly-discovered non-canonical α4 complex in vivo has been previously shown (L. J. Hammack et al., 2017; Lindsay J. Hammack & Kusmierczyk). Their abundance in early intermediates and eventual disappearance in later assembly intermediates suggest their particular role in the early stages of proteasome assembly, especially in α subunit interaction. Since these Hsp70 group proteins have ATP binding domains, their interaction with $\alpha_{1\text{-}4}$ subunits could be ATP dependent. It is not surprising to see Ssb1/ Ssb2 in the complex as they are known proteasome mutant suppressors (Ohba, 1994). Moreover, the Ssb1 contains a nuclear export sequence (NES) in its C-terminus and certain proteasome α subunits also include NLS like sequences. Their association indicates they may contribute to assembly intermediate localization. It will be interesting to analyze further the association of Hsp70 family proteins with early assembly intermediates to understand the factors necessary for initiation of proteasome assembly.

CHAPTER 4. HIGH MOLECULAR WEIGHT COMPLEXES

4.1 Abstract

The proteasome is a multi-subunit protease complex that plays a major role in the degradation of ubiquitin tagged proteins. Structurally, the 20S proteasome is composed of four coaxially arranged rings. The two outer α rings, and two inner β rings, are each made up of seven homologous but distinct subunits. Proteasome assembly is a complex and highly ordered process that requires the assistance of assembly chaperones. The assembly chaperone Pba3-Pba4 assists in the formation of the α ring, which is an early event in proteasome assembly. Due to the rapid nature of these events, the exact order of the α subunit addition to form an α ring, and the precise role of Pba3-Pba4 in this process, remain unclear. This chapter focus on investigating the early events in proteasome assembly by the recombinant expression of *Saccharomyces cerevisiae* α subunits in *Escherichia coli*. Recombinant co-expression of several α subunit combinations, such as α7α1, α6α7α1 and α5α6α7α1, results in the formation of high molecular weight complexes (HMWC). An engineered disulfide crosslinking strategy shows that all of these complexes are double α rings. Interestingly, the co-expression of Pba3-Pba4 with α5α6α7α1 prevents the formation of this HMWC, whereas the Pba3-Pba4 cannot disrupt a preformed α5α6α7α1 complex. More importantly, the crosslinking strategy suggests that similar HMWCs may form in vivo when Pba3-Pba4 is absent. These data suggest that α subunits have a tendency to form non-canonical ring complexes and one of the roles of Pba3-Pba4 is to prevent the formation of these likely dead-end species.

4.2 Introduction

The 20S proteasome or core particle (CP) is a multi-subunit protease complex involved in the degradation of the majority of proteins. Structurally, it is made of 14 distinct α and β subunits that form four heteroheptameric α-rings and β-rings arranged as α1-7, β1-7, β1-7, α1-7 (Groll et al., 1997). Among the seven β subunits, β1, β2, and β5 are catalytically active bearing the Thr1 nucleophile, and are synthesized as proproteins (Arendt & Hochstrasser, 1999; P. Chen & Hochstrasser, 1996; Groll et al., 1997; S. Witt et al., 2006). The inner β-rings form the catalytic chamber and the outer α rings form a gated pore which, when in open conformation, allows passage

of the substrate into the catalytic chamber (Groll et al., 2000; Groll et al., 1997; Religa et al., 2010). Often, activators like the 19S regulatory particle (RP) bind to the ring to open the gate, and function in substrate recognition, unfolding and translocating to the catalytic core of the 20S proteasome (Groll et al., 2000).

The CP assembly is a complex, yet highly efficient process supported by several assembly chaperones (Fig. 1.2) (Budenholzer et al., 2017; Howell et al., 2017; Kunjappu & Hochstrasser, 2013). Assembly starts with α subunit interactions leading to the formation of α rings. These rings act as a base for the subsequent addition of β subunits (Hirano et al., 2006; Zwickl et al., 1994). Sequential addition of β2, β3, β4 followed by β1, β5, β6 is defined by intermediates 13S and 15S respectively (Hirano et al., 2008; X. Li et al., 2007; Marques et al., 2007). Addition of β7 completes the β ring to form a half proteasome intermediate. Two half proteasomes dimerize to yield a preholoproteasome (PHP) that structurally resembles CP but has intact β subunit propeptides (X. Li et al., 2007). Autocatalytic removal of the propeptides exposes the Thr1 residue, transforming the PHP into the mature CP. Several assembly chaperones are known to support proteasome assembly. Ump1 assists in the dimerization step of half proteasomes (X. Li et al., 2007). Pba1-Pba2 is involved in α- ring assembly, and perform a safety function to prevent premature association of activators to CP intermediates (Kusmierczyk et al., 2011). Pba3-Pba4 functions in α-ring assembly by ensuring the correct placement of α3 between α2 and α4 subunits (Kusmierczyk et al., 2008). In the absence of Pba3-Pba4, yeast forms a subpopulation of the evolutionary conserved α4-α4 proteasome that has an additional copy of α4 subunit positioned in place of α3 (Kusmierczyk et al., 2008; Padmanabhan et al., 2016; Velichutina et al., 2004).

The early event of the proteasome assembly, α-ring formation, is the least understood step to date. Recombinant expression of archaeal and specific eukaryotic α subunits *in vitro* has revealed their inherent tendency to readily form high molecular weight complexes (HMWC) with different subunit stoichiometries (Gerards, de Jong, Bloemendal, et al., 1998; Gerards et al., 1997; Groll et al., 2003; Ishii et al., 2015; Panfair et al., 2015; Yao et al., 1999; Zwickl et al., 1994). However, such HMWC does not form *in vivo*. The assembly chaperones may function in preventing unproductive association of proteasome subunits (Hirano et al., 2005; Takagi et al., 2014). The focus of this chapter is to study the α-ring assembly and determine the role of assembly

chaperones involved. The results show recombinant expression of specific *S. cerevisiae* α subunits forming double ringed HMWCs. Presence of Pba3-Pba4 prevents the formation of such complexes *in vitro*. The crosslinking data provide evidence of similar HMWC formation *in vivo* when Pba4 is absent. These results demonstrate the role of Pba3-Pba4 in preventing formation of these likely off-pathway products.

4.3 Materials and Methods

4.3.1 Bacterial Protein Expression and Purification

Bacterial expression plasmids, including those enabling polycistronic gene expression from a single mRNA, were generated as described (Kusmierczyk et al., 2008). Plasmids used in this study are listed in Supplementary Table 4 in Appendix C. Proteins were expressed as described in (Kusmierczyk et al., 2008; Panfair & Kusmierczyk, 2016). Proteins were induced at 30 °C or, where indicated, specific protein induction was carried out at 37 ^{0}C. Small scale (6 ml) cultures were used for recombinant protein expression except for AKB 349. After transformation of AKB 349 plasmid into the BL21 cells, single colonies were inoculated in 6 ml of LB medium supplemented with ampicillin. After 6 hours of growth at 37 °C with shaking, the primary culture was diluted to an OD_{600} of 0.2 in 200 ml of LB with ampicillin and reincubated at 37 °C for 40 mins. The cultures were then transferred to 30 °C and incubated for another 30 mins before adding 1 mM IPTG to induce protein expression. After 14 hours of induction, the culture was split into four 50 ml aliquots and pelleted down by centrifugation for 10 mins at 13000rpm. The pellets were stored at -80 °C. The frozen pellet lysis and immobilized cobalt affinity resin (ICAR) purification were carried out as described in (Panfair & Kusmierczyk, 2016) with two changes in AKB349 lysis. The pellets were lysed in 1ml of lysis buffer and for the total, soluble and pellet fraction analysis by denaturing gels, the lysates were diluted to 50% with lysis buffer and 5 µl of samples were loaded.

4.3.2 Yeast lysis and Flag purification

The yeast strains used are listed Supplementary Table 5 in Appendix C. Yeast growth conditions and manipulations were carried out according to established protocols (C. Guthrie, 1991). Protein purifications, depletion analysis and electrophoresis were carried out as described (Hammack & Kusmierczyk, 2017; Kusmierczyk et al., 2008).

4.3.3 Disulfide Crosslinking

Disulfide crosslinking was performed as described in (Kusmierczyk et al., 2011). Crosslinked and non-crosslinked samples were mixed with 2 x SDS sample buffer without DTT and loaded onto 12% SDS PAGE step gradient gels. Where indicated, a 25 µl aliquot of each sample was reduced with 2 µl of 1M DTT at room temperature for 15 minutes.

4.3.4 Lysate Mixing and Purified Protein Mixing

For lysate mixing experiments, equal volumes of soluble bacterial lysates of desired samples were mixed and incubated at 30 °C with slow shaking for 30 min. Following incubation, mixed lysates were subjected to ICAR purification as described previously in (Panfair & Kusmierczyk, 2016). For purified protein mixing, equal amounts of ICAR purified proteins of desired samples were mixed at 30 °C for 30 minutes followed by native PAGE analysis.

4.3.5 Electrophoresis

Samples were subjected to SDS-PAGE and native PAGE as previously described (Kusmierczyk et al., 2011) except 5% and 4–15% non-denaturing polyacrylamide gradient gels, as well 12% SDS-PAGE gels were used as indicated. For all the gels, the migration of molecular size standards is indicated to the left of each gel image in the Figures. The 4–15 % gradient gels were precast Mini-PROTEAN TGX (Bio-Rad) while all others were poured in lab. Non-denaturing gradient gels were run at 60 V for 11 hours at 4 °C, 5% non-denaturing gels were run at 55V for 3.5 hours. The native gels were stained with Imperial Protein Stain (ThermoScientific). Loading control samples were run on reducing 12% SDS-PAGE. All SDS-PAGE gels were stained with GelCode blue (ThermoScientific).

4.3.6 Mass Spectrometry Analysis

Gel slices were submitted to the Indiana University School of Medicine Proteomics Core Facility (IUSM-PCF) on a fee-for-service basis. Protein contents of the gel slices were identified by LC-MS/MS as described (Lindsay J. Hammack & Andrew R. Kusmierczyk, 2017). Annotated data is presented in the Sup Fig. 23.

4.4 Results

4.4.1 α Subunits Form Non-canonical Complexes

To study the events involved in the α-ring formation, *S. cerevisiae* α subunits in *E. coli* were expressed. When expressed individually, all the subunits were mostly insoluble (data not shown). The subunits were coexpressed with their native neighbor within α-ring in different combinations. Among several combinations, expression of C-terminal hexahistidine tagged α1 (α1H) with α7 increased the solubility of both subunits (Sup Fig. 20 a). Further extending the coverage of α-ring, two other neighboring subunits, α5 and α6, were sequentially added that resulted in improved solubility of all the included subunits in α6α7α1H, α5α6α7α1H samples (Fig. 4.1b and Sup Fig. 20 b). Their likely interaction contributes to their enhanced solubility. Native PAGE analysis of purified proteins by ICAR revealed coexpression of α7α1, α6α7α1, α5α6α7α1 subunits combinations forms HMWCs (Fig. 4.1a, lanes 1-3). Excision of the bands followed by elution of the proteins within and analysis by SDS-PAGE confirmed the composition of these complexes correlates with the co-expressed subunits (Ramamurthy unpublished).

Interestingly, when the proteins were induced at a higher temperature (37 °C), an additional band, migrating similar to the α7α1 band, was observed in α6α7α1 sample (Fig. 4.1a, lane 5). The soluble fractions of α6α7α1 lysate analyzed by SDS PAGE revealed a much-reduced solubility of α6 at a higher temperature (Fig. 4.1b lane 2 vs. lane 5). The reduced solubility lowered the relative level of α6 compared to α7 and α1 levels. The excess of α7 and α1 formed the α7α1 complex which migrates faster than α6α7α1 complex (Fig. 1a lane 4 and 5). The α6 subunit did not show sensitivity towards higher temperature in the presence of its native neighbor α5 in the α5α6α7α1sample suggesting α5α6 interaction increases the stability of α6 subunit (Sup Fig. 20 b, lane 2 vs. lane 5). The loading control shows a faint α6 band compared to α7 and α1 in the α6α7α1coexpression lane suggesting a sub-stoichiometric level of α6 in the α6α7α1 complex (Fig. 4.1a, Bottom lane 2). However, such a stoichiometric difference was not observed in the α5α6α7α1 sample (Fig. 4.1b, lane 3) suggesting the α5-α6 interaction promotes α6 incorporation in the HMWC. These results were consistent when the subunit levels within the complex were compared by excising the bands and analyzing the eluted protein by SDS-PAGE (Ramamurthy unpublished).

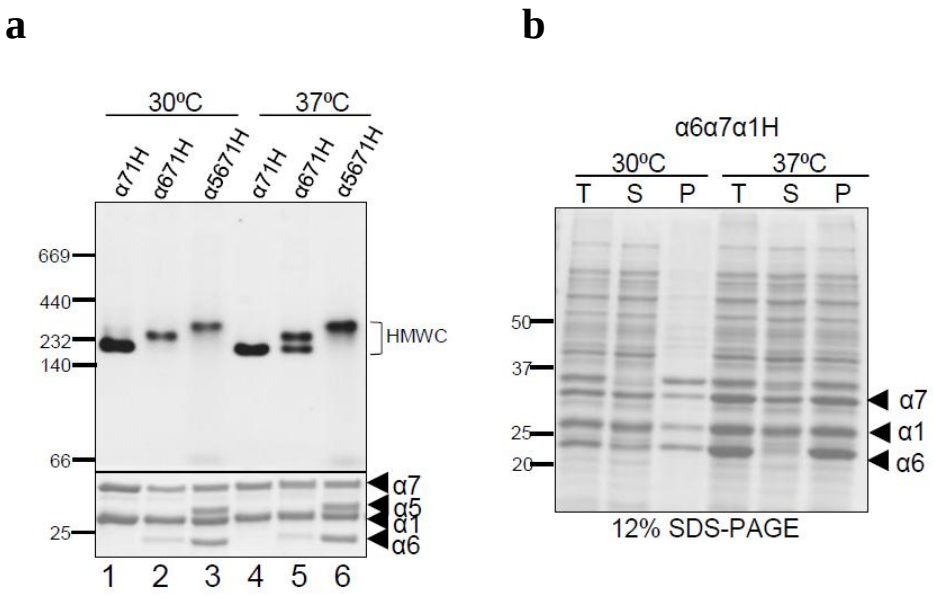

Figure 4.1: Recombinant coexpression of α subunits forms HMWC
(a) Purified proteins (10µg) from the coexpression of α subunit in combinations as indicated were analyzed by 5% native PAGE (top) and SDS PAGE (bottom) The α1 subunit has the hexahistidine tag (α1H). The HMWC are shown by bracket. The individual subunits in the loading control gels are indicated by the arrows. (b) Total (T), Soluble (S) and Pellet (P) fractions of extracts from *E. coli* expressing α6, α7, and α1H induced at 30 °C and 37 °C. The migration of individual subunits is labeled. All the gels were stained by GelCode blue. Migration of molecular size standards in kDa is indicated on the left.

The key interaction in the formation of the α5α6α7α1complex is likely α7 and α1, since they can interact independently. The presence of a single complex in co-expression of α5, α6, α7, and α1 despite the capability of α6, α7, α1 (and α7 and α1) to form other complexes, suggests that formation of the α5α6α7α1 complex is more favorable. Given that co-expressing 4 of the 7 alpha subunits (α5α6α7α1) is arguably more physiologically relevant than co-expressing 2 or 3, we chose to characterize this complex further.

4.4.2 Characterization of the α5α6α7α1 Complex

Purified α5α6α7α1 complex observed under negative-stain electron microscopy (EM) appeared as rings having an approximate diameter of 11 nm, a size consistent with proteasome α rings (Sup Fig. 21b) (Groll et al., 1997). Mass spectrometry analysis estimated a molecular mass for this complex of ~457 kDa (Sup Fig. 21a). The average molecular mass of the α5, α6, α7, and α1 subunits is 28 kDa. Based on this, the mass of a single and double heptameric ring would be

around 196 kDa and 392 kDa respectively. However, if the rings were octameric, the mass of such a double ring would be around 448 kDa, much closer to the observed mass of this HMWC. These results suggest that the α5α6α7α1HMWC is most likely an octameric double ringed species.

In chapter 2, the identity of an archaeal double α-ring was confirmed via cross-linking two α subunits by suitably placing a cysteine residue in the H1 helix (Panfair et al., 2015). The crosslink only forms when two α subunits (α/α, where / indicates a trans interaction) interact like an α and β subunit (α/β). Here, the same cross-linking strategy was applied to investigate whether the HMWC is double ring species. Using multiple sequence alignment revealed the corresponding position in the H1 helix of yeast α subunits to introduce the cysteines for crosslinking. The likelihood of observing a crosslink involving either α7 or α1 subunits in the HMWC was greater as these two subunits appear to nucleate HMWC formation. The alanine at position 102 was changed to cysteine in the α1 subunit, now referred to as α1cc. Gel extracted proteins from the HMWC band, formed by co-expressing α5, α6, α7 and α1cc, were analyzed by non-reducing SDS PAGE and showed an α1-α1 dimer band. This result suggests that HMWC contains at least one pair of α1 subunit sitting across each other thereby confirms the double ring conformation of the complex (Sup Fig. 22).

4.4.3 Pba3-Pba4 Prevents the Formation of HMWC *in vitro*

The ability of certain α subunits to form HMWC *in vitro* has been reported across other species (Gerards, de Jong, Bloemendal, et al., 1998; Yao et al., 1999; Zwickl et al., 1994). However, these complexes are not common *in vivo*. There must exist a mechanism to prevent their formation or disintegrate them if formed. Out of the six known assembly chaperones assisting proteasome assembly, four are involved in α-ring formation. Perhaps the chaperone presence may prevent spontaneous off pathway α subunit interaction, which in turn might prevent HMWC formation. To test this hypothesis *in vitro*, assembly chaperone Pba3-Pba4 was chosen for two reasons. First, they are exclusively involved in the α-ring formation, and their absence results in altered order of α subunits within α-ring, suggesting their role in maintaining the order of subunits (Hirano et al., 2006; Kusmierczyk et al., 2008; Takagi et al., 2014). Second, they show strong binding to α5, and weak binding α1 subunit, both of which are present in the α5α6α7α1 HMWC (Kusmierczyk et al., 2008; Le Tallec et al., 2007; Yashiroda et al., 2008)

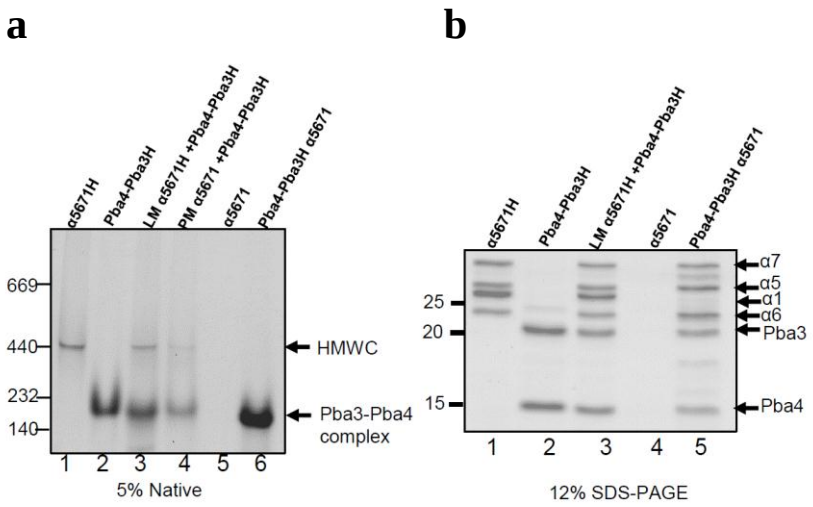

Figure 4.2: Pba3-Pba4 prevents the formation of α5α6α7α1 complex
(a) Native PAGE analysis of ICAR purified proteins from coexpressed hexahistidine tagged Pba3 (pba3H)-Pba4 α5α6α7α1 along with separate expression as controls. Lysate mixing (LM) and purified protein mixing (PM) of separately expressed Pba4-Pba3H and α5α6α7α1H was carried out at 30 °C for 30 min (lane 3-4). The Pba3-Pba4 complex and HMWC are indicated by the arrows. (b) Aliquots from (a) analyzed by SDS PAGE. A faint band present between α5 and α7 subunit in lane 5 is clipped α7 subunit likely arising due to non-specific proteolysis post lysis. Both the gels were stained with GelCode blue.

To see if this assembly chaperone prevents the formation of HMWC, C-terminally his tagged Pba3 (Pba3H) and Pba4 were co-expressed with α5, α6, α7, α1 subunit followed by protein purification and native PAGE analysis. Consistent with the earlier report, when co-expressed, Pba3-Pba4 multimerize to form a complex (Fig. 4.2, lane 2) (Kusmierczyk et al., 2008; Yashiroda et al., 2008). In the presence of Pba3-Pba4, co-expression of α5, α6, α7, and α1 did not show the HMWC band (Fig. 4.2, lane 6 vs. lane 1). The band migrating at the position of Pba3-Pba4 complex in lane 5 is resolved into three separate bands when analyzed on 4-15% gradient PAGE and contains multimers of Pba3-Pba4, α5, α6, α7 and to some extent α1 (See chapter 3, Fig 3.4a, band 3-8, Sup Fig. 18). The loading control showed Pba3-Pba4 pulled down α5, α6, α7 but very little α1, indicating the assembly chaperone somehow prevents the key interaction between the α7 and α1 subunits (Fig. 4.2b, lane 5). An additional faint band migrating between α5 and α7 subunit in lanes 1, 3 and 5 is likely truncated α7 subunit resulting from non-specific proteolysis after lysis. Its higher intensity in lane 5 could be the result of the subunit being more accessible to proteolysis when not present within the HMWC.

Pba3-Pba4 could prevent the α7 and α1 interaction in two possible ways: First, when co-expressed, the preferential binding of Pba3-Pba4 to α5 happens first. Sequential binding of α7 and α6 to the Pba3-Pba4-α5 trimer may alter the conformation of the bound α subunits such that they could no longer associate with α1. Second, the involved α subunits interact first, and a later binding of Pba3-Pba4 to α5 brings conformational change in the subunits that leads to dissociation of α1 subunit. The earlier hypothesis is preferable based on the lysate mixing and purified protein mixing results. When a preformed HMWC was mixed with the Pba3-Pba4 complex, both by purified protein mixing and lysate mixing, the HMWC band remained intact suggesting the Pba3-Pba4 complex could not dissociate a preformed HMWC complex (Fig. 4.2, lane 3 and 4).

4.4.4 Pba3-Pba4 prevents the Formation of HMWC *in vivo*

If Pba3-Pba4 can prevent the formation of HMWC, then its absence should trigger this complex formation *in vivo*. To test this, a C terminally flag epitope-tagged α1cc mutant (with all

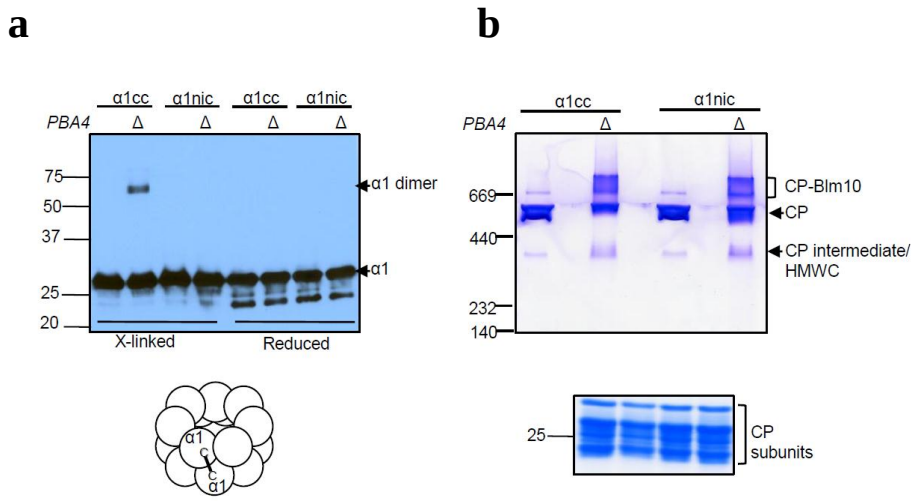

Figure 4.3: Absence of assembly chaperone Pba4 leads to HMWC formation *in vivo*
(a) Flag purified proteins from the indicated yeast strains containing either α1cc (crosslinkable) or α1nic (no internal cysteine) mutant were crosslinked using CuCl2 followed by SDS PAGE under non-reducing (lanes 1-4) and reducing (lanes 5-8) conditions and immunoblotting using anti-Flag antibody. Arrowheads denotes the position of a crosslinked α1 dimer and an α1cc monomer. Bottom shows schematic of the crosslinkable α1 subunit (α1cc) and the resulting crosslink of adjacent α1 subunits in opposite α-ring in the α5α6α7α1 complex. (b) An aliquot (20µg) of native samples from (a) before crosslinking was analyzed by imperial stained 4-15% TGX non-denaturing gel. Core particle (CP), CP-bound Blm10 hybrid species and HMWC are labeled. Bottom shows loading control focused on CP subunits (bracket) analyzed on 12%SDS PAGE stained by GelCode blue.

the internal cysteines removed and bearing only the crosslinking mutation A102C in the H1 helix), and its α1nic mutant control (no internal cysteines), were introduced into wild-type and *pba4Δ* yeast strains. The α1cc will detect putative HMWC(s), if present, by showing the signature dimer band. Flag purified proteins from the indicated strains, after $CuCl_2$ mediated crosslinking followed by non-reducing SDS PAGE and immunoblotting, showed the presence of α1 dimer band, between 50-75 kDa, when *PBA4* gene was deleted in the α1cc mutant (Fig. 4.3, lane 2). The band disappeared under reducing conditions as expected from a crosslinked species. Moreover, this band did not appear in *pba4Δ* α1nic mutant lane suggesting the α1 dimerization is specific to the introduced cysteine in the H1 helix (Fig. 4.3 lane 4).

One could argue that the observed crosslinking arises from dimerization of the free α1 subunits which might accumulate in *pba4Δ* cells because proteasome assembly is known to be perturbed in these cells. To eliminate this possibility, purified proteins from the indicated samples were analyzed by native PAGE. The major band in all the samples, migrating near 669 kDa size, was the CP (Fig. 4.3b). About 20-50% of CP in *pba4Δ* samples are α4-α4 proteasomes (Kusmierczyk et al., 2008). Bands migrating slower than CP are likely complexes of Blm10 and CP; these were more prominent in *pba4Δ* samples because Blm10 preferentially binds to open gate CP and α4-α4 proteasome are hypothesized to have open gates (Lehmann et al., 2008). The MS analysis of these bands confirmed Blm10 association with CP (Sup Fig. 23b). Species migrating faster than CP were also observed. These are likely CP assembly intermediates. A closer look at the faster migrating species shows there may be two closely migrating bands in the *pba4Δ* samples. Increased intensity of these faster migrating band(s) in the *pba4Δ* samples could be due to any (or all) of the following three possibilities. First, the known CP assembly intermediates accumulate in the absence of Pba4, resulting in the more intense band(s). Second, a previously reported aberrant complex (similar to the13S intermediate except it has an additional α2 that takes the place of α4) formed in the absence of Pba4, would be expected to migrate near this position. Third, HMWC(s) (similar to, or even identical with, the α5α6α7α1 complex) would also be expected to migrate near this position.

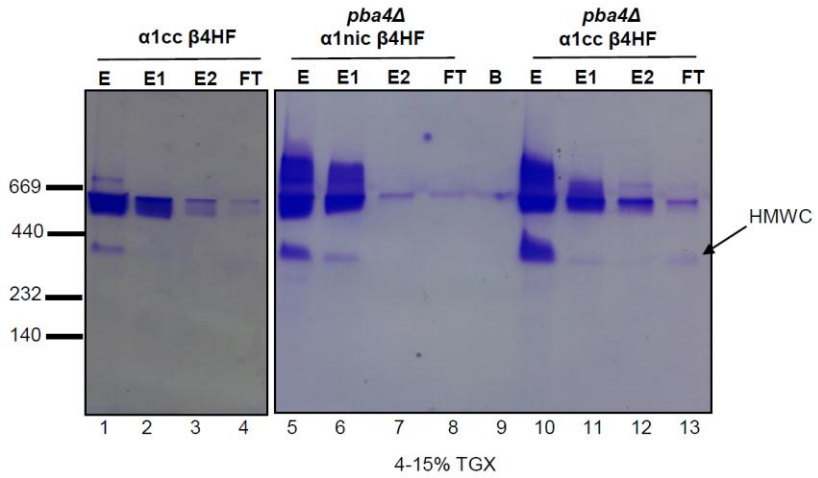

Figure 4.4: Depletion analysis for isolating HMWC
Aliquots of flag purified CP from the indicated yeast strains were subjected to native PAGE (Eluate E). The remainder of the flag-purified material was depleted of his-tagged proteins via two rounds of binding to immobilized-cobalt affinity resin (ICAR). Aliquots of ICAR bound proteins, eluate 1 (E1) and eluate 2 (E2) from round 1 and round 2 binding respectively, and the flow through (FT) from round 2, were loaded on the same native gel. (B) Indicates blank. Arrow denotes a faster migrating species that remains after depletion.

To address these three possibilities and determine if HMWC(s) are present in the faster migrating band(s), a depletion approach (diagrammed in Sup Fig. 24) was employed. This strategy was recently used to detect non-canonical α4 complexes *in vivo*, which are obscured on native PAGE by "normal" assembly intermediates (Lindsay J. Hammack & Andrew R. Kusmierczyk, 2017). Briefly, a C-terminal hexahistidine-and-flag tagged β4 subunit (β4HF) was generated in the context of a *pba4Δ* α1cc strain (recall the cross-linkable α1cc is also flag tagged). After flag purification, the sample should contain assembly intermediates, aberrant 13S like complexes, and putative HMWC when analyzed by native PAGE (Fig.4.4 lane 10). However, when the flag purified material is subjected to depletion through TALON resin, because of histidine tag on β4, all the CP, assembly intermediates, and aberrant 13S like complexes should bind to the resin. Since the HMWC likely does not contain the β4 subunit, the flow through (FT) should contain the HMWC. Two rounds of TALON resin binding were performed to enhance depletion.

Native PAGE after depletion showed a faint band in the β4HF *pba4Δ* α1cc FT lane (Fig. 4.4 lane 13) migrating near the 440 kDa size standard. An absence of this band in the FT of the corresponding wild-type sample suggests that the complex does not form when Pba3-Pba4 is

present, as would be expected. And an absence of this band in the FT of the corresponding *pba4Δ* α1nic control suggests its formation can only be detected on native PAGE using a cross-linkable α1. The high abundance of CP makes its complete depletion difficult, even with two rounds of ICAR binding, which is why a small amount of it still persists in the FT lanes. The composition of the HMWC band in the FT lane of the *pba4Δ* α1cc sample remains to be determined.

4.5 Discussion

The ability of α subunits to form high molecular weight complexes (HMWC) and its prevention by the assembly chaperone Pba3-Pba4 is demonstrated *in vitro* and *in vivo*. Recombinant expression of *S. cerevisiae* proteasome subunits α5, α6, α7, and α1 subunits in combinations results in the formation of HMWC as long as both α1 and α7 are present (Fig. 4.1 a). The α5α6α7α1 complex is physiologically relevant compared to other HMWCs as it appears more stable and contains the maximum number of subunits that can be successfully coexpressed *in vitro*. Negative stain EM and MS analysis suggested the HMWC is likely a double octameric ringed species (Sup Fig. 21). The crosslinking strategy adopted from (Panfair et al., 2015) showed the presence α1 crosslinks within this complex further corroborated the double ring conformation of this complex (Sup Fig. 22). While the order of the subunits in the complex is not clear, based on the crosslinking data, at least one pair of α1 subunits is positioned across from each other in the two adjoining rings (Fig. 4.3c). It is also likely, given that α5α6α7α1 (in that order) are neighbors within an α-ring *in vivo*, that this subunit order is maintained within each ring of the HMWC to maximize native subunit contacts.

A similar tendency of certain recombinant α subunits forming such double ringed HMWC has been demonstrated in different species (Gerards, de Jong, Bloemendal, et al., 1998; Yao et al., 1999). Such complexes highlight the tendency of specific α subunits to interact spontaneously. Despite such easiness in their formation, HMWCs are not common *in vivo*. A double α-ring, whether in archaea or in eukaryotes, are considered dead end complexes, and there must exist some mechanism to prevent their formation. Since only specific α subunit interaction triggers HMWC formation, perhaps interaction of these subunits is well coordinated in a timely manner that might prevent such aberrant complex formation. Assembly chaperones, particularly ones that are involved in the α-ring formation, such as Pba3-Pba4, are known to direct specific α subunit

interactions. These proteins were the likely candidates for further investigation. Indeed, coexpression of assembly chaperone Pba3-Pba4 with α5, α6, α7, and α1 subunits prevented the formation of HMWC (Fig. 4.2a lane 6). In the presence of Pba3-Pba4, while stoichiometric levels of α5, α6 and α7 subunit coprecipitated, sub-stoichiometric levels of α1 subunit was pulled down (Fig. 4.2b lane 5). The poor association of Pba3-Pba4 with α1 subunit has also been shown in a previous report (Kusmierczyk et al., 2008). Perhaps isolation of the α1 subunit inhibits the critical interaction between α1-α7 subunit which is likely responsible for triggering the HMWC formation. However, Pba3-Pba4 could not dissociate a preformed HMWC as shown by the lysate mixing and purified protein mixing (Fig. 4.2a lane 3 and 4). This underscores the importance of having assembly chaperones present from the start of proteasome biogenesis. These results demonstrate Pba3-Pba4 prevents α5α6α7α1 complex formation.

Further evidence for the involvement of assembly chaperone in preventing the formation of HMWC was investigated by looking for aberrant complexes *in vivo* in the absence of Pba3-Pba4. If aberrant complex does form in the absence of Pba3-Pba4, they would likely contain the α1 crosslink, a characteristic of the HMWCs *in vitro*. Indeed, the non-reducing SDS PAGE showed an α1 crosslinking only when assembly chaperone *PBA4* gene was deleted and the crosslinkable α1 mutant (α1cc) was used (Fig. 4.3a, lane 2). Native PAGE of the same strains showed an increase in levels of a faster migrating species in the *pba4Δ* strain, which could be a mix of assembly intermediates and HMWC (Fig. 4.3b). The depletion strategy removed assembly intermediates and left behind a very faint faster migrating band, likely a HMWC (Fig. 4.4 lane 13).

The low abundance of the putative HMWC in *pba4Δ* cells, even after using a large-scale yeast culture, indicates perhaps other factors may be involved in preventing the HMWC formation. These could be assembly chaperones Pba1-Pba2 and/or the presence of other proteasome subunits that compete for binding. The absence of this band in the wild-type sample indicates that this putative HMWC does not form under normal conditions (Fig. 4.4 lane 4). The HMWC complex did not appear in the absence of Pba4 when the non-crosslinkable mutant of α1 subunit (α1nic) was used (Fig. 4.4 lane 8) suggesting the necessity of crosslinking mutation for enabling complex's detection. This argues that this putative HMWC may not be stable enough to survive electrophoresis on its own, and why it might have escaped detection until now. A labile non-

canonical complex formed by α4 subunits was recently reported whose detection on native PAGE also relied on crosslinking (Lindsay J. Hammack & Andrew R. Kusmierczyk, 2017). Further analysis of the putative HMWC complex is required to show it as a novel non-canonical complex and to determine its composition. Eventually, a structural analysis would provide conformational details of the complex.

Overall, the results provide evidence of α subunit interaction following an alternate assembly pathway, one that leads to the formation of a dead-end complex. The assembly chaperone Pba3-Pba4 prevents this non-productive pathway by directing productive α subunit interactions and thereby increases the efficiency of proteasome assembly. These results further suggest the proteasome subunit interactions are not linear. They can interact in multiple ways, and ancillary proteins promote productive pathways.

CHAPTER 5. SUMMARY AND CONCLUSION

5.1 Overview

The 20S proteasome contains 14 distinct types of α and β subunits that are arranged into four heptameric rings. The support of assembly chaperones makes the assembly process highly efficient. Assembly of these subunits is believed to follow a linear pathway that begins with the formation of α-rings onto which the β subunits are sequentially added, forming assembly intermediates that eventually lead to form mature 20S proteasome. Different proteasome isoforms observed in specific tissues assemble slightly different from the canonical 20S proteasome. Dedicated assembly chaperones Pba1-Pba2, Pba3-Pba4, and Ump1 are involved at various stages guiding the productive interactions. The assembly pathway has been well studied over the past few decades, yet some of the steps, especially the early events, are still not well understood.

Proteasome dysfunction is linked to several types of cancers, neurodegenerative diseases and cardiovascular diseases (McNaught & Olanow, 2006; Paul, 2008; Schmidt & Finley, 2014). In addition to other factors, an assembly defect in the proteasome could lead to proteasome dysfunction (Arima et al., 2011; Asai et al., 2009; Day et al., 2013; Treise et al., 2018). In some cases, the defects may be limited to a specific population of the proteasome. The proteasome is already a target of several FDA-approved medicines. While the current approaches to treatment cannot distinguish different proteasome populations, a better understanding of the assembly pathway may help design new strategies in therapeutics to target a specific population of the proteasome. This dissertation expands our knowledge of proteasome assembly via three significant contributions. First, archaeal proteasome can assemble in an α-ring independent pathway, the first evidence of α-ring independent proteasome assembly outside of bacteria. Second, a novel early assembly intermediate, sub-13S, is discovered in yeast that contains a subset of α and β subunits. Its existence argues that α-ring independent proteasome assembly pathways may be present in eukaryotes as well. Finally, Pba3-Pba4 enhance the efficiency of proteasome assembly by preventing the formation of aberrant complexes.

5.2 Archaeal Proteasome Can Assemble by Two Separate Pathways

The archaeal proteasome is compositionally simpler and shares many assembly features with their eukaryotic counterparts. For this reason, early proteasome assembly studies were initiated in archaea by recombinant expression of α subunits. Expression of α subunits in *E. coli* formed a single ring, and a double ring (DR) likely by dimerization of two single rings (Fig. 2.1). This was confirmed using a crosslinking strategy that showed the α subunits interact between the adjacent rings through H1 helices (α/α interaction, / denotes H1 helix-based interaction in adjacent rings) similar to an α/β interaction in a half proteasome intermediate (Fig. 2.1 and Sup. Fig. 1). When the α rings were destabilized using site directed mutagenesis, some level of DR was still observed, which indicated the DR formation could form independent of the single ring (Fig 2.2). The inability of DR to form proteasome showed that the DR is an assembly incompetent species (Fig 2.6). Combining the ring destabilizing α subunit mutants with β subunits resulted in formation of the proteasome, indicating the proteasome assembly can occur without the formation of α rings (Fig. 2.3). Proteasome also formed when the size exclusion chromatography fractions containing unassembled ring disrupting α subunits mutants were mixed with lysates containing β subunit (Fig. 2.6). This experiment ruled out the possibility of some level of undetected single rings being the reason for proteasome formation.

These results emphasized two things. First, they linked the bacterial proteasome assembly pathway (α-ring independent) to archaea, from which the bacteria were hypothesized to have acquired proteasomes through HGT. One could now advance a reasonable hypothesis for why bacterial proteasome assembly was long considered "different". Simply put, bacterial proteasomes lost the α-ring dependent pathway shortly after HGT and retained only the α-ring independent pathway. Second, the ability of bacterial and archaeal proteasomes to assemble independently of α-ring formation suggested this mechanism might be broader and perhaps even present in eukaryotes.

5.3 A Novel Early Assembly Intermediate Sub-13S

A depletion strategy implemented to purify proteasome intermediates and their potential binding partners in another study from our laboratory identified a novel species containing

proteasome subunits α_{1-4} and β_{2-4} (L. J. Hammack et al., 2017). This species migrated faster than the 13S intermediate on native PAGE, so it was referred to as the sub-13S.

The sub-13S does not fit within the accepted assembly pathway for eukaryotes due to the lack of a complete α ring. Eukaryotic proteasome assembly initiates with the formation of an α-ring (Hirano et al., 2005). This was also assumed to be the case in archaea, whose proteasomes have long served as models for studying 20S CP assembly (Zwickl et al., 1994). However, the results from chapter 2 showed proteasome assembly in archaea could also initiate through an α and β subunit interaction, bypassing the α-ring formation. This suggested that the sub-13S intermediate likely originates from a similar α-ring independent pathway that may also exist in eukaryotes.

The sub-13S resembles a 13S intermediate lacking α5, α6, and α7. Because of this similarity, it was hypothesized that sub-13S might be a precursor to the 13S. The observation of sub-13S in some strains, but not others, was attributed to the mild perturbations in assembly caused by tagging different proteasome subunits (Fig.3.1). To test the idea of a precursor-product relationship of sub-13S and 13S, 13S assembly was disturbed by slowing down the rate at which α5 could incorporate using an α5 mutant. The results were consistent with sub-13S being the immediate precursor to the 13S. Slowing down assembly in strains that produced low levels of sub-13S caused more sub-13S accumulation with a consequent reduction in 13S level (Fig 3.2). Furthermore, slowing down assembly with the α5 mutant induced the formation of sub-13S in strains where it was previously not detected (Sup. Fig. 11b). To rule out the possibility of sub-13S being an off-pathway intermediate, the missing subunits (α5, α6, and α7) and assembly chaperone Pba3 and Pba4 were mixed with the sub-13S intermediate. Based on the observed band shift on native PAGE, sub-13S converted to a 13S like intermediate (Fig. 3.4 and Sup. Fig 19). Pba3-Pba4 are required to keep the α subunits in free form as they would otherwise form a dead-end complex (shown in chapter 4). The assembly chaperone may also assist in band shift. The MS analysis of the slower migrating band will confirm the identity of the complex by showing its composition.

The evidence provided argues for this novel sub-13S species participating within an alternative assembly pathway, initiating through the interaction of α and β subunits. Perhaps, this

novel intermediate is unique to yeast, since α-rings were never formally detected in this species. But it is also possible that eukaryotes, like archaea, can use more than one assembly pathway.

5.4 Pba3-Pba4 Prevents HMWC Formation

To study α-ring formation, *S. cerevisiae* α subunits were expressed in *E. coli*. Coexpression of α7α1, α6α7α1, and α5α6α7α1 formed high molecular weight complexes (HMWC) (Fig. 4.1). The α5α6α7α1 HMWC was chosen for further study because it is more physiologically relevant than the other complexes (it contained 4 of the 7 subunits). Mass spectrometry, negative stain EM and crosslinking strategy (similar to archaea, Chapter 2) showed the HMWC complex is a double octamer ring having at least one pair of α1 subunit interacting via H1 helices (α1/α1) (Sup. Fig. 21 and 22). Assembly chaperone Pba3-Pba4 prevented the formation of this complex when coexpressed with α5, α6, α7, and α1. However, Pba3-Pba4 could not dissociate a preformed complex (Fig. 4.2). This is consistent with the previously hypothesized roles of assembly chaperones in preventing off-pathway interactions. The crosslinking strategy detected an α1 dimer indicative of a putative HMWC *in vivo* when the assembly chaperone gene *PBA4* was deleted in yeast (Fig 4.3). Native PAGE analysis showed a more intense, faster-migrating complex in the *pba4Δ* strains (Fig 4.3). To determine if the putative HMWC is present within the intense band, a depletion strategy was employed. Native PAGE after depletion showed a presence of a unique band in the *pba4Δ* strain that contained crosslinking mutation suggesting the crosslinking stabilized HMWC and enabled its detection (Fig 4.4).

The results argue that Pba3-Pba4 prevent the formation of aberrant complexes that likely results from an off-pathway interaction. Similar roles were demonstrated for assembly chaperone Pba1-Pba2 in mammalian cells (Hirano et al., 2005). Whether β subunits are present in this complex or it is strictly an α subunit aberrant complex is not known. Mass spectrometry of the unique band on native PAGE will disclose its subunit composition. These results further add to the multiple pathway theme of proteasome assembly advanced in this dissertation: whereas some pathways (both α-ring dependent and α-ring independent) are productive, there are some pathways that are nonproductive. Assembly chaperones can help ensure the productive interactions are preferred, perhaps by preventing subunit interactions that produce dead end species (like the HMWC).

5.5 Concluding Remarks

The data resulting from this dissertation led to three discoveries: 1. the existence of alternative assembly proteasome assembly pathways in archaea and yeast; 2. evidence of a novel assembly intermediate; 3. the establishment of an additional role of assembly chaperone Pba3-Pba4 in yeast.

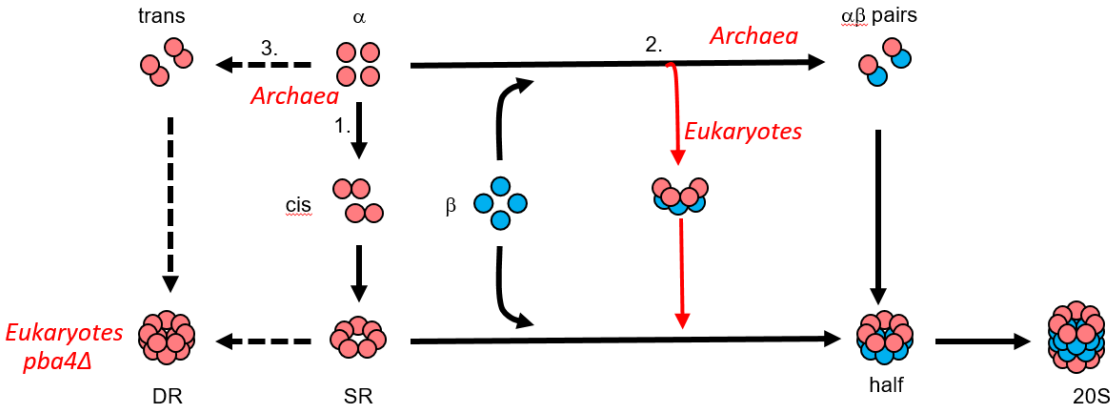

Figure 5.1: Contributions to the 20S proteasome assembly pathway
This schematic is modified from the schematic shown in Figure 2.7. The findings from this dissertation are included and labeled in red.

The data converge to support the existence of a proteasome assembly network containing multiple productive pathways (pathways 1 and 2) and non-productive pathways (pathway 3), in which the ancillary proteins/ β subunits prevent the unproductive route of assembly pathway (pathway 3) (Fig. 5.1). The demonstration of an assembly network also connects the seemingly separate bacterial proteasome assembly pathway with rest of the proteasome realm. It is not yet known if these productive pathways operate simultaneously or a preference exists for a specific pathway in vivo. However, having multiple pathways may offer an advantage to the cell by enabling assembly of proteasomes via an alternate pathway in the event of a defect in one pathway.

LIST OF REFERENCES

Adams, J. (2004). The proteasome: a suitable antineoplastic target. Nat Rev Cancer, 4(5), 349-360. doi:10.1038/nrc1361

Akiyama, K., Kagawa, S., Tamura, T., Shimbara, N., Takashina, M., Kristensen, P., . . . Ichihara, A. (1994). Replacement of proteasome subunits X and Y by LMP7 and LMP2 induced by interferon-gamma for acquirement of the functional diversity responsible for antigen processing. FEBS Lett, 343(1), 85-88. doi:0014-5793(94)80612-8 [pii]

Arendt, C. S., & Hochstrasser, M. (1999). Eukaryotic 20S proteasome catalytic subunit propeptides prevent active site inactivation by N-terminal acetylation and promote particle assembly. EMBO J, 18(13), 3575-3585. doi:10.1093/emboj/18.13.3575

Arima, K., Kinoshita, A., Mishima, H., Kanazawa, N., Kaneko, T., Mizushima, T., . . . Yoshiura, K. (2011). Proteasome assembly defect due to a proteasome subunit beta type 8 (PSMB8) mutation causes the autoinflammatory disorder, Nakajo-Nishimura syndrome. Proc Natl Acad Sci U S A, 108(36), 14914-14919. doi:1106015108 [pii]10.1073/pnas.1106015108

Asai, M., Tsukamoto, O., Minamino, T., Asanuma, H., Fujita, M., Asano, Y., . . . Kitakaze, M. (2009). PKA rapidly enhances proteasome assembly and activity in in vivo canine hearts. J Mol Cell Cardiol, 46(4), 452-462. doi:10.1016/j.yjmcc.2008.11.001

Asher, G., Reuven, N., & Shaul, Y. (2006). 20S proteasomes and protein degradation "by default". Bioessays, 28(8), 844-849. doi:10.1002/bies.20447

Asher, G., & Shaul, Y. (2005). p53 proteasomal degradation: poly-ubiquitination is not the whole story. Cell Cycle, 4(8), 1015-1018. doi:10.4161/cc.4.8.1900

Bai, M., Zhao, X., Sahara, K., Ohte, Y., Hirano, Y., Kaneko, T., . . . Murata, S. (2014). Assembly mechanisms of specialized core particles of the proteasome. Biomolecules, 4(3), 662-677. doi:10.3390/biom4030662

Bajorek, M., Finley, D., & Glickman, M. H. (2003). Proteasome disassembly and downregulation is correlated with viability during stationary phase. Curr Biol, 13(13), 1140-1144.

Barthelme, D., & Sauer, R. T. (2012). Identification of the Cdc48*20S proteasome as an ancient AAA+ proteolytic machine. Science, 337(6096), 843-846. doi:10.1126/science.1224352[pii]

Barthelme, D., & Sauer, R. T. (2013). Bipartite determinants mediate an evolutionarily conserved interaction between Cdc48 and the 20S peptidase. Proc Natl Acad Sci U S A, 110(9), 3327-3332. doi:10.1073/pnas.1300408110 [pii]

Basler, M., Kirk, C. J., & Groettrup, M. (2013). The immunoproteasome in antigen processing and other immunological functions. Curr Opin Immunol, 25(1), 74-80. doi:10.1016/j.coi.2012.11.004

Baugh, J. M., Viktorova, E. G., & Pilipenko, E. V. (2009). Proteasomes can degrade a significant proportion of cellular proteins independent of ubiquitination. J Mol Biol, 386(3), 814-827. doi:10.1016/j.jmb.2008.12.081

Benaroudj, N., & Goldberg, A. L. (2000). PAN, the proteasome-activating nucleotidase from archaebacteria, is a protein-unfolding molecular chaperone. Nat Cell Biol, 2(11), 833-839. doi:10.1038/35041081

Bolten, M., Delley, C. L., Leibundgut, M., Boehringer, D., Ban, N., & Weber-Ban, E. (2016). Structural Analysis of the Bacterial Proteasome Activator Bpa in Complex with the 20S Proteasome. Structure, 24(12), 2138-2151. doi:10.1016/j.str.2016.10.008

Budenholzer, L., Leng Cheng, C., Li, Y., & Hochstrasser, M. (2017). Proteasome Structure and Assembly (Vol. 429).

Burri, L., Hockendorff, J., Boehm, U., Klamp, T., Dohmen, R. J., & Levy, F. (2000). Identification and characterization of a mammalian protein interacting with 20S proteasome precursors. Proc Natl Acad Sci U S A, 97(19), 10348-10353. doi:10.1073/pnas.190268597 [pii]

Cascio, P., Call, M., Petre, B. M., Walz, T., & Goldberg, A. L. (2002). Properties of the hybrid form of the 26S proteasome containing both 19S and PA28 complexes. EMBO J, 21(11), 2636-2645. doi:10.1093/emboj/21.11.2636

Chen, P., & Hochstrasser, M. (1995). Biogenesis, structure and function of the yeast 20S proteasome. EMBO J, 14(11), 2620-2630.

Chen, P., & Hochstrasser, M. (1996). Autocatalytic subunit processing couples active site formation in the 20S proteasome to completion of assembly. Cell, 86(6), 961-972. doi:S0092-8674(00)80171-3 [pii]

Chen, S., Wu, J., Lu, Y., Ma, Y. B., Lee, B. H., Yu, Z., . . . Mao, Y. (2016). Structural basis for dynamic regulation of the human 26S proteasome. Proc Natl Acad Sci U S A, 113(46), 12991-12996. doi:10.1073/pnas.1614614113

Choi, W. H., de Poot, S. A., Lee, J. H., Kim, J. H., Han, D. H., Kim, Y. K., . . . Lee, M. J. (2016). Open-gate mutants of the mammalian proteasome show enhanced ubiquitin-conjugate degradation. Nat Commun, 7, 10963. doi:10.1038/ncomms10963

Ciechanover, A. (2005). Intracellular protein degradation: from a vague idea, through the lysosome and the ubiquitin-proteasome system, and onto human diseases and drug targeting (Nobel lecture). Angew Chem Int Ed Engl, 44(37), 5944-5967. doi:10.1002/anie.200501428

Ciechanover, A., & Schwartz, A. L. (2004). The ubiquitin system: pathogenesis of human diseases and drug targeting. Biochim Biophys Acta, 1695(1-3), 3-17. doi:10.1016/j.bbamcr.2004.09.018

Crawford, L. J., Walker, B., & Irvine, A. E. (2011). Proteasome inhibitors in cancer therapy. J Cell Commun Signal, 5(2), 101-110. doi:10.1007/s12079-011-0121-7

Cromm, P. M., & Crews, C. M. (2017). The Proteasome in Modern Drug Discovery: Second Life of a Highly Valuable Drug Target. ACS Cent Sci, 3(8), 830-838. doi:10.1021/acscentsci.7b00252

Dambacher, C. M., Worden, E. J., Herzik, M. A., Martin, A., & Lander, G. C. (2016). Atomic structure of the 26S proteasome lid reveals the mechanism of deubiquitinase inhibition. Elife, 5, e13027. doi:10.7554/eLife.13027

Dange, T., Smith, D., Noy, T., Rommel, P. C., Jurzitza, L., Cordero, R. J., . . . Schmidt, M. (2011). Blm10 protein promotes proteasomal substrate turnover by an active gating mechanism. J Biol Chem, 286(50), 42830-42839. doi:10.1074/jbc.M111.300178 [pii]

Darwin, K. H., Ehrt, S., Gutierrez-Ramos, J. C., Weich, N., & Nathan, C. F. (2003). The proteasome of Mycobacterium tuberculosis is required for resistance to nitric oxide. Science, 302(5652), 1963-1966. doi:10.1126/science.1091176302/5652/1963 [pii]

Darwin, K. H., Lin, G., Chen, Z., Li, H., & Nathan, C. F. (2005). Characterization of a Mycobacterium tuberculosis proteasomal ATPase homologue. Mol Microbiol, 55(2), 561-571. doi:10.1111/j.1365-2958.2004.04403.x

Day, S. M., Divald, A., Wang, P., Davis, F., Bartolone, S., Jones, R., & Powell, S. R. (2013). Impaired assembly and post-translational regulation of 26S proteasome in human end-stage heart failure. Circ Heart Fail, 6(3), 544-549. doi:10.1161/circheartfailure.112.000119

De, M., Jayarapu, K., Elenich, L., Monaco, J. J., Colbert, R. A., & Griffin, T. A. (2003). Beta 2 subunit propeptides influence cooperative proteasome assembly. J Biol Chem, 278(8), 6153-6159. doi:10.1074/jbc.M209292200[pii]

De Mot, R., Nagy, I., & Baumeister, W. (1998). A self-compartmentalizing protease in *Rhodococcus*: the 20S proteasome. Antonie Van Leeuwenhoek, 74(1-3), 83-87.

De Mot, R., Schoofs, G., & Nagy, I. (2007). Proteome analysis of Streptomyces coelicolor mutants affected in the proteasome system reveals changes in stress-responsive proteins. Arch Microbiol, 188(3), 257-271. doi:10.1007/s00203-007-0243-8

Delley, C. L., Laederach, J., Ziemski, M., Bolten, M., Boehringer, D., & Weber-Ban, E. (2014). Bacterial proteasome activator bpa (rv3780) is a novel ring-shaped interactor of the mycobacterial proteasome. PLoS ONE, 9(12), e114348-e114348. doi:10.1371/journal.pone.0114348

Dubiel, W., Pratt, G., Ferrell, K., & Rechsteiner, M. (1992). Purification of an 11 S regulator of the multicatalytic protease. J Biol Chem, 267(31), 22369-22377.

Fehlker, M., Wendler, P., Lehmann, A., & Enenkel, C. (2003). Blm3 is part of nascent proteasomes and is involved in a late stage of nuclear proteasome assembly. EMBO Rep, 4(10), 959-963. doi:10.1038/sj.embor.embor938[pii]

Finley, D., Ulrich, H. D., Sommer, T., & Kaiser, P. (2012). The ubiquitin-proteasome system of Saccharomyces cerevisiae. Genetics, 192(2), 319-360. doi:10.1534/genetics.112.140467192/2/319 [pii]

Forster, A., Masters, E. I., Whitby, F. G., Robinson, H., & Hill, C. P. (2005). The 1.9 A structure of a proteasome-11S activator complex and implications for proteasome-PAN/PA700 interactions. Mol Cell, 18(5), 589-599. doi:S1097-2765(05)01279-7 [pii]10.1016/j.molcel.2005.04.016

Frankenberg, R. J., Hsu, T. S., Yakota, H., Kim, R., & Clark, D. S. (2001). Chemical denaturation and elevated folding temperatures are required for wild-type activity and stability of recombinant Methanococcus jannaschii 20S proteasome. Protein Sci, 10(9), 1887-1896. doi:10.1110/ps.ps.05801

Frankland-Searby, S., & Bhaumik, S. R. (2012). The 26S proteasome complex: an attractive target for cancer therapy. Biochim Biophys Acta, 1825(1), 64-76. doi:10.1016/j.bbcan.2011.10.003

Frentzel, S., Pesold-Hurt, B., Seelig, A., & Kloetzel, P. M. (1994). 20 S proteasomes are assembled via distinct precursor complexes. Processing of LMP2 and LMP7 proproteins takes place in 13-16 S preproteasome complexes. J Mol Biol, 236(4), 975-981. doi:0022-2836(94)90003-5 [pii]

Funakoshi, M., Li, X., Velichutina, I., Hochstrasser, M., & Kobayashi, H. (2004). Sem1, the yeast ortholog of a human BRCA2-binding protein, is a component of the proteasome regulatory particle that enhances proteasome stability. J Cell Sci, 117(Pt 26), 6447-6454. doi:jcs.01575 [pii]10.1242/jcs.01575

Gaczynska, M., Rock, K. L., & Goldberg, A. L. (1993). Gamma-interferon and expression of MHC genes regulate peptide hydrolysis by proteasomes. Nature, 365(6443), 264-267. doi:10.1038/365264a0

Gerards, W. L., de Jong, W. W., Bloemendal, H., & Boelens, W. (1998). The human proteasomal subunit HsC8 induces ring formation of other alpha-type subunits. J Mol Biol, 275(1), 113-121. doi:S0022-2836(97)91429-7 [pii]10.1006/jmbi.1997.1429

Gerards, W. L., de Jong, W. W., Boelens, W., & Bloemendal, H. (1998). Structure and assembly of the 20S proteasome. Cell Mol Life Sci, 54(3), 253-262.

Gerards, W. L., Enzlin, J., Haner, M., Hendriks, I. L., Aebi, U., Bloemendal, H., & Boelens, W. (1997). The human alpha-type proteasomal subunit HsC8 forms a double ringlike structure, but does not assemble into proteasome-like particles with the beta-type subunits HsDelta or HsBPROS26. J Biol Chem, 272(15), 10080-10086.

Glickman, M. H., Rubin, D. M., Coux, O., Wefes, I., Pfeifer, G., Cjeka, Z., . . . Finley, D. (1998). A subcomplex of the proteasome regulatory particle required for ubiquitin-conjugate degradation and related to the COP9-signalosome and eIF3. Cell, 94(5), 615-623. doi:S0092-8674(00)81603-7 [pii]

Griffin, T. A., Nandi, D., Cruz, M., Fehling, H. J., Kaer, L. V., Monaco, J. J., & Colbert, R. A. (1998). Immunoproteasome assembly: cooperative incorporation of interferon gamma (IFN-gamma)-inducible subunits. J Exp Med, 187(1), 97-104.

Griffin, T. A., Slack, J. P., McCluskey, T. S., Monaco, J. J., & Colbert, R. A. (2000). Identification of proteassemblin, a mammalian homologue of the yeast protein, Ump1p, that is required for normal proteasome assembly. Mol Cell Biol Res Commun, 3(4), 212-217. doi:10.1006/mcbr.2000.0213S1522472400902137 [pii]

Groettrup, M., Standera, S., Stohwasser, R., & Kloetzel, P. M. (1997). The subunits MECL-1 and LMP2 are mutually required for incorporation into the 20S proteasome. Proc Natl Acad Sci U S A, 94(17), 8970-8975.

Groll, M., Bajorek, M., Kohler, A., Moroder, L., Rubin, D. M., Huber, R., . . . Finley, D. (2000). A gated channel into the proteasome core particle. Nat Struct Biol, 7(11), 1062-1067. doi:10.1038/80992

Groll, M., Brandstetter, H., Bartunik, H., Bourenkow, G., & Huber, R. (2003). Investigations on the maturation and regulation of archaebacterial proteasomes. J Mol Biol, 327(1), 75-83. doi:S0022283603000809 [pii]

Groll, M., Ditzel, L., Lowe, J., Stock, D., Bochtler, M., Bartunik, H. D., & Huber, R. (1997). Structure of 20S proteasome from yeast at 2.4 A resolution. Nature, 386(6624), 463-471. doi:10.1038/386463a0

Guillaume, B., Chapiro, J., Stroobant, V., Colau, D., Van Holle, B., Parvizi, G., . . . Van den Eynde, B. J. (2010). Two abundant proteasome subtypes that uniquely process some antigens presented by HLA class I molecules. Proc Natl Acad Sci U S A, 107(43), 18599-18604. doi:1009778107 [pii]10.1073/pnas.1009778107

Hammack, L. (2017). 20S Proteasome Assembly: Alternative Pathways and Complexes, PhD Dissertation. Indiana University Purdue University Indianapolis (IUPUI).

Hammack, L. J., Firestone, K., Chang, W., & Kusmierczyk, A. R. (2017). Molecular chaperones of the Hsp70 family assist in the assembly of 20S proteasomes. Biochem Biophys Res Commun, 486(2), 438-443. doi:10.1016/j.bbrc.2017.03.059

Hammack, L. J., & Kusmierczyk, A. R. Assembly of proteasome subunits into non-canonical complexes in vivo. Biochem Biophys Res Commun. doi:http://dx.doi.org/10.1016/j.bbrc.2016.11.024

Hammack, L. J., & Kusmierczyk, A. R. (2017). Assembly of proteasome subunits into non-canonical complexes in vivo. Biochem Biophys Res Commun, 482(1), 164-169. doi:10.1016/j.bbrc.2016.11.024

Hammack, L. J., & Kusmierczyk, A. R. (2017). Assembly of proteasome subunits into non-canonical complexes in vivo. Biochem Biophys Res Commun. doi:http://dx.doi.org/10.1016/j.bbrc.2016.11.024

Hanssum, A., Zhong, Z., Rousseau, A., Krzyzosiak, A., Sigurdardottir, A., & Bertolotti, A. (2014). An inducible chaperone adapts proteasome assembly to stress. Mol Cell, 55(4), 566-577. doi:10.1016/j.molcel.2014.06.017

Hatanaka, A., Chen, B., Sun, J. Q., Mano, Y., Funakoshi, M., Kobayashi, H., . . . Oki, M. (2011). Fub1p, a novel protein isolated by boundary screening, binds the proteasome complex. Genes Genet Syst, 86(5), 305-314.

Heinemeyer, W., Fischer, M., Krimmer, T., Stachon, U., & Wolf, D. H. (1997). The active sites of the eukaryotic 20 S proteasome and their involvement in subunit precursor processing. J Biol Chem, 272(40), 25200-25209.

Hendil, K. B., Khan, S., & Tanaka, K. (1998). Simultaneous binding of PA28 and PA700 activators to 20 S proteasomes. Biochem J, 332 (Pt 3), 749-754.

Hendil, K. B., Kriegenburg, F., Tanaka, K., Murata, S., Lauridsen, A. M., Johnsen, A. H., & Hartmann-Petersen, R. (2009). The 20S proteasome as an assembly platform for the 19S regulatory complex. J Mol Biol, 394(2), 320-328. doi:S0022-2836(09)01165-6 [pii]10.1016/j.jmb.2009.09.038

Hill, C. P., Masters, E. I., & Whitby, F. G. (2002). The 11S regulators of 20S proteasome activity. Curr Top Microbiol Immunol, 268, 73-89.

Hirano, Y., Hayashi, H., Iemura, S., Hendil, K. B., Niwa, S., Kishimoto, T., . . . Murata, S. (2006). Cooperation of multiple chaperones required for the assembly of mammalian 20S proteasomes. Mol Cell, 24(6), 977-984. doi:S1097-2765(06)00786-6 [pii]10.1016/j.molcel.2006.11.015

Hirano, Y., Hendil, K. B., Yashiroda, H., Iemura, S., Nagane, R., Hioki, Y., . . . Murata, S. (2005). A heterodimeric complex that promotes the assembly of mammalian 20S proteasomes. Nature, 437(7063), 1381-1385. doi:nature04106 [pii]10.1038/nature04106

Hirano, Y., Kaneko, T., Okamoto, K., Bai, M., Yashiroda, H., Furuyama, K., . . . Murata, S. (2008). Dissecting beta-ring assembly pathway of the mammalian 20S proteasome. EMBO J, 27(16), 2204-2213. doi:emboj2008148 [pii]10.1038/emboj.2008.148

Hochstrasser, M. (1996). Ubiquitin-dependent protein degradation. Annu Rev Genet, 30, 405-439. doi:10.1146/annurev.genet.30.1.405

Hochstrasser, M., Deng, M., Kusmierczyk, A. R., Li, X., Kreft, S. G., Ravid, T., . . . Xie, Y. (2008). Molecular genetics of the ubiquitin-proteasome system: lessons from yeast. Ernst Schering Found Symp Proc(1), 41-66.

Howell, L., Tomko Jr, R., & Kusmierczyk, A. (2017). Putting it all together: intrinsic and extrinsic mechanisms governing proteasome biogenesis.

Hu, G., Lin, G., Wang, M., Dick, L., Xu, R. M., Nathan, C., & Li, H. (2006). Structure of the Mycobacterium tuberculosis proteasome and mechanism of inhibition by a peptidyl boronate. Mol Microbiol, 59(5), 1417-1428. doi:10.1111/j.1365-2958.2005.05036.x

Huang, X., Luan, B., Wu, J., & Shi, Y. (2016). An atomic structure of the human 26S proteasome. Nat Struct Mol Biol, 23(9), 778-785. doi:10.1038/nsmb.3273

Huber, E. M., Basler, M., Schwab, R., Heinemeyer, W., Kirk, C. J., Groettrup, M., & Groll, M. (2012). Immuno- and constitutive proteasome crystal structures reveal differences in substrate and inhibitor specificity. Cell, 148(4), 727-738. doi:10.1016/j.cell.2011.12.030

Huber, E. M., & Groll, M. (2017). The Mammalian Proteasome Activator PA28 Forms an Asymmetric alpha4beta3 Complex. Structure, 25(10), 1473-1480.e1473. doi:10.1016/j.str.2017.07.013

Humbard, M. A., Zhou, G., & Maupin-Furlow, J. A. (2009). The N-terminal penultimate residue of 20S proteasome alpha1 influences its N(alpha) acetylation and protein levels as well as growth rate and stress responses of Haloferax volcanii. J Bacteriol, 191(12), 3794-3803. doi:JB.00090-09 [pii]10.1128/JB.00090-09

Imajoh-Ohmi, S., Kawaguchi, T., Sugiyama, S., Tanaka, K., Omura, S., & Kikuchi, H. (1995). Lactacystin, a specific inhibitor of the proteasome, induces apoptosis in human monoblast U937 cells. Biochem Biophys Res Commun, 217(3), 1070-1077.

Ishii, K., Noda, M., Yagi, H., Thammaporn, R., Seetaha, S., Satoh, T., . . . Uchiyama, S. (2015). Disassembly of the self-assembled, double-ring structure of proteasome alpha7 homo-tetradecamer by alpha6. Sci Rep, 5, 18167. doi:10.1038/srep18167

Jager, S., Groll, M., Huber, R., Wolf, D. H., & Heinemeyer, W. (1999). Proteasome beta-type subunits: unequal roles of propeptides in core particle maturation and a hierarchy of active site function. J Mol Biol, 291(4), 997-1013. doi:10.1006/jmbi.1999.2995S0022-2836(99)92995-9 [pii]

Jastrab, J. B., Wang, T., Murphy, J. P., Bai, L., Hu, K., Merkx, R., . . . Darwin, K. H. (2015). An adenosine triphosphate-independent proteasome activator contributes to the virulence of Mycobacterium tuberculosis. Proceedings of the National Academy of Sciences, 112(14), E1763-E1772. doi:10.1073/pnas.1423319112

Jung, T., Catalgol, B., & Grune, T. (2009). The proteasomal system. Mol Aspects Med, 30(4), 191-296. doi:10.1016/j.mam.2009.04.001

Kane, R. C., Farrell, A. T., Sridhara, R., & Pazdur, R. (2006). United States Food and Drug Administration approval summary: bortezomib for the treatment of progressive multiple myeloma after one prior therapy. Clin Cancer Res, 12(10), 2955-2960. doi:10.1158/1078-0432.ccr-06-0170

Kaur, G., & Batra, S. (2016). Emerging role of immunoproteasomes in pathophysiology. Immunol Cell Biol, 94(9), 812-820. doi:10.1038/icb.2016.50

Kingsbury, D. J., Griffin, T. A., & Colbert, R. A. (2000). Novel propeptide function in 20 S proteasome assembly influences beta subunit composition. J Biol Chem, 275(31), 24156-24162. doi:10.1074/jbc.M001742200 [pii]

Klare, N., Seeger, M., Janek, K., Jungblut, P. R., & Dahlmann, B. (2007). Intermediate-type 20 S proteasomes in HeLa cells: "asymmetric" subunit composition, diversity and adaptation. J Mol Biol, 373(1), 1-10. doi:10.1016/j.jmb.2007.07.038

Knowlton, J. R., Johnston, S. C., Whitby, F. G., Realini, C., Zhang, Z., Rechsteiner, M., & Hill, C. P. (1997). Structure of the proteasome activator REGalpha (PA28alpha). Nature, 390(6660), 639-643. doi:10.1038/37670

Kock, M., Nunes, M. M., Hemann, M., Kube, S., Dohmen, R. J., Herzog, F., . . . Wendler, P. (2015). Proteasome assembly from 15S precursors involves major conformational changes and recycling of the Pba1-Pba2 chaperone. Nat Commun, 6, 6123. doi:10.1038/ncomms7123

Komander, D., & Rape, M. (2012). The ubiquitin code. Annu Rev Biochem, 81, 203-229. doi:10.1146/annurev-biochem-060310-170328

Kuhn, D. J., Chen, Q., Voorhees, P. M., Strader, J. S., Shenk, K. D., Sun, C. M., . . . Orlowski, R. Z. (2007). Potent activity of carfilzomib, a novel, irreversible inhibitor of the ubiquitin-proteasome pathway, against preclinical models of multiple myeloma. Blood, 110(9), 3281-3290. doi:10.1182/blood-2007-01-065888

Kulathu, Y., & Komander, D. (2012). Atypical ubiquitylation - the unexplored world of polyubiquitin beyond Lys48 and Lys63 linkages. Nat Rev Mol Cell Biol, 13(8), 508-523. doi:10.1038/nrm3394

Kumoi, K., Satoh, T., Murata, K., Hiromoto, T., Mizushima, T., Kamiya, Y., . . . Kato, K. (2013). An archaeal homolog of proteasome assembly factor functions as a proteasome activator. PLoS ONE, 8(3), e60294. doi:10.1371/journal.pone.0060294PONE-D-12-23454 [pii]

Kunjappu, M. J., & Hochstrasser, M. (2013). Assembly of the 20S proteasome. Biochim Biophys Acta. doi:S0167-4889(13)00099-2 [pii]10.1016/j.bbamcr.2013.03.008

Kupperman, E., Lee, E. C., Cao, Y., Bannerman, B., Fitzgerald, M., Berger, A., . . . Bolen, J. (2010). Evaluation of the proteasome inhibitor MLN9708 in preclinical models of human cancer. Cancer Res, 70(5), 1970-1980. doi:10.1158/0008-5472.can-09-2766

Kusmierczyk, A. R., & Hochstrasser, M. (2008). Some assembly required: dedicated chaperones in eukaryotic proteasome biogenesis. Biol Chem, 389(9), 1143-1151. doi:10.1515/bc.2008.130

Kusmierczyk, A. R., Kunjappu, M. J., Funakoshi, M., & Hochstrasser, M. (2008). A multimeric assembly factor controls the formation of alternative 20S proteasomes. Nat Struct Mol Biol, 15(3), 237-244. doi:10.1038/nsmb.1389

Kusmierczyk, A. R., Kunjappu, M. J., Kim, R. Y., & Hochstrasser, M. (2011). A conserved 20S proteasome assembly factor requires a C-terminal HbYX motif for proteasomal precursor binding. Nat Struct Mol Biol, 18(5), 622-629. doi:10.1038/nsmb.2027

Kwon, Y. D., Nagy, I., Adams, P. D., Baumeister, W., & Jap, B. K. (2004). Crystal structures of the *Rhodococcus* proteasome with and without its pro-peptides: implications for the role of the pro-peptide in proteasome assembly. J Mol Biol, 335(1), 233-245. doi:S0022283603010623 [pii]

Lander, G. C., Estrin, E., Matyskiela, M. E., Bashore, C., Nogales, E., & Martin, A. (2012). Complete subunit architecture of the proteasome regulatory particle. Nature, 482(7384), 186-191. doi:10.1038/nature10774[pii]

Le Tallec, B., Barrault, M. B., Courbeyrette, R., Guerois, R., Marsolier-Kergoat, M. C., & Peyroche, A. (2007). 20S proteasome assembly is orchestrated by two distinct pairs of chaperones in yeast and in mammals. Mol Cell, 27(4), 660-674. doi:S1097-2765(07)00415-7 [pii]10.1016/j.molcel.2007.06.025

Lee, S. H., Moon, J. H., Yoon, S. K., & Yoon, J. B. (2012). Stable incorporation of ATPase subunits into 19 S regulatory particle of human proteasome requires nucleotide binding and C-terminal tails. J Biol Chem, 287(12), 9269-9279. doi:M111.316208 [pii]10.1074/jbc.M111.316208

Lehmann, A., Jechow, K., & Enenkel, C. (2008). Blm10 binds to pre-activated proteasome core particles with open gate conformation. EMBO Rep, 9(12), 1237-1243. doi:embor2008190 [pii]10.1038/embor.2008.190

Levin, A., Minis, A., Lalazar, G., Rodriguez, J., & Steller, H. (2018). PSMD5 Inactivation Promotes 26S Proteasome Assembly during Colorectal Tumor Progression. Cancer Research, 78(13), 3458-3468. doi:10.1158/0008-5472.can-17-2296

Li, B., Fu, J., Chen, P., Ge, X., Li, Y., Kuiatse, I., . . . Orlowski, R. Z. (2015). The Nuclear Factor (Erythroid-derived 2)-like 2 and Proteasome Maturation Protein Axis Mediate Bortezomib Resistance in Multiple Myeloma. J Biol Chem, 290(50), 29854-29868. doi:10.1074/jbc.M115.664953

Li, D., Li, H., Wang, T., Pan, H., & Lin, G. (2010). Structural basis for the assembly and gate closure mechanisms of the Mycobacterium tuberculosis 20S proteasome. EMBO J, 29(12), 2037-2047. doi:emboj201095 [pii]10.1038/emboj.2010.95

Li, G., Elder, R. T., Dubrovsky, L., Liang, D., Pushkarsky, T., Chiu, K., . . . Zhao, R. Y. (2010). HIV-1 replication through hHR23A-mediated interaction of Vpr with 26S proteasome. PLoS ONE, 5(6), e11371. doi:10.1371/journal.pone.0011371

Li, X., Kusmierczyk, A. R., Wong, P., Emili, A., & Hochstrasser, M. (2007). beta-Subunit appendages promote 20S proteasome assembly by overcoming an Ump1-dependent checkpoint. EMBO J, 26(9), 2339-2349. doi:10.1038/sj.emboj.7601681

Li, X., Li, Y., Arendt, C. S., & Hochstrasser, M. (2016). Distinct Elements in the Proteasomal beta5 Subunit Propeptide Required for Autocatalytic Processing and Proteasome Assembly. J Biol Chem, 291(4), 1991-2003. doi:10.1074/jbc.M115.677047

Li, X., Mooney, P., Zheng, S., Booth, C., Braunfeld, M. B., Gubbens, S., . . . Cheng, Y. (2013). Electron counting and beam-induced motion correction enable near atomic resolution single particle cryoEM. Nature methods, 10(6), 584-590. doi:10.1038/nmeth.2472

Lin, G., Hu, G., Tsu, C., Kunes, Y. Z., Li, H., Dick, L., . . . Nathan, C. (2006). Mycobacterium tuberculosis prcBA genes encode a gated proteasome with broad oligopeptide specificity. Mol Microbiol, 59(5), 1405-1416. doi:MMI5035 [pii]10.1111/j.1365-2958.2005.05035.x

Lowe, J., Stock, D., Jap, B., Zwickl, P., Baumeister, W., & Huber, R. (1995). Crystal structure of the 20S proteasome from the archaeon *T. acidophilum* at 3.4 A resolution. Science, 268(5210), 533-539.

Marques, A. J., Glanemann, C., Ramos, P. C., & Dohmen, R. J. (2007). The C-terminal extension of the beta7 subunit and activator complexes stabilize nascent 20 S proteasomes and promote their maturation. J Biol Chem, 282(48), 34869-34876. doi:M705836200 [pii]10.1074/jbc.M705836200

Masson, P., Andersson, O., Petersen, U. M., & Young, P. (2001). Identification and characterization of a Drosophila nuclear proteasome regulator. A homolog of human 11 S REGgamma (PA28gamma). J Biol Chem, 276(2), 1383-1390. doi:10.1074/jbc.M007379200[pii]

Maupin-Furlow, J. (2012). Proteasomes and protein conjugation across domains of life. Nat Rev Microbiol, 10(2), 100-111. doi:10.1038/nrmicro2696 [pii]

Maupin-Furlow, J. A., Aldrich, H. C., & Ferry, J. G. (1998). Biochemical characterization of the 20S proteasome from the methanoarchaeon Methanosarcina thermophila. J Bacteriol, 180(6), 1480-1487.

McNaught, K. S., & Olanow, C. W. (2006). Proteasome inhibitor-induced model of Parkinson's disease. Ann Neurol, 60(2), 243-247. doi:10.1002/ana.20936

Moreau, P. (2014). The emerging role of carfilzomib combination therapy in the management of multiple myeloma. Expert Rev Hematol, 7(2), 265-290. doi:10.1586/17474086.2014.873699

Murata, S., Takahama, Y., & Tanaka, K. (2008). Thymoproteasome: probable role in generating positively selecting peptides. Curr Opin Immunol, 20(2), 192-196. doi:10.1016/j.coi.2008.03.002

Nandi, D., Woodward, E., Ginsburg, D. B., & Monaco, J. J. (1997). Intermediates in the formation of mouse 20S proteasomes: implications for the assembly of precursor beta subunits. EMBO J, 16(17), 5363-5375. doi:10.1093/emboj/16.17.5363

Nitta, T., Kochi, Y., Muro, R., Tomofuji, Y., Okamura, T., Murata, S., . . . Takayanagi, H. (2017). Human thymoproteasome variations influence CD8 T cell selection. Sci Immunol, 2(12). doi:10.1126/sciimmunol.aan5165

Ohba, M. (1994). A 70-kDa heat shock cognate protein suppresses the defects caused by a proteasome mutation in Saccharomyces cerevisiae (Vol. 351).

Orlowski, R. Z., & Kuhn, D. J. (2008). Proteasome inhibitors in cancer therapy: lessons from the first decade. Clin Cancer Res, 14(6), 1649-1657. doi:10.1158/1078-0432.ccr-07-2218

Padmanabhan, A., Vuong, S. A.-T., & Hochstrasser, M. (2016). Assembly of an Evolutionarily Conserved Alternative Proteasome Isoform in Human Cells. Cell reports, 14(12), 2962-2974. doi:10.1016/j.celrep.2016.02.068

Panfair, D., & Kusmierczyk, A. R. (2016). Examining Proteasome Assembly with Recombinant Archaeal Proteasomes and Nondenaturing PAGE: The Case for a Combined Approach. (118), e54860. doi:doi:10.3791/54860

Panfair, D., Ramamurthy, A., & Kusmierczyk, A. R. (2015). Alpha-ring Independent Assembly of the 20S Proteasome. Scientific reports, 5.

Park, S., Roelofs, J., Kim, W., Robert, J., Schmidt, M., Gygi, S. P., & Finley, D. (2009). Hexameric assembly of the proteasomal ATPases is templated through their C termini. Nature, 459(7248), 866-870. doi:nature08065 [pii] 10.1038/nature08065

Paul, S. (2008). Dysfunction of the ubiquitin-proteasome system in multiple disease conditions: therapeutic approaches. Bioessays, 30(11-12), 1172-1184. doi:10.1002/bies.20852

Qian, M. X., Pang, Y., Liu, C. H., Haratake, K., Du, B. Y., Ji, D. Y., . . . Qiu, X. B. (2013). Acetylation-mediated proteasomal degradation of core histones during DNA repair and spermatogenesis. Cell, 153(5), 1012-1024. doi:10.1016/j.cell.2013.04.032S0092-8674(13)00508-4 [pii]

Ramamurthy, A. (2014). Investigating the early events in proteasome assembly, Master's thesis. Indiana University Purdue University Indianapolis (IUPUI).

Ramos, P. C., Hockendorff, J., Johnson, E. S., Varshavsky, A., & Dohmen, R. J. (1998). Ump1p is required for proper maturation of the 20S proteasome and becomes its substrate upon completion of the assembly. Cell, 92(4), 489-499. doi:S0092-8674(00)80942-3 [pii]

Ramos, P. C., Marques, A. J., London, M. K., & Dohmen, R. J. (2004). Role of C-terminal extensions of subunits beta2 and beta7 in assembly and activity of eukaryotic proteasomes. J Biol Chem, 279(14), 14323-14330. doi:10.1074/jbc.M308757200 [pii]

Realini, C., Dubiel, W., Pratt, G., Ferrell, K., & Rechsteiner, M. (1994). Molecular cloning and expression of a gamma-interferon-inducible activator of the multicatalytic protease. J Biol Chem, 269(32), 20727-20732.

Religa, T. L., Sprangers, R., & Kay, L. E. (2010). Dynamic regulation of archaeal proteasome gate opening as studied by TROSY NMR. Science, 328(5974), 98-102. doi:328/5974/98 [pii]10.1126/science.1184991

Sa-Moura, B., Funakoshi, M., Tomko, R. J., Jr., Dohmen, R. J., Wu, Z., Peng, J., & Hochstrasser, M. (2013). A conserved protein with AN1 zinc finger and ubiquitin-like domains modulates Cdc48 (p97) function in the ubiquitin-proteasome pathway. J Biol Chem, 288(47), 33682-33696. doi:10.1074/jbc.M113.521088

Sadre-Bazzaz, K., Whitby, F. G., Robinson, H., Formosa, T., & Hill, C. P. (2010). Structure of a Blm10 complex reveals common mechanisms for proteasome binding and gate opening. Mol Cell, 37(5), 728-735. doi:S1097-2765(10)00116-4 [pii]10.1016/j.molcel.2010.02.002

Saeki, Y., & Tanaka, K. (2012). Assembly and function of the proteasome. Methods Mol Biol, 832, 315-337. doi:10.1007/978-1-61779-474-2_22

Schmidt, M., & Finley, D. (2014). Regulation of proteasome activity in health and disease. Biochim Biophys Acta, 1843(1), 13-25. doi:10.1016/j.bbamcr.2013.08.012

Schmidt, M., Haas, W., Crosas, B., Santamaria, P. G., Gygi, S. P., Walz, T., & Finley, D. (2005). The HEAT repeat protein Blm10 regulates the yeast proteasome by capping the core particle. Nat Struct Mol Biol, 12(4), 294-303. doi:nsmb914 [pii]10.1038/nsmb914

Schmidtke, G., Kraft, R., Kostka, S., Henklein, P., Frommel, C., Lowe, J., . . . Schmidt, M. (1996). Analysis of mammalian 20S proteasome biogenesis: the maturation of beta-subunits is an ordered two-step mechanism involving autocatalysis. EMBO J, 15(24), 6887-6898.

Schreiner, P., Chen, X., Husnjak, K., Randles, L., Zhang, N., Elsasser, S., . . . Groll, M. (2008). Ubiquitin docking at the proteasome through a novel pleckstrin-homology domain interaction. Nature, 453(7194), 548-552. doi:nature06924 [pii]10.1038/nature06924

Schweitzer, A., Aufderheide, A., Rudack, T., Beck, F., Pfeifer, G., Plitzko, J. M., . . . Baumeister, W. (2016). Structure of the human 26S proteasome at a resolution of 3.9 Å. Proceedings of the National Academy of Sciences, 113(28), 7816-7821. doi:10.1073/pnas.1608050113

Seemuller, E., Lupas, A., & Baumeister, W. (1996). Autocatalytic processing of the 20S proteasome. Nature, 382(6590), 468-471. doi:10.1038/382468a0

Sharon, M., Witt, S., Glasmacher, E., Baumeister, W., & Robinson, C. V. (2007). Mass spectrometry reveals the missing links in the assembly pathway of the bacterial 20 S proteasome. J Biol Chem, 282(25), 18448-18457. doi:M701534200 [pii]10.1074/jbc.M701534200

Shinohara, K., Tomioka, M., Nakano, H., Tone, S., Ito, H., & Kawashima, S. (1996). Apoptosis induction resulting from proteasome inhibition. Biochem J, 317 (Pt 2), 385-388.

Sikdar, A., Satoh, T., Kawasaki, M., & Kato, K. (2014). Crystal structure of archaeal homolog of proteasome-assembly chaperone PbaA. Biochem Biophys Res Commun, 453(3), 493-497. doi:10.1016/j.bbrc.2014.09.114

Stadtmueller, B. M., & Hill, C. P. (2011). Proteasome activators. Mol Cell, 41(1), 8-19. doi:S1097-2765(10)01005-1 [pii]10.1016/j.molcel.2010.12.020

Stadtmueller, B. M., Kish-Trier, E., Ferrell, K., Petersen, C. N., Robinson, H., Myszka, D. G., . . . Hill, C. P. (2012). Structure of a proteasome Pba1-Pba2 complex: implications for proteasome assembly, activation, and biological function. J Biol Chem, 287(44), 37371-37382. doi:10.1074/jbc.M112.367003[pii]

Striebel, F., Hunkeler, M., Summer, H., & Weber-Ban, E. (2010). The mycobacterial Mpa-proteasome unfolds and degrades pupylated substrates by engaging Pup's N-terminus. EMBO J, 29(7), 1262-1271. doi:emboj201023 [pii]10.1038/emboj.2010.23

Takagi, K., Saeki, Y., Yashiroda, H., Yagi, H., Kaiho, A., Murata, S., . . . Kato, K. (2014). Pba3-Pba4 heterodimer acts as a molecular matchmaker in proteasome alpha-ring formation. Biochem Biophys Res Commun, 450(2), 1110-1114. doi:10.1016/j.bbrc.2014.06.119

Takeuchi, J., Chen, H., Hoyt, M. A., & Coffino, P. (2008). Structural elements of the ubiquitin-independent proteasome degron of ornithine decarboxylase. Biochem J, 410(2), 401-407. doi:BJ20071239 [pii]10.1042/BJ20071239

Tamura, T., Nagy, I., Lupas, A., Lottspeich, F., Cejka, Z., Schoofs, G., . . . Baumeister, W. (1995). The first characterization of a eubacterial proteasome: the 20S complex of *Rhodococcus*. Curr Biol, 5(7), 766-774. doi:S0960-9822(95)00153-9 [pii]

Tanahashi, N., Murakami, Y., Minami, Y., Shimbara, N., Hendil, K. B., & Tanaka, K. (2000). Hybrid proteasomes. Induction by interferon-gamma and contribution to ATP-dependent proteolysis. J Biol Chem, 275(19), 14336-14345.

Tanaka, K. (1994). Role of proteasomes modified by interferon-gamma in antigen processing. J Leukoc Biol, 56(5), 571-575.

Teicher, B. A., & Tomaszewski, J. E. (2015). Proteasome inhibitors. Biochem Pharmacol, 96(1), 1-9. doi:10.1016/j.bcp.2015.04.008

Thompson, D., Hakala, K., & DeMartino, G. N. (2009). Subcomplexes of PA700, the 19 S regulator of the 26 S proteasome, reveal relative roles of AAA subunits in 26 S proteasome assembly and activation and ATPase activity. J Biol Chem, 284(37), 24891-24903. doi:M109.023218 [pii]10.1074/jbc.M109.023218

Tian, G., Park, S., Lee, M. J., Huck, B., McAllister, F., Hill, C. P., . . . Finley, D. (2011). An asymmetric interface between the regulatory and core particles of the proteasome. Nat Struct Mol Biol, 18(11), 1259-1267. doi:10.1038/nsmb.2147 [pii]

Tomko, R. J., Jr., & Hochstrasser, M. (2013). Molecular architecture and assembly of the eukaryotic proteasome. Annu Rev Biochem, 82, 415-445. doi:10.1146/annurev-biochem-060410-150257

Treise, I., Huber, E. M., Klein-Rodewald, T., Heinemeyer, W., Grassmann, S. A., Basler, M., . . . Busch, D. H. (2018). Defective immuno- and thymoproteasome assembly causes severe immunodeficiency. Sci Rep, 8(1), 5975. doi:10.1038/s41598-018-24199-0

Uechi, H., Hamazaki, J., & Murata, S. (2014). Characterization of the testis-specific proteasome subunit alpha4s in mammals. J Biol Chem, 289(18), 12365-12374. doi:10.1074/jbc.M114.558866

Unno, M., Mizushima, T., Morimoto, Y., Tomisugi, Y., Tanaka, K., Yasuoka, N., & Tsukihara, T. (2002a). Structure determination of the constitutive 20S proteasome from bovine liver at 2.75 A resolution. J Biochem, 131(2), 171-173.

Unno, M., Mizushima, T., Morimoto, Y., Tomisugi, Y., Tanaka, K., Yasuoka, N., & Tsukihara, T. (2002b). The structure of the mammalian 20S proteasome at 2.75 A resolution. Structure, 10(5), 609-618. doi:S0969212602007487 [pii]

Ustrell, V., Hoffman, L., Pratt, G., & Rechsteiner, M. (2002). PA200, a nuclear proteasome activator involved in DNA repair. EMBO J, 21(13), 3516-3525. doi:10.1093/emboj/cdf333

Ustrell, V., Pratt, G., Gorbea, C., & Rechsteiner, M. (2005). Purification and assay of proteasome activator PA200. Methods Enzymol, 398, 321-329. doi:S0076-6879(05)98026-9 [pii]10.1016/S0076-6879(05)98026-9

Varambally, S., Cao, Q., Mani, R. S., Shankar, S., Wang, X., Ateeq, B., . . . Chinnaiyan, A. M. (2008). Genomic loss of microRNA-101 leads to overexpression of histone methyltransferase EZH2 in cancer. Science, 322(5908), 1695-1699. doi:10.1126/science.1165395

Varshavsky, A. (2012). The Ubiquitin System, an Immense Realm. Annual Review of Biochemistry, 81(1), 167-176. doi:10.1146/annurev-biochem-051910-094049

Velichutina, I., Connerly, P. L., Arendt, C. S., Li, X., & Hochstrasser, M. (2004). Plasticity in eucaryotic 20S proteasome ring assembly revealed by a subunit deletion in yeast. EMBO J, 23(3), 500-510. doi:10.1038/sj.emboj.7600059[pii]

Vinitsky, A., Cardozo, C., Sepp-Lorenzino, L., Michaud, C., & Orlowski, M. (1994). Inhibition of the proteolytic activity of the multicatalytic proteinase complex (proteasome) by substrate-related peptidyl aldehydes. J Biol Chem, 269(47), 29860-29866.

Volker, C., & Lupas, A. N. (2002). Molecular evolution of proteasomes. Curr Top Microbiol Immunol, 268, 1-22.

Walerych, D., Lisek, K., Sommaggio, R., Piazza, S., Ciani, Y., Dalla, E., . . . Del Sal, G. (2016). Proteasome machinery is instrumental in a common gain-of-function program of the p53 missense mutants in cancer. Nat Cell Biol, 18(8), 897-909. doi:10.1038/ncb3380

Wani, P. S., Rowland, M. A., Ondracek, A., Deeds, E. J., & Roelofs, J. (2015). Maturation of the proteasome core particle induces an affinity switch that controls regulatory particle association. Nat Commun, 6, 6384. doi:10.1038/ncomms7384

Weberruss, M. H., Savulescu, A. F., Jando, J., Bissinger, T., Harel, A., Glickman, M. H., & Enenkel, C. (2013). Blm10 facilitates nuclear import of proteasome core particles. EMBO J. doi:10.1038/emboj.2013.192[pii]

Wilk, S., Chen, W. E., & Magnusson, R. P. (2000). Properties of the beta subunit of the proteasome activator PA28 (11S REG). Arch Biochem Biophys, 384(1), 174-180. doi:S0003-9861(00)92112-X [pii]10.1006/abbi.2000.2112

Williamson, J. R. (2008). Cooperativity in macromolecular assembly. Nat Chem Biol, 4(8), 458-465. doi:10.1038/nchembio.102[pii]

Wilson, H. L., Ou, M. S., Aldrich, H. C., & Maupin-Furlow, J. (2000). Biochemical and physical properties of the Methanococcus jannaschii 20S proteasome and PAN, a homolog of the ATPase (Rpt) subunits of the eucaryal 26S proteasome. J Bacteriol, 182(6), 1680-1692.

Witt, E., Zantopf, D., Schmidt, M., Kraft, R., Kloetzel, P. M., & Kruger, E. (2000). Characterisation of the newly identified human Ump1 homologue POMP and analysis of LMP7(beta 5i) incorporation into 20 S proteasomes. J Mol Biol, 301(1), 1-9. doi:10.1006/jmbi.2000.3959S0022-2836(00)93959-7 [pii]

Witt, S., Kwon, Y. D., Sharon, M., Felderer, K., Beuttler, M., Robinson, C. V., . . . Jap, B. K. (2006). Proteasome assembly triggers a switch required for active-site maturation. Structure, 14(7), 1179-1188. doi:S0969-2126(06)00258-9 [pii]10.1016/j.str.2006.05.019

Wolf, S., Nagy, I., Lupas, A., Pfeifer, G., Cejka, Z., Muller, S. A., . . . Baumeister, W. (1998). Characterization of ARC, a divergent member of the AAA ATPase family from *Rhodococcus* erythropolis. J Mol Biol, 277(1), 13-25. doi:10.1006/jmbi.1997.1589

Yao, Y., Toth, C. R., Huang, L., Wong, M. L., Dias, P., Burlingame, A. L., . . . Wang, C. C. (1999). alpha5 subunit in Trypanosoma brucei proteasome can self-assemble to form a cylinder of four stacked heptamer rings. Biochem J, 344 Pt 2, 349-358.

Yashiroda, H., Mizushima, T., Okamoto, K., Kameyama, T., Hayashi, H., Kishimoto, T., . . . Tanaka, K. (2008). Crystal structure of a chaperone complex that contributes to the assembly of yeast 20S proteasomes. Nat Struct Mol Biol, 15(3), 228-236. doi:nsmb.1386 [pii]10.1038/nsmb.1386

Yashiroda, H., Toda, Y., Otsu, S., Takagi, K., Mizushima, T., & Murata, S. (2015). N-terminal alpha7 deletion of the proteasome 20S core particle substitutes for yeast PI31 function. Mol Cell Biol, 35(1), 141-152. doi:10.1128/mcb.00582-14

Yu, Z., Livnat-Levanon, N., Kleifeld, O., Mansour, W., Nakasone, M. A., Castaneda, C. A., . . . Glickman, M. H. (2015). Base-CP proteasome can serve as a platform for stepwise lid formation. Biosci Rep. doi:10.1042/BSR20140173

Zhang, X., Schulz, R., Edmunds, S., Kruger, E., Markert, E., Gaedcke, J., . . . Dobbelstein, M. (2015). MicroRNA-101 Suppresses Tumor Cell Proliferation by Acting as an Endogenous Proteasome Inhibitor via Targeting the Proteasome Assembly Factor POMP. Mol Cell, 59(2), 243-257. doi:10.1016/j.molcel.2015.05.036

Zhong, L., & Belote, J. M. (2007). The testis-specific proteasome subunit Prosalpha6T of D. melanogaster is required for individualization and nuclear maturation during spermatogenesis. Development, 134(19), 3517-3525. doi:dev.004770 [pii]10.1242/dev.004770

Zimmerman, S. B., & Trach, S. O. (1991). Estimation of macromolecule concentrations and excluded volume effects for the cytoplasm of *Escherichia coli*. J Mol Biol, 222(3), 599-620.

Zuhl, F., Seemuller, E., Golbik, R., & Baumeister, W. (1997). Dissecting the assembly pathway of the 20S proteasome. FEBS Lett, 418(1-2), 189-194. doi:S0014-5793(97)01370-7 [pii]

Zuhl, F., Tamura, T., Dolenc, I., Cejka, Z., Nagy, I., De Mot, R., & Baumeister, W. (1997). Subunit topology of the *Rhodococcus* proteasome. FEBS Lett, 400(1), 83-90. doi:S0014-5793(96)01403-2 [pii]

Zwickl, P., Kleinz, J., & Baumeister, W. (1994). Critical elements in proteasome assembly. Nat Struct Biol, 1(11), 765-770.

Zwickl, P., Ng, D., Woo, K. M., Klenk, H. P., & Goldberg, A. L. (1999). An archaebacterial ATPase, homologous to ATPases in the eukaryotic 26 S proteasome, activates protein breakdown by 20 S proteasomes. J Biol Chem, 274(37), 26008-26014.

Zwickl, P., Voges, D., & Baumeister, W. (1999). The proteasome: a macromolecular assembly designed for controlled proteolysis. Philos Trans R Soc Lond B Biol Sci, 354(1389), 1501-1511. doi:10.1098/rstb.1999.0494

APPENDIX A. SUPPLEMENTARY FOR CHAPTER 2

Supplementary Note

On the function of β subunit propeptides (Kusmierczyk et al., 2011)

In Figure 2.5, we demonstrate that the archaeal β subunit propeptide is dispensable for CP assembly even when archaeal α subunits cannot form rings; assembly occurs with comparable efficiency with or without the propeptide. The bacterial β subunit propeptide is also not required for CP assembly (Lin et al., 2006; Zuhl, Seemuller, et al., 1997) hence the dispensable nature of the propeptide is conserved in archaeal and bacterial CP assembly. However, this is not to argue that the purpose of the propeptide is identical in both. A number of differences are worth discussing.

The cis α-α subunit interface in bacterial proteasomes is much smaller than in eukaryotic/archaeal counterparts (Hu et al., 2006; Kwon et al., 2004). This likely contributes to the inability of bacterial α subunits to form stable α rings on their own (Zuhl, Seemuller, et al., 1997), though dimers and trimers are apparently possible (Sharon et al., 2007). Consequently, bacterial β subunit propeptides are large in part to provide this missing contact surface and function as a "glue" to stabilize bacterial α-rings (Kwon et al., 2004). Consistent with this, in the absence of the β subunit propeptide, assembly of CP from *Rhodococcus erythropolis* is very inefficient (Zuhl, Seemuller, et al., 1997). Interestingly, assembly of CP from *Mycobacterium tuberculosis* is not affected by the absence of its corresponding propeptide (Lin et al., 2006). This argues that the "glue" function, while important, likely cannot be the only role for a bacterial β subunit propeptide in assembly. The visualization of the *Mycobacterium* propeptides outside (and below) the α-ring in a half proteasome (G. Li et al., 2010), and their ability to negatively impact assembly (Lin et al., 2006), are consistent with this view.

Unlike bacterial propeptides, archaeal β subunit propeptides are much shorter. Clearly, the "glue" function is not required by archaeal proteasomes since their α subunits can form stable α-rings independently. Also, archaeal β subunit propeptides are completely dispensable for assembly (J. A. Maupin-Furlow et al., 1998; Wilson et al., 2000; Zwickl et al., 1994). Our data suggests that

assembly is equally efficient in their presence or absence, even when archaeal α subunits cannot form rings. So, what is their role? One possible function is to ensure that the active site threonine is only exposed upon completion of assembly where it is safely enclosed within the central cavity. Numerous observations, for proteasomes from all three domains of life, that propeptide processing is coupled to assembly support this view (P. Chen & Hochstrasser, 1996; D. Li et al., 2010; Schmidtke et al., 1996; Seemuller, Lupas, & Baumeister, 1996; Sharon et al., 2007; S. Witt et al., 2006). Related to this function is the finding that the active site threonine can also be inactivated by N-acetylation if exposed to the cytosolic milieu (Arendt & Hochstrasser, 1999); a propeptide would again serve in a protective role until assembly is nearly complete. A third possible function is that propeptides can allosterically convey assembly status. A previous report demonstrated the ability of PbaA, the putative archaeal ortholog of the Pba1-Pba2 assembly factor that binds to the outer α-ring surface, to preferentially bind to propeptide-containing intermediates (Kusmierczyk et al., 2011). This binding became progressively weaker with increased β subunit processing and let us to propose a "safety" function for this assembly factor: by recognizing propeptide-containing intermediates, assembly factors like PbaA and Pba1-Pba2 could prevent the premature association of activators (such as PAN in archaea, or RP in eukaryotes) to incompletely assembled CP (Kusmierczyk et al., 2011). This safety function was recently confirmed for Pba1-Pba2 in yeast (Wani et al., 2015).

All three of these functions are not mutually exclusive, but all of them can be satisfied by a small propeptide like those found in archaea. Since all three of these functions reduce the incidence of undesirable events, this could help explain the non-essential nature of these propeptides, namely: assembly per se is not affected in their absence, only the incidence of (undesirable) side-reactions would increase. Most pertinent to this study, all three of these functions are compatible with an α-ring dependent and an α-ring independent assembly mechanism, both of which are shown here to be possible for the archaeal CP. Other functions beyond those suggested here are also possible and may come to light with increasing experimental evidence.

On the formation of αβ heterodimers

In Supplementary Figure 9, and the accompanying main text, we describe experiments aimed at determining if SR-independent assembly of archaeal proteasomes can proceed through the formation of αβ heterodimers. Lysate mixing was used to initiate proteasome assembly, and after 30 min, an assembly reaction was subjected to ICAR and the purified proteins loaded onto a size exclusion column. Fractions 15 to 18 contained coeluting α and β subunits and corresponded to assembled proteasomes (and other large species). Fractions 25 to 30 also contained coeluting α and β subunits and we present arguments in the main text supporting our claim that these fractions could contain the putative αβ heterodimers. Here, we put forth additional arguments based on our data to support this claim.

First, the overlap between the nonR peak of α-his subunits and the presence of β subunits in fractions 25 to 30 would be expected given that nonR species (i.e. mostly free α subunits) are the immediate precursor to αβ heterodimers. Second, the only way β subunits should end up in fractions 25 to 30 (or any fractions for that matter) is via complex formation with α-his subunits because free untagged β subunits do not bind to the metal-affinity resin (ICAR purification) that immediately precedes the size exclusion separation. Finally, the elution of β subunits in fractions 25 to 30 is not observed when β subunits are fractionated on a size exclusion column in the absence of α subunits; free β subunits elute in fractions 32 to 34 (Sup Fig. 8). This shift in elution profile (from fractions 32-34 to fractions 25-30) implies a higher molecular mass and thus complex formation with α subunits.

Taken together, our data support the existence of archaeal αβ heterodimers but they also do not rule out other interpretations (i.e. heterotrimers). However, it is important to note that this lack of absolute certainty is also the case with bacterial αβ heterodimers. A mass-spectrometry analysis has provided the first, and to date the only, physical evidence of bacterial αβ heterodimer formation (Sharon et al., 2007). However, all the αβ heterodimer species identified in that study contained truncated β subunits that lacked no fewer than 25 N-terminal amino acids of the 65 amino acid propeptide (Sharon et al., 2007). The authors themselves offered an alternate explanation for these complexes as “trapped” species, not capable of assembly (Sharon et al., 2007). The formation of αβ heterodimers is the most plausible explanation for how proteasome

assembly can occur in the absence of SR formation. Nevertheless, despite data in bacteria (Kwon et al., 2004; Sharon et al., 2007; Zuhl, Seemuller, et al., 1997) and now in archaea (this study) that strongly support this view, one must allow that a bona fide heterodimer (consisting of a full length α subunit bound to a full length β subunit) functioning as an assembly-competent species remains to be unequivocally demonstrated for any proteasome.

Supplementary Table 1: Plasmids used in chapter 2

Name	Genotype	Source
AKB191	pET42 psmA-his	(Kusmierczyk et al., 2011)
AKB254	pET42 psmA (R88D)-his	This study
AKB257	pET42 psmA (K59E)-his	This study
AKB946	pET42 psmB	This study
AKB950	pET42 psmB Δpro	This study
AKB951	pET42 psmB (T1A)	This study
AKB952	pET42 psmB (R166W)	This study
AKB464	pET42 psmA-his psmB	(Kusmierczyk et al., 2011)
AKB600	pET42 psmA (Q99C)-his	This study
AKB628	pET42 psmA-his psmB Δpro	(Kusmierczyk et al., 2011)
AKB572	pET42 psmA-his psmB (T1A)	(Kusmierczyk et al., 2011)
AKB573	pET42 psmA-his psmB (R166W)	This study
AKB706	pET42 psmA (A98C)-his	This study
AKB707	pET42 psmA (M100C)-his	This study
AKB708	pET42 psmA (Δcys)-his	This study
AKB709	pET42 psmA (Q99C Δcys)-his	This study
AKB727	pET42 psmA (K59E)-his psmB	This study
AKB943	pET42 psmA (K59E)-his psmB (R166W)	This study
AKB944	pET42 psmA (K59E)-his psmB (T1A)	This study
AKB945	pET42 psmA (K59E)-his psmBΔpro	This study
AKB949	pET42 psmA (R88D)-his psmB	This study
AKB953	pET42 psmB-his	This study
AKB964	pET42 psmA (R88D)-his psmBΔpro	This study
AKB965	pET42 psmA (R88D)-his psmB (T1A)	This study
AKB966	pET42 psmA (R88D)-his psmB (R166W)	This study
AKB976	pET42 psmB (K29E)	This study
AKB988	pET42 psmB (K29E)-his	This study

psmA = α subunit from *Methanococcus maripaludis*
psmB = β subunit from *Methanococcus maripaludis*

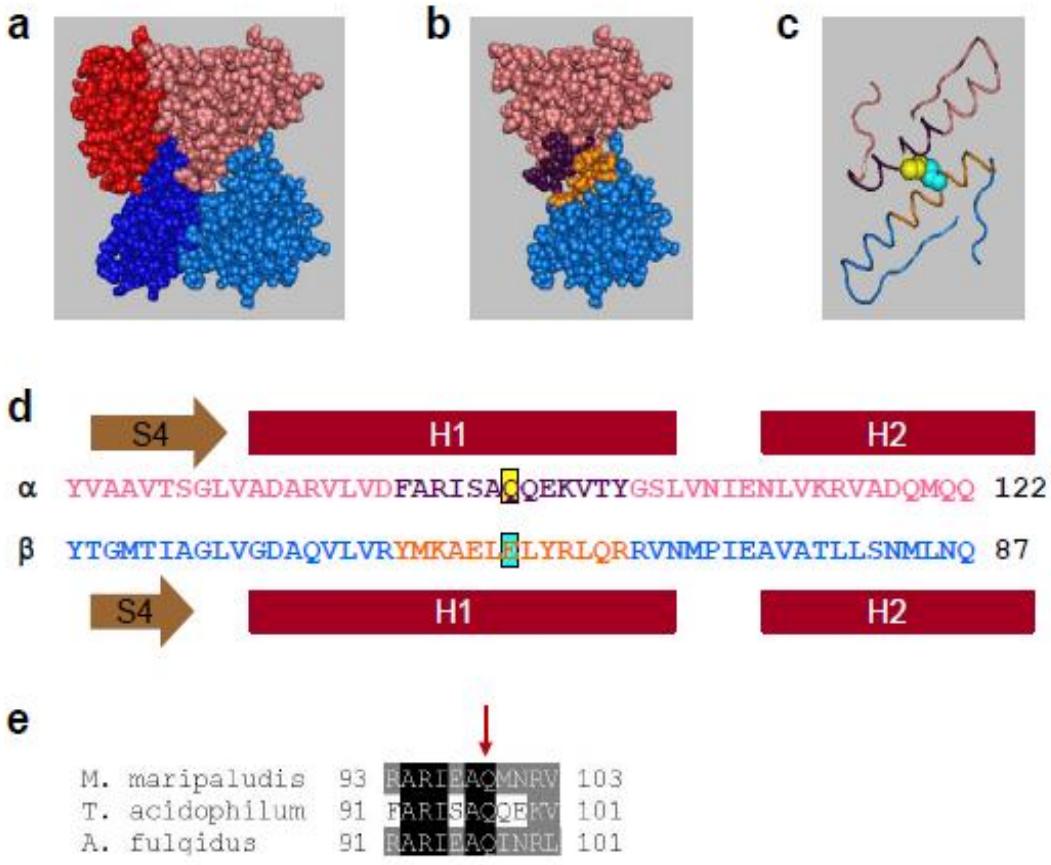

Supplementary Figure 1: The H1 helices of α and β subunits contribute to inter-ring contacts
Structural models based on the *T. acidophilum* crystal structure (1PMA) and generated with the program Cn3D. (a) Subunit contacts between two neighboring α (red/pink) and two β (blue) subunits viewed from inside the 20S cavity. (b) Subunit contacts and color scheme as in (a), with an α-β subunit pair isolated for emphasis. The C- terminal halves of helices H1 in each subunit are indicated in purple and orange. Close-up of H1 helices (c) and sequence alignment of relevant region (d) with color scheme as in (a, b). Glutamine 97 in the H1 helix of the *T. acidophilum* α subunit (yellow) is juxtaposed with the corresponding aligned residue (glutamate 62; teal) in the β subunit. Hence, if a second α subunit were to take the place of the β subunit, as hypothesized for a double α-ring, the indicated glutamine might be suitably positioned for an engineered disulfide cross-link. The equivalent position in the *M. maripaludis* α subunit is Q99 (e).

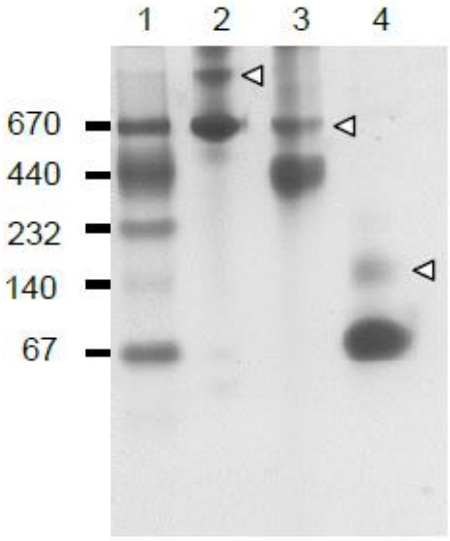

Supplementary Figure 2: Gel-induced higher order species artifacts
In order to better visualize some lower-abundance species, native gels in this study were frequently heavily loaded with protein (10–20 µg per lane). When this was done, however, one could sometimes observe higher order species migrating above the band of interest. These are identified by white arrowheads in the main Figures and they are gel-induced artifacts. Formation of gel-induced artifacts can be illustrated in the nondenaturing 4–15% gradient gel above, stained with GelCode blue. Lane 1 contains the molecular size standards used throughout this study. In lanes 2–4 (2: 670 kDa standard {Thyroglobulin}, 3: 440 kDa standard {Ferritin} and 4: 67 kDa standard {Bovine serum albumin}), some of these standards are heavily loaded and run individually. In addition to the correctly running major band, the heavily loaded samples exhibit higher order species to varying degrees (white arrowheads).

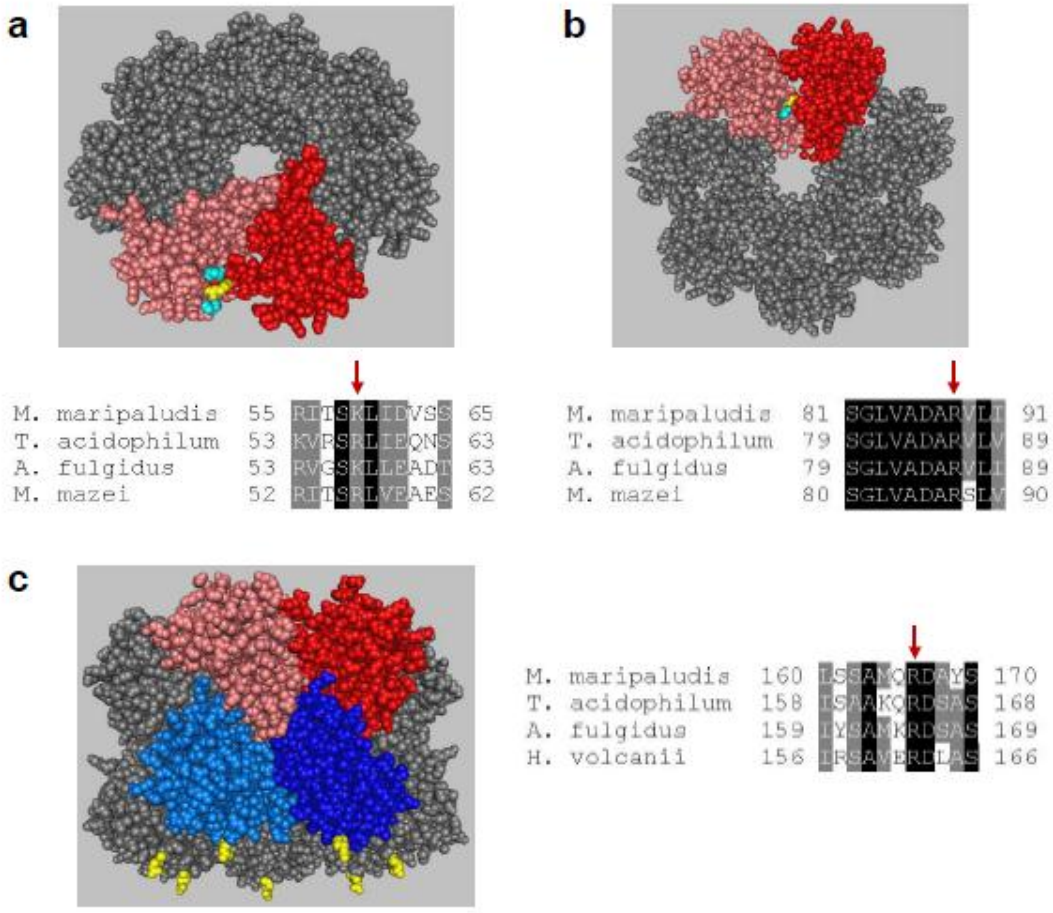

Supplementary Figure 3: Residues selected for mutagenesis

Space filling models based on the T. acidophilum crystal structure (1PMA) and generated with the program Cn3D. (a,b) Highly conserved charged residues (yellow) in one α subunit (red) are juxtaposed with highly conserved residues of opposite charge (teal) located within 5 angstroms on the neighboring α subunit (pink). (a) Top view of α-ring with R57 of T. acidophilum (yellow). The equivalent position in M. maripaludis α subunit is K59. (b) Bottom view of α-ring with R86 of T. acidophilum (yellow). The equivalent position in M. maripaludis α subunit is R88. (c) Side view of the half-proteasome, angled upward, showing highly conserved β subunit arginine 164 (yellow). Two α and β subunits are colored for reference. Numbering in the sequence alignment is based on the N-terminal catalytic threonine being assigned position1; hence in M. maripaludis the β subunit arginine is at position 166.

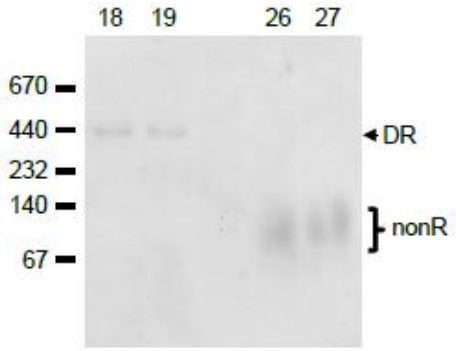

Supplementary Figure 4: The K59E mutant form some DR without apparently forming SR
Following the fractionation of the α (K59E) mutant by size exclusion chromatography (Fig. 2.2b main text), aliquots of fractions 18, 19, 26, and 27 were analyzed by native PAGE on a nondenaturing 4–15% gradient gel shown here stained with Imperial Stain This analysis confirmed the assignment of the major peak in fractions 25–28 as the nonR peak, and the minor peak in fractions 17– 19 as the DR peak (see main text). The data are consistent with the α (K59E) mutation interfering with the assembly of SR, yet still allowing some DR to form.

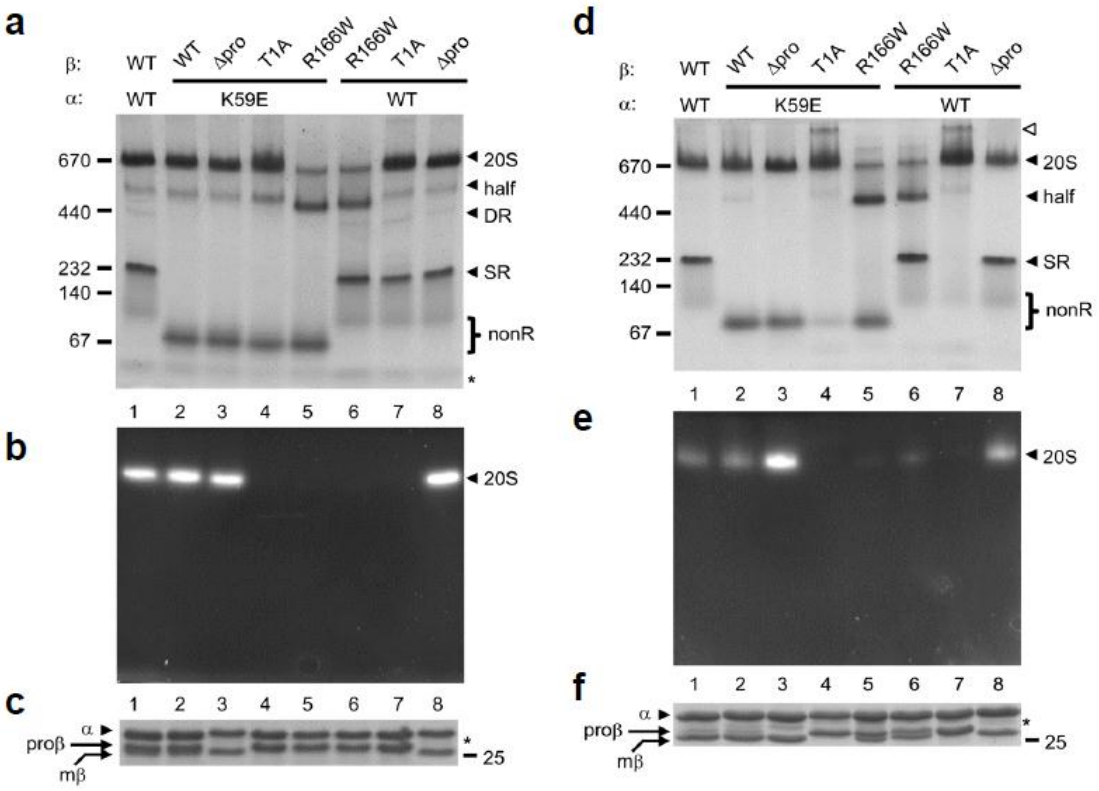

Supplementary Figure 5: Assembly of archaeal proteasomes exhibits bacterial-like features
The experiments described in the panels above use the α (K59E) mutant but are otherwise identical to those carried out with the α (R88D) mutant described in the main text (Fig. 2.5). Indeed, the Figure legend to Figure 2.5 applies here exactly, with K59E substituted for R88D. The results of this Figure support the same conclusions drawn from the main text (Fig. 2.5) namely: (i) that archaeal 20S assembly can proceed along a bacterial-like pathway, independent of SR; (ii) that this SR-independent pathway still proceeds through a half-proteasome; (iii) that the SR-independent pathway does not depend on the β subunit propeptide; and (iv) that the same conclusions could be drawn regardless of the approach, lysate mixing versus coexpression, though the latter approach results in more efficient assembly (see main text pertaining to Fig. 2.5).

As stated in the main text, there are two minor differences between lysate mixing and coexpression approaches. These differences do not affect the aforementioned conclusions, but they are worth noting here. First, in lysate mixing experiments, levels of the half proteasomes were similar within wild-type α subunit samples (Fig. 2.5a and Supplementary Fig. 5a, lanes 1, 7, 8), and within mutant samples (Fig. 2.5a and Supplementary Fig. 5a, lanes 2, 3, 4), regardless of the β subunit propeptide variant employed. By contrast, this uniformity was absent during coexpression (see corresponding lanes in Fig. 2.5d and Supplementary Fig. 5d). This was likely due to slower assembly in lysate mixing where the rate limiting step might be (i) the association of α subunits into SR and/or (ii) the association of α and β subunits into half-proteasomes.

Supplementary Figure 5 (continued)

Second, in coexpression experiments, the samples employing β (T1A) exhibited sharp decreases in SR and nonR (Fig. 2.5d and Supplementary Fig. 5d, lanes 4 and 7). By contrast, SR and nonR levels were constant in lysate mixing regardless of which β subunit variant was being used. This suggests that under coexpression conditions, where assembly is already more efficient than lysate mixing, the T1A mutant is even more efficient at interacting with free subunit, and/or SR, than a wild-type β subunit. However, the reason for this is unknown.

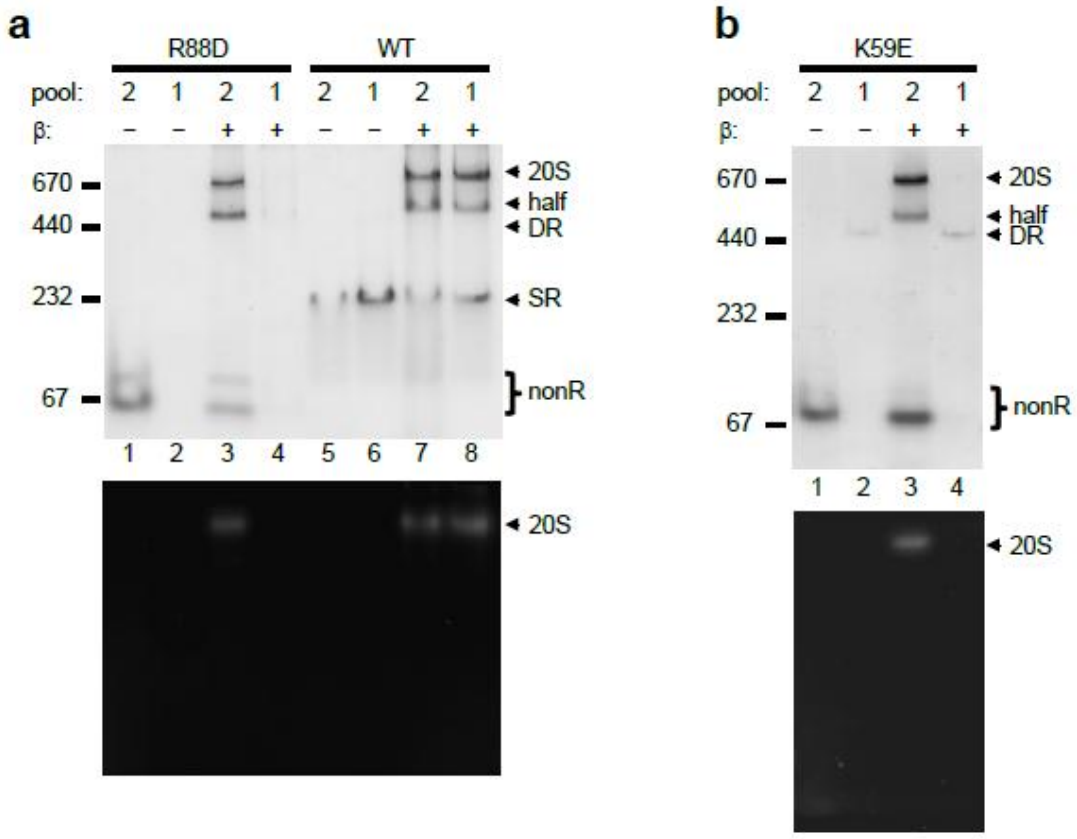

Supplementary Figure 6: Ring independent assembly of archaeal 20S proteasomes
This is another iteration of the same experiment as described in Figure 2.6. The difference is that in this version, the isolated pool 1 and pool 2 samples for each of the α-his proteins (a, wild-type and R88D; b, K59E) were split in half. One half was mixed with an equal volume of lysate from E. coli expressing wild-type archaeal β subunits (+) and the other half was not (−). Following incubation to allow assembly to occur, the proteins were repurified by ICAR and equal volumes of each eluate were electrophoresed on a nondenaturing 5–10% gradient gel. Immediately prior to GelCode staining (top panels), the polyacrylamide gel was overlaid with buffer solution containing the fluorogenic peptide substrate Suc-LLVY-AMC to detect peptidase activity (bottom panel). Black arrowheads denote the positions of assembled 20S core particle (20S), half-proteasome (half), double α-ring (DR) and single α-ring (SR). The position of α subunit species that do not assemble into any ring (nonR), and are mostly free α subunits, is shown with a bracket. The migration of several molecular size standards (in kDa) is indicated.

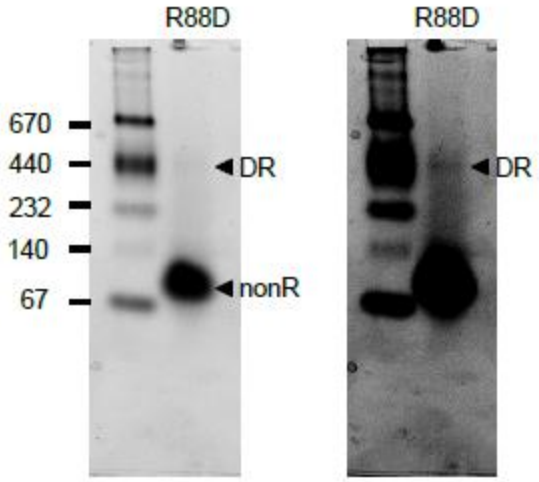

Supplementary Figure 7: On the severity of the R88D mutation
The α (K59E) mutant does not appear capable for forming any detectable SR, though it does form some DR, while the α (R88D) mutant appears to form neither SR nor DR (Figs. 2.2, 2.3). Both mutants exist primarily as nonR (mostly free α subunits) species. Although the effect of the R88D mutation on ring assembly is profound, it is not absolute. When purified α (R88D) protein is heavily overloaded on a nondenaturing 4–15% gradient gel, one can begin to discern a very faint DR band (left panel). Adjusting the brightness and contrast of this image makes this band a bit easier to visualize (right panel). No SR band is ever seen. Hence, the α (R88D) mutation can be thought of as a more extreme version of the α (K59E) mutation i.e. neither forms SR but α (R88D) is much more severe in its effect on DR.

Since the levels of DR in the α (R88D) mutant sample are almost but not quite zero, this can help explain why pool 1 from this mutant also gave rise to barely-perceptible levels of 20S (Fig. 2.6a, lane 4 and Supplementary Fig. 6a, lane 4). Although present at much lower levels than the α (K59E) DR, the α (R88D) DR is inherently less stable and will dissociate more readily into assembly competent nonR (mostly free α subunits). Because such a large amount of protein is loaded onto the Sephacryl S-300 column (780 µg), there should be enough DR present in pool 1 that, upon concentration and mixing with β-subunit-containing lysates, vanishingly small but detectable levels of 20S species will form. Regardless, these tiny levels of 20S in the pool 1 samples do not alter the main point (Fig. 2.6 and Sup Fig. 6) that free α subunits (pool 2) can serve as the starting point for efficient CP assembly along a pathway that does not require SR to form.

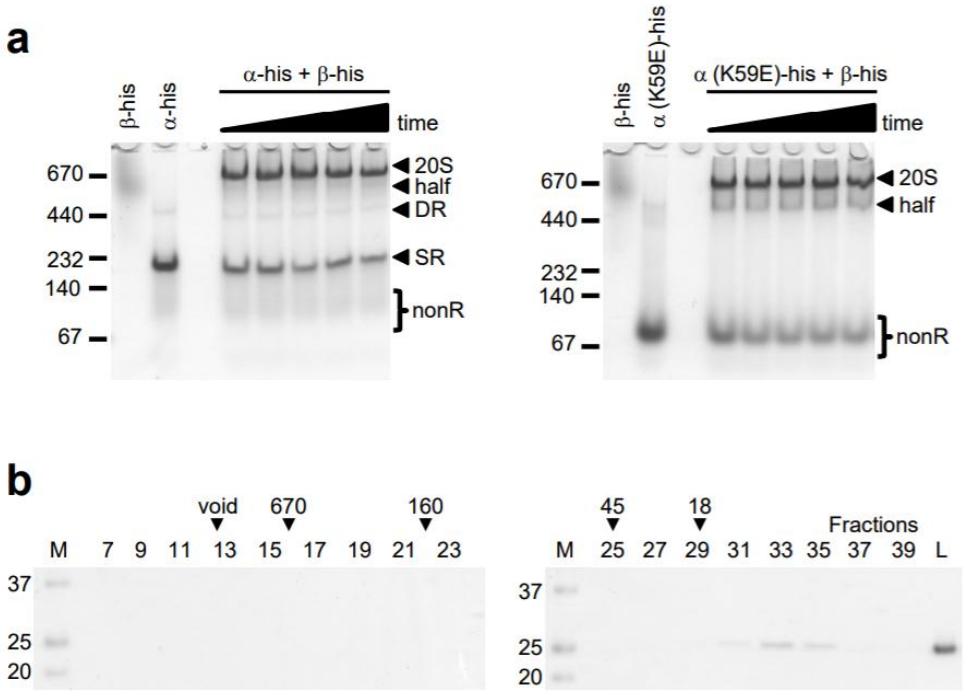

Supplementary Figure 8: Rapid assembly of 20S proteasomes following subunit mixing
To visualize additional assembly intermediates, we sought to carry out mixing experiments using separately expressed wild-type, or mutant, α-his and wild-type β- his subunits that were first purified via ICAR. (a) Purified wild-type, or K59E mutant, α-his (10 µg) was mixed with purified wild-type β-his (10 µg) and incubated for increasing amounts of time (0 to 20 min) prior to loading onto a nondenaturing 5-10% gradient gel. The dead time of the experiment was ~8 mins. This is the time it takes to withdraw an aliquot of the assembly mixture, add nondenaturing sample buffer, load the sample, turn on the voltage, and have the sample enter the gel. Assembly can continue during the dead time because the sample is always under nondenaturing conditions and it is only when protein enters the gel (and free α and β subunits begin to separate from each other) that assembly is no longer happening. The data suggest that most of the assembly observed occurred during the dead time. Black arrowheads denote the positions of assembled 20S core particle (20S), half- proteasome (half), double α-ring (DR) and single α-ring (SR). The position of α subunit species that do not assemble into any ring (nonR), and are mostly free α subunits, is shown with a bracket. The migration of several molecular size standards (in kDa) is indicated. As stated in the main text, no new assembly intermediates (i.e. αβ heterodimers) were evident in mixing experiments. This could be because αβ heterodimers are transient and very rapidly assemble into half -proteasomes, or because αβ heterodimers are not stable enough to survive electrophoresis, or both.

Supplementary Figure 8 (continued).

While purified α-his subunits (wild-type or mutant) resulted in distinct species when separated by nondenaturing PAGE, purified β-his subunits produced a slowly migrating smear (a). We attribute this to the high predicted isoelectric point for β -his (pI = 8.39). Since the pH of the nondenaturing gel is 8.8, β -his may not be appreciably negatively charged at this pH to easily enter the gel. In support of this, we fractionated purified β-his by size exclusion chromatography. (b) ICAR-purified recombinant β-his subunits were subjected to size exclusion chromatography on a Sephacryl S-300 column. Aliquots of every other fraction were analyzed by 12% SDS-PAGE followed by staining with Imperial Stain. Black arrowheads indicate the column void volume and the elution peaks of molecular size standards (in kDa). M, molecular size standards (size in kDa indicated at left). L, aliquot of the sample load. Purified β-his elutes late as a single peak. No β-his was observed near the void volume or in high molecular weight fractions, consistent with purified β-his behaving as a monomer. The slightly later elution of the β -his protein (predicted M_r of 24.6 kDa) relative to the molecular size standards could reflect weak affinity of the β-his subunit for the Sephacryl resin. At the near neutral pH of the size exclusion column, the basic β -his protein (predicted pI = 8.39) may weakly bind to the low levels of carboxylates in the Sephacryl matrix thereby slowing its elution

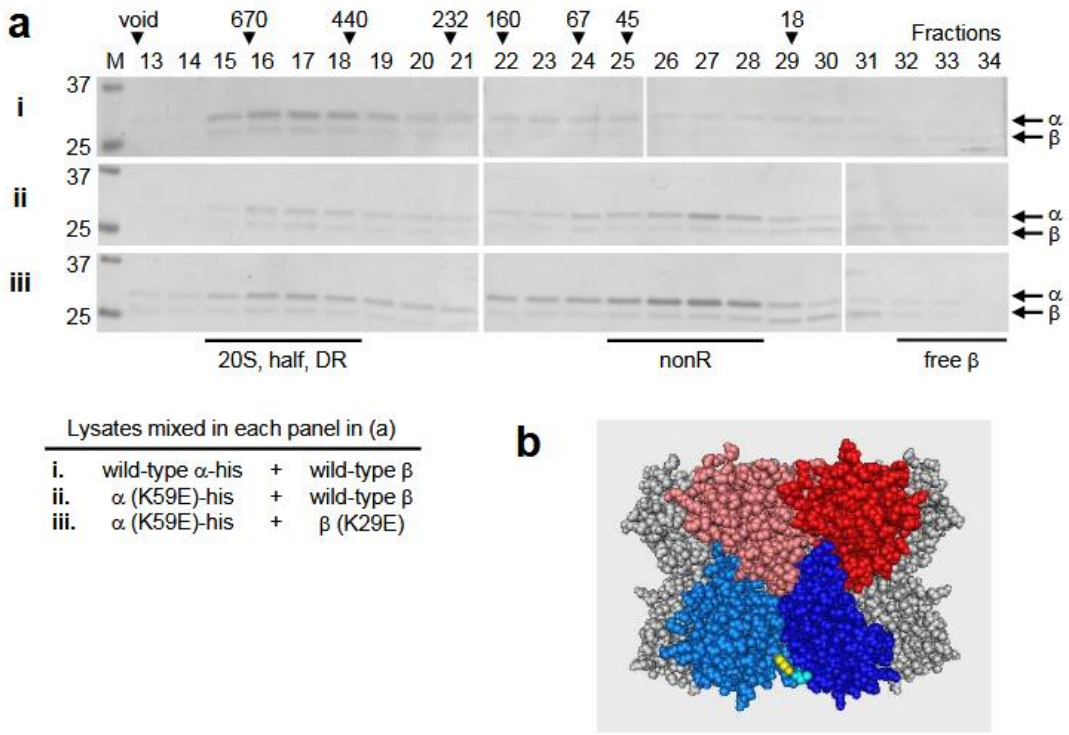

Supplementary Figure 9: SR-independent assembly likely proceeds via αβ heterodimer
(a) Proteasome assembly was initiated by mixing equal volumes of lysates from cells separately expressing the indicated α-his and β subunits. After 30 minutes, proteins were purified by ICAR and loaded onto a Sephacryl S-300 size exclusion column and 3 ml fractions were collected. Aliquots (50 µl) of the indicated fractions were analyzed by three 12% SDS-PAGE gels and stained with Imperial stain. Black lines delineate the position of the 20S peak (also containing half-proteasomes and DR) as well as the α subunit nonR peak and free β subunit peak. We note that both wild-type (Sup Fig. 8) and mutant β subunits (K29E; not shown) elute in fractions 32-34 when expressed on their own. The locations of the column void volume and the elution peaks of the indicated molecular size standards (in kDa) are indicated with black arrowheads. M, molecular size standards (size in kDa indicated at left). Panels (ii) and (iii) show progressively increasing amounts of β subunits eluting in fractions 25-30, consistent with αβ heterodimer formation. (b) Side view of the half-proteasome based on the *T. acidophilum* crystal structure (1PMA) and generated with the program Cn3D. Two α and β subunits are colored for reference. A conserved lysine (K29; yellow) in one β subunit is shown juxtaposed with a conserved residue of opposite charge (teal) located within 5 angstroms on the neighboring β subunit. Numbering is based on the N-terminal catalytic threonine being assigned position1; in *M. maripaludis* this β subunit lysine is also at position 29.

APPENDIX B. SUPPLEMENTARY FOR CHAPTER 3

Supplementary Table 2: Yeast strains used in chapter 3

Name	Genotype	Source
AKY709	MATa *his3-Δ200 leu2-3,112 ura3-52 lys2-801 trp1-1 PRE1*-6XGLY-3XFlag::kanMX6	(Sa-Moura et al., 2013)
AKY889	MATa *his3-Δ200 leu2-3,112 ura3-52 lys2-801 trp1-1 pre6*Δ::HIS3 [pRS315 pre6-Flag]	(L. J. Hammack & A. R. Kusmierczyk, 2017)
AKY1066	MATa *his3-Δ200 leu2-3,112 ura3-52 lys2-801 trp1-1 pre8*-HF(URA)	(L. J. Hammack & A. R. Kusmierczyk, 2017)
AKY1368	MATa *his3-Δ200 leu2-3,112 ura3-52 lys2-801 trp1- pre6*Δ::HIS3 *rpn4*Δ*::hphMX6* [pRS315 pre6-Flag]	
AKY1346	MATa *his3-Δ200 leu2-3,112 ura3-52 lys2-801 trp1-1 pre6*Δ::HIS3 *DOA5*-HF::hphMX6 [pRS315 pre6-Flag]	
AKY1347	MATa *his3-Δ200 leu2-3,112 ura3-52 lys2-801 trp1-1 pre6*Δ::HIS3 *doa5*Δ::HIS3 [pRS315 pre6-Flag] [Ycplac22 *doa5-1*]	
AKY1375	MATa *his3-Δ200 leu2-3,112 ura3-52 lys2-801 trp1-1 pre8*-HF(URA) *rpn4*Δ*::hphMX6*	
AKY1377	MATa *his3-Δ200 leu2-3,112 ura3-52 lys2-801 trp1-1 DOA5*-HF::hphMX6 *rpn4*Δ*::hphMX6 pre6*Δ::HIS3	
AKY1379	MATa *his3-Δ200 leu2-3,112 ura3-52 lys2-801 trp1-1 DOA5*-HF::hphMX6 *PRE1*-6XGLY- 3XFlag::kanMX6	
AKY1402	MATa *his3-Δ200 leu2-3,112 ura3-52 lys2-801 trp1-1 pre8*-HF(URA) *doa5*Δ::HIS3 [Ycplac22 *doa5-1*]	

Unless otherwise indicated strains were generated in this study.

Supplementary Table 3: Plasmids used in chapter 3

Name	Genotype	Source
AKB 70	Pet42 α5α6α7his	(Kusmierczyk et al., 2008)
AKB 349	pET42 Pba4-Pba3his α5α6α7α1	this study

a

	α4F		α2HF	α5HF	β4F
	1	2	3	4	5
α1	31	46	28	34	28
α2	15	29	15	30	20
α3	18	28	23	26	27
α4	21	27	8	17	29
α5	14	7	16	21	20
α6	23	0	24	24	37
α7	12	5	12	14	15
β1	5	4	5	8	8
β2	7	10	7	9	6
β3	9	11	12	11	18
β4	14	16	10	14	13
β5	4	4	6	7	8
β6	0	0	0	5	4
β7	0	0	0	5	4
Pba1	9	0	13	17	25
Pba2	5	5	5	8	11
Pba3	1	0	0	0	0
Pba4	2	0	0	0	0
Ump1	0	5	0	7	8
Ssa1/2	27	83	0	2	0
Ssb2	0	0	0	0	0
Ssc1	0	12	0	0	0
Sse1/2	0	30	0	0	0
Blm10	4	0	0	11	3
Ecm29	9	0	5	0	6

b

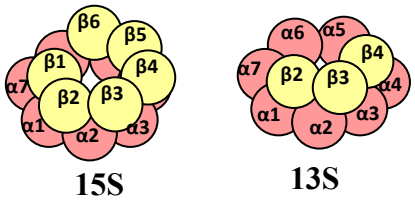

15S **13S**

Band 1,3,4, and 5

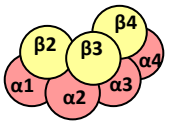

sub-13S

Band 2

Supplementary Figure 10: Composition of bands from Fig. 3.1b

Contents of bands were analyzed by LC-MS/MS. The table indicates the total count of PSMs (peptide spectral matches) for peptides derived from individual proteins. (b) Shows the identity of likely complexes and intermediates. Band 2 is sub-13S complex comprising of proteasome subunits $\alpha_{1\text{-}4}$ and $\beta_{2\text{-}4}$ as per the analysis done in a previous study (Lindsay J. Hammack & Andrew R. Kusmierczyk, 2017). MS analysis of band 2 showed the expected abundance of the $\alpha_{1\text{-}4}$ subunit. The PSMs for $\beta_{2\text{-}4}$ subunit are higher than other β subunits, but overall PSM count is relatively low to make a significant comparison. This is likely due to low protein amount as indicated by the faint appearance of these bands. Also, since these samples are not generated from a depletion strain, a strain created by strategically tagging specific subunit to isolate the species of interest**,** low PSMs for additional subunits also appears.

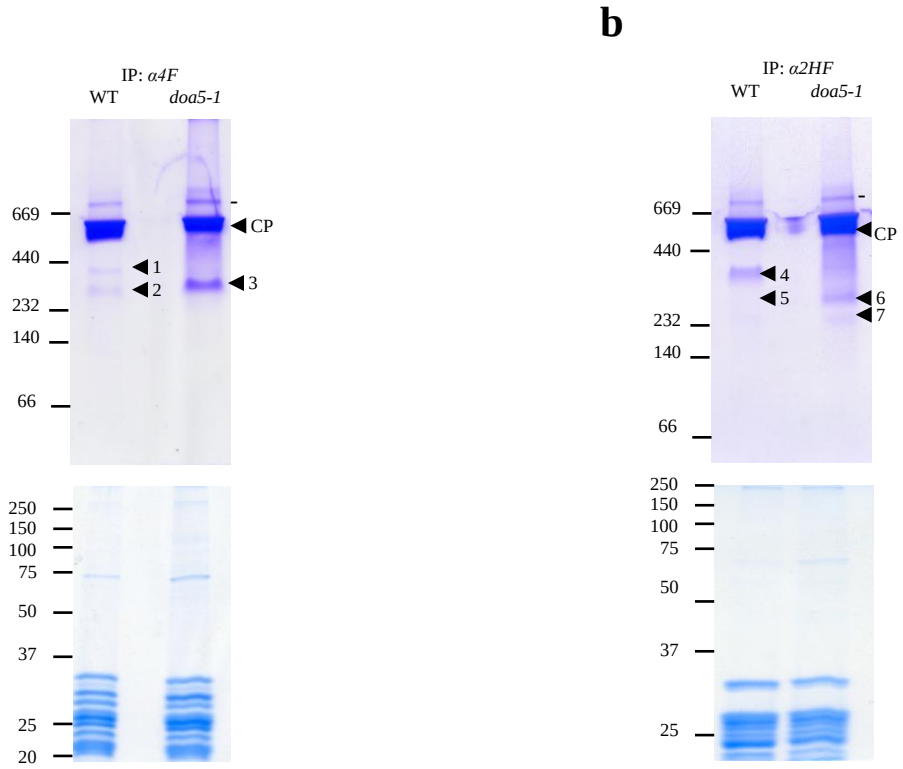

Supplementary Figure 11: Induction of sub-13S in *doa5-1* mutants
Equal amounts (25 µg) of Flag purified proteins from indicated yeast strains were analyzed by native PAGE. Species of interest are indicated by arrowheads. (-) Denotes Blm10-CP complex. These bands were gel excised and analyzed by MS. Loading controls from the native gel in are shown in the bottom. These figures are derived from (L. Hammack, 2017).

a

	α4F		α4F *doa5-1*	α2HF		α2hF *doa5-1*	
	1	2	3	4	5	6	7
α1	70	124	434	72	14	140	62
α2	38	55	176	48	5	62	21
α3	44	75	234	41	15	69	21
α4	42	42	153	39	6	42	13
α5	29	14	1	42	11	3	5
α6	38	7	2	48	3	5	8
α7	22	11	12	29	4	13	7
β1	9	10	0	12	4	7	5
β2	15	27	103	24	7	31	12
β3	15	19	67	22	2	17	4
β4	25	44	165	31	3	49	8
β5	7	5	2	10	1	3	3
β6	6	5	2	5	2	3	4
β7	0	1	0	0	0	0	0
Pba1	21	7	4	24	5	5	2
Pba2	15	4	2	37	4	6	3
Pba3	0	0	0	0	0	0	0
Pba4	3	0	0	0	0	0	0
Ump1	18	34	71	23	3	42	5
Ssa1/2	91	96	180	2	1	63	92
Ssb2	0	15	1	0	0	1	17
Ssc1	0	14	1	0	0	15	34
Sse1/2	0	13	36	0	0	0	27
hsp60	11	0	0	3	0	0	0
Blm10	6	0	3	6	0	0	0

b

Band 1, 2, and 4

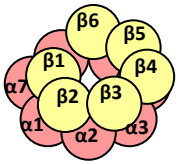

15S

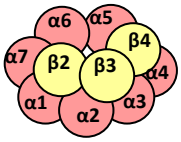

13S

Band 2, 3, 6 and 7

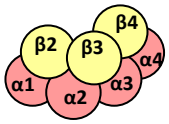

sub-13S

Supplementary Figure 12: Composition of bands from Sup Fig. 11
Contents of bands were analyzed by LC-MS/MS. The table indicates the total count of PSMs for peptides derived from individual proteins. (b) Represents the identity of likely complexes and intermediates.

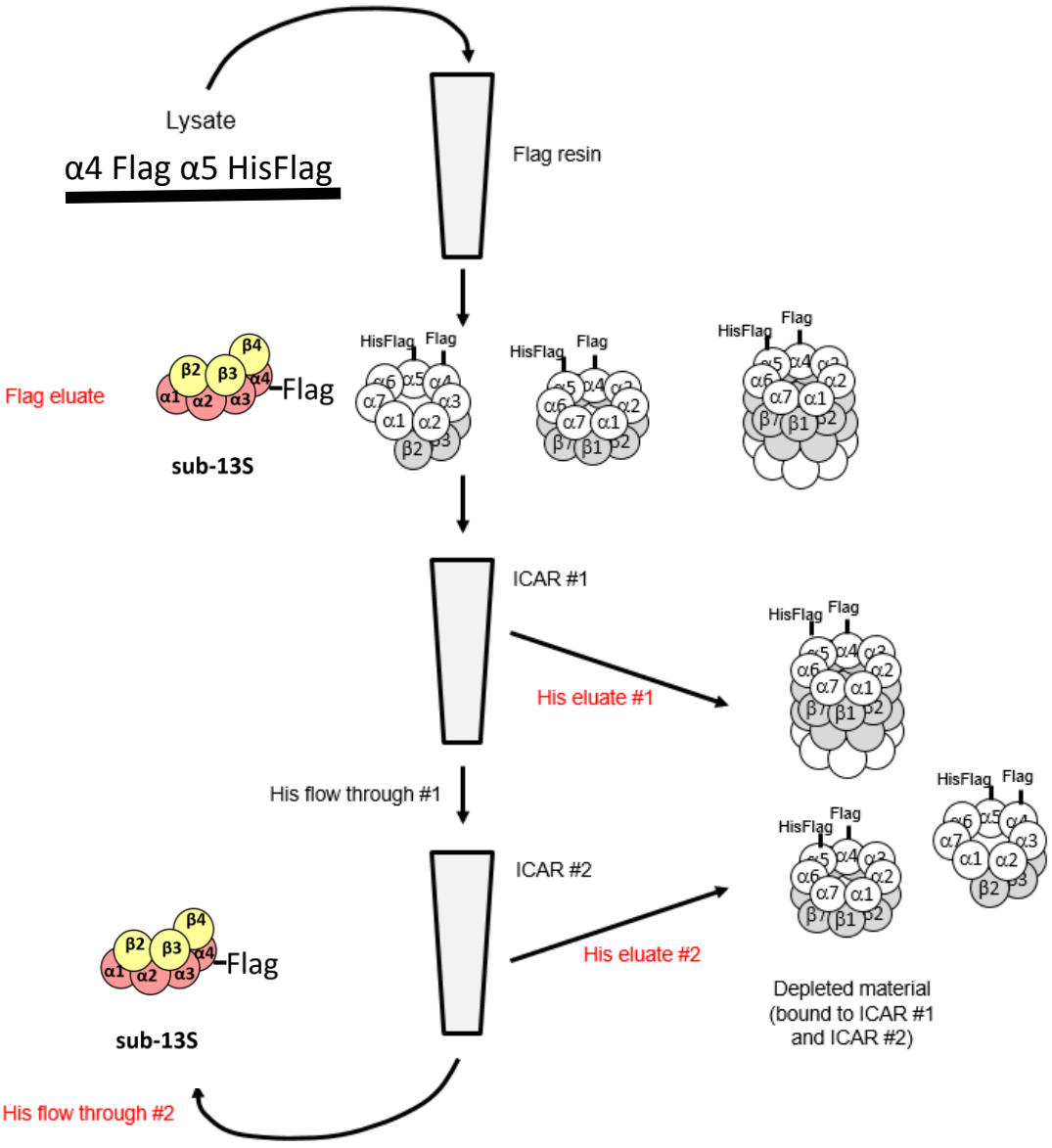

Supplementary Figure 13: Depletion strategy for isolating sub-13S
First yeast lysate is Flag-purified. The purified eluates are subjected to two rounds of ICAR that leads to binding of all histidine tagged proteins/complexes to TALON resin, including the 13S. The sub-13S complex, lacking the histidine tag, should remain present in the His flow through after depletion. Results of this strategy are depicted in Fig 3.3 and Sup. Fig. 14.

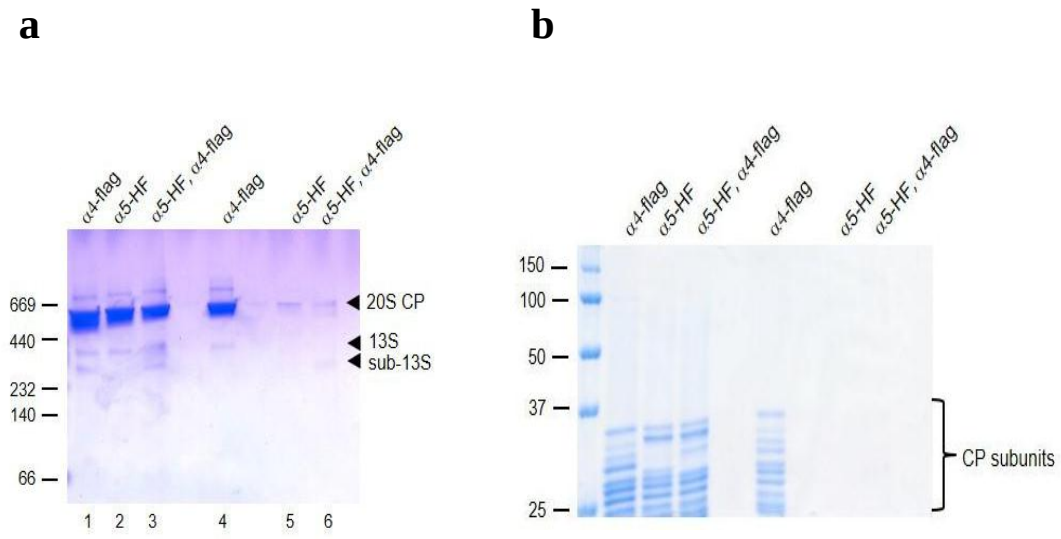

Supplementary Figure 14: Depletion analysis to test for gel artifact
(a) Native PAGE analysis of Flag-purified CP (α4-Flag) from the indicated yeast strains (lanes 1 to 3). The Flag-purified material was subjected to two rounds of depletion by ICAR to remove his-tagged proteins. Aliquots of the flow through from the second ICAR round were analyzed on the same native PAGE gel (lanes 4 to 6). Arrowheads denote CP and other bands of interest. Figure source (L. Hammack, 2017)

a

	α4F α5HF
	2
α1	41
α2	19
α3	22
α4	28
α5	5
α6	8
α7	1
β1	3
β2	7
β3	8
β4	16
β5	3
β6	3
β7	0
Pba1	2
Pba2	4
Pba3	2
Pba4	3
Ump1	4
Ssa1/2	234
Ssb1/2	67
Ssc1	18
Sse1/2	19
hsp60	0
Blm10	10

b

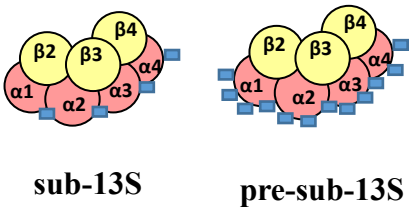

sub-13S **pre-sub-13S**

Supplementary Figure 15: Composition of band 2 from Figure 3.3
Contents of the band were analyzed by LC-MS/MS. The table indicates the total count of PSMs for peptides derived from individual proteins. (b) Represents the identity of the likely complex. Blue rectangle indicates Hsp70 group proteins including Ssa1/2, Ssb1/2, Ssc1, Sse1/2. These proteins are more abundant in the pre-sub-13S complex as depicted by more blue squares.

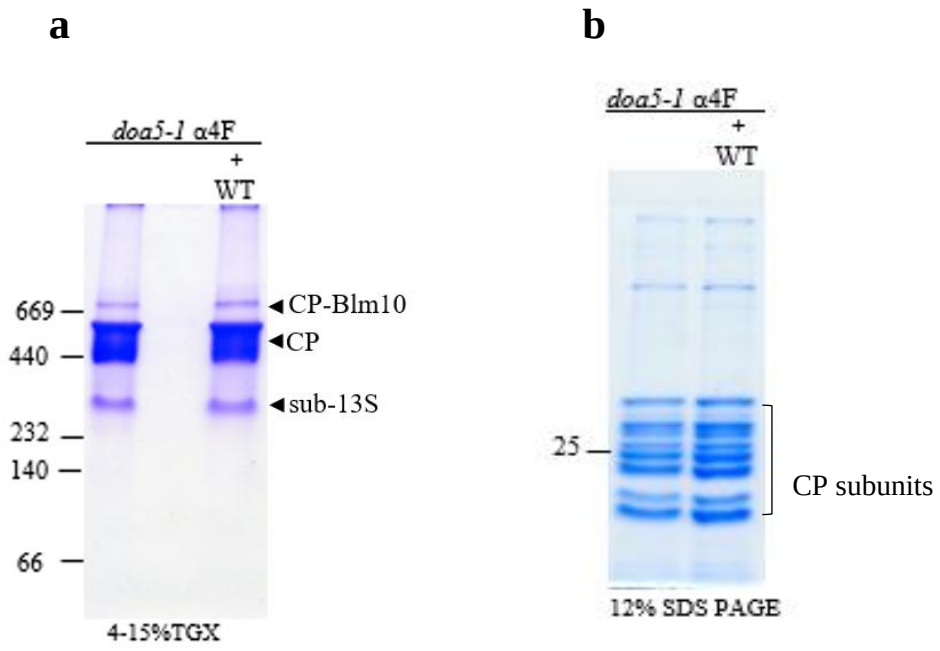

Supplementary Figure 16: Lysate mixing of WT yeast with *doa5-1* mutant
(a) Lysate of yeast mutant α4F *doa5-1* was mixed with wild-type yeast lysate at 30 °C for 30 mins followed by flag purification and native PAGE analysis. There was no difference in the lysate mixed and individual sample profile. (b) Shows the loading control. The migration of several molecular size standards (in kDa) is indicated on left.

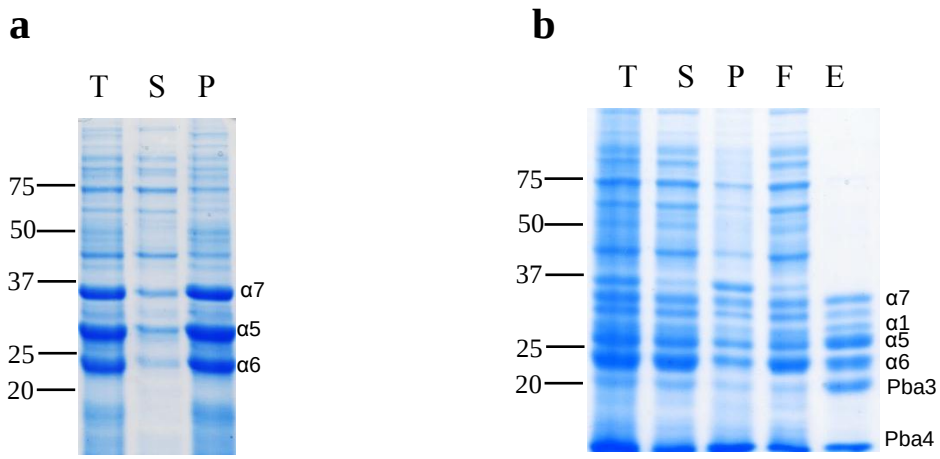

Supplementary Figure 17: Recombinant expression of yeast proteasome subunits in *E. coli*
Lysates of *E. coli* coexpressing α5, α6, and α7H (a), Pba4, Pba3H, α5, α6, α7, and α1 (b) are fractionated into total (T), soluble (S), pellet(P) fractions, (F) flow through and (E) eluate (after ICAR purification) fractions followed by 12% SDS PAGE analysis shows subunit expression and solubility. The migration of several molecular size standards (in kDa) is indicated on left. A faint band present between α5 and α7 subunit in lane 5 is clipped α7 subunit likely arising due to non-specific proteolysis post lysis. Both the gels were stained with GelCode blue.

a

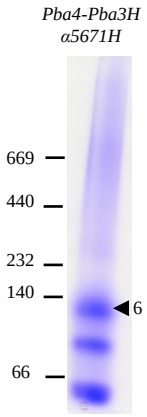

b

	α4F doa5-1	Pba4-Pba3H α5671H + α4F doa5-1				Pba4-Pba3H α5671H		
	1	2	3	4	5	6	7	8
α1	441	261	41	32	8	4	14	5
α2	213	98	11	1	0	0	0	0
α3	101	68	30	39	20	0	3	2
α4	126	125	15	4	2	0	0	1
α5	9	74	313	455	870	26	816	294
α6	10	127	467	260	33	28	656	118
α7	9	80	198	33	33	12	26	8
β1	12	10	10	10	4	0	1	0
β2	195	98	11	8	5	0	0	0
β3	54	42	12	10	6	0	0	0
β4	120	77	6	4	2	0	1	2
β5	5	6	5	0	1	0	0	0
β6	8	14	2	1	1	0	0	0
β7	0	0	0	0	0	0	0	0
Pba1	2	2	0	1	6	0	1	0
Pba2	1	0	0	1	6	0	1	0
Pba3	1	36	400	153	459	41	472	133
Pba4	4	29	246	233	346	49	324	207
Ump1	54	37	3	1	4	0	0	1
Ssa1/2	79	40	138	7	0	0	0	0
Ssb2	0	0	0	0	0	0	0	0
Ssc1	2	0	0	0	0	0	0	0
Sse1/2	0	0	0	0	0	0	0	0
hsp60	0	0	1	0	0	0	0	0
Blm10	0	6	0	0	0	0	0	0

Supplementary Figure 18: Composition of bands from Fig. 3.4a
(a) Analysis of indicated sample from Fig 3.4 lane 3 is analyzed on a separate 4-15% TGX gel followed by imperial blue stain. The migration of several molecular size standards (in kDa) is indicated on left. Contents of bands from Fig 3.4a were analyzed by LC-MS/MS. (b) The table indicates total count of PSMs for peptides derived from individual proteins. Band 6 was excised from the (a).

a

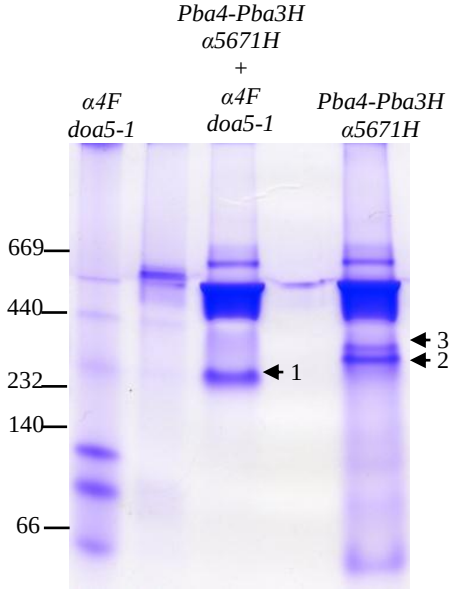

b

	α4F doa5-1	Pba4-Pba3H α5671H + α4F doa5-1	
	1	2	3
α1	418	206	136
α2	266	138	72
α3	206	101	77
α4	272	162	216
α5	55	126	78
α6	30	147	72
α7	21	143	71
β1	10	5	8
β2	132	75	37
β3	65	35	26
β4	131	93	33
β5	5	4	6
β6	9	10	10
β7	0	0	0
Pba1	14	12	13
Pba2	0	5	7
Pba3	14	80	34
Pba4	100	140	140
Ump1	58	40	35
Ssa1/2	148	118	121
Ssb2	0	0	0
Ssc1	6	0	0
Sse1/2	0	0	0
hsp60	0	0	4
Blm10	41	54	64
Ecm29	0	0	34

Supplementary Figure 19: Sub13S is an assembly competent species
(a) This is the same experiment as shown in Figure 3.4 except the protein mixing ratio for Pba3-Pba4α5α6α7α1 to *doa5-1* mutant is 1:4. The migration of several molecular size standards (in kDa) is indicated on left. (b) Contents of the indicated bands from (a) were analyzed by LC-MS/MS. The table indicates total count of PSMs for peptides derived from individual proteins.

APPENDIX C. SUPPLEMENTARY FOR CHAPTER 4

Supplementary Table 4: Yeast strains used in chapter 4

Name	Genotype	Source
AKY 1062	*MAT***a** *his3-Δ200 leu2-3,112 ura3-52 lys2-801 trp1-1 gal2 scl1Δ::natMX4 [pRS315α1nic]*	This study
AKY1097	*MAT***α** *his3-Δ200 leu2-3,112 ura3-52 lys2-801 trp1-1 gal2 scl1Δ::natMX4 pba4Δ::hphMX[pRS315α1nic]*	This study
AKY1064	*MAT***a** *his3-Δ200 leu2-3,112 ura3-52 lys2-801 trp1-1 gal2 scl1Δ::natMX4 [pRS315scl1(A102C)]*	This study
AKY1063	*MAT***α** *his3-Δ200 leu2-3,112 ura3-52 lys2-801 trp1-1 gal2 scl1Δ::natMX4 pba4Δ::hphMX [pRS315scl1(A102C)]*	This study
AKY1243	*MAT***a** *his3-Δ200 leu2-3,112 ura3-52 lys2-801 trp1-1 gal2 scl1Δ::natMX4 pba4Δ::hphMX [pRS315scl1(A102C)]*	This study
AKY1257	*MAT***a** *his3-Δ200 leu2-3,112 ura3-52 lys2-801 trp1-1 gal2 scl1Δ::natMX4[pRS315scl1(A102C)]*	This study
AKY1261	*MAT***a** *his3-Δ200 leu2-3,112 ura3-52 lys2-801 trp1-1 gal2 scl1Δ::natMX4 pba4Δ::hphMX[pRS315α1nic]*	This study

Supplementary Table 5: Plasmids used in chapter 4

Name	Genotype	Source
AKB49	pET11a α5α6α7α1	This study
AKB80	pET11a α5α6α7α1his	This study
AKB143	pET11a α7α1his	This study
AKB145	pET11a α6α7α1his	This study
AKB268	pET42 Pba4-Pba3his	This study
AKB349	pET42 Pba4-Pba3his α5α6α7α1	This study
AKB 788	pET11a α5α6α7α1(A102C) his	This study
AKB1010	pRS315 *SCL1*(A102C) Flag	This study
AKB1011	pRS315 *SCL1*(NIC)Flag	This study
AKB1035	pRS315 *SCL1*Flag	This study

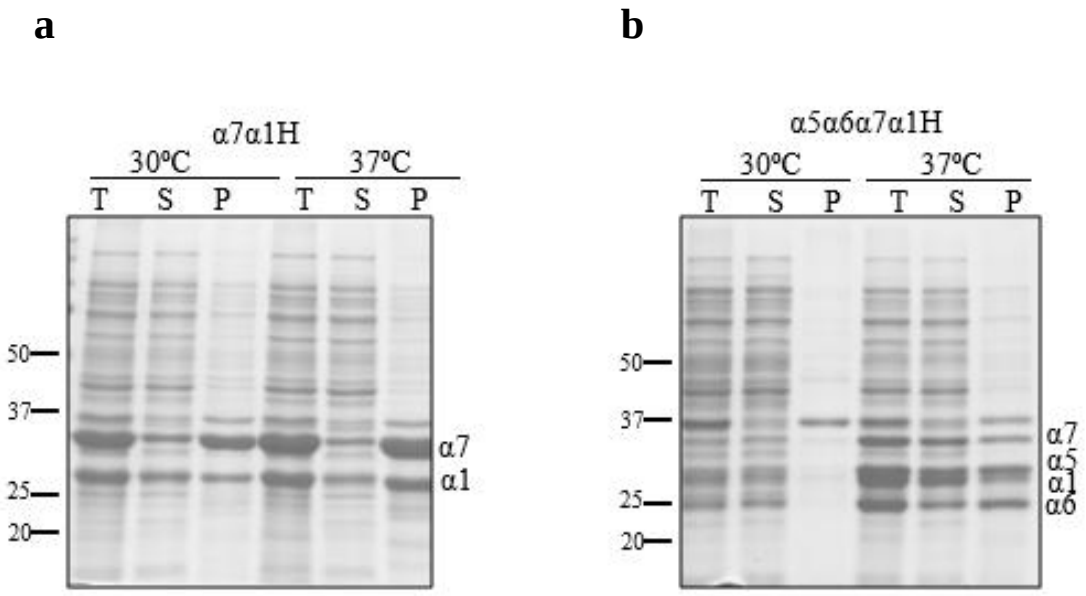

Supplementary Figure 20: Fractionation of *E. coli* lysates expressing indicated α subunits
(a, b) Total (T), Soluble (S) and Pellet (P) fractions of extracts from *E. coli* expressing α7, and α1H and α5, α6, α7, and α1H induced at 30 °C and 37 °C. The migration of individual subunit is labeled. All the gels were stained by GelCode blue. Migration of molecular size standards in kDa is indicated on the left.

a **b**

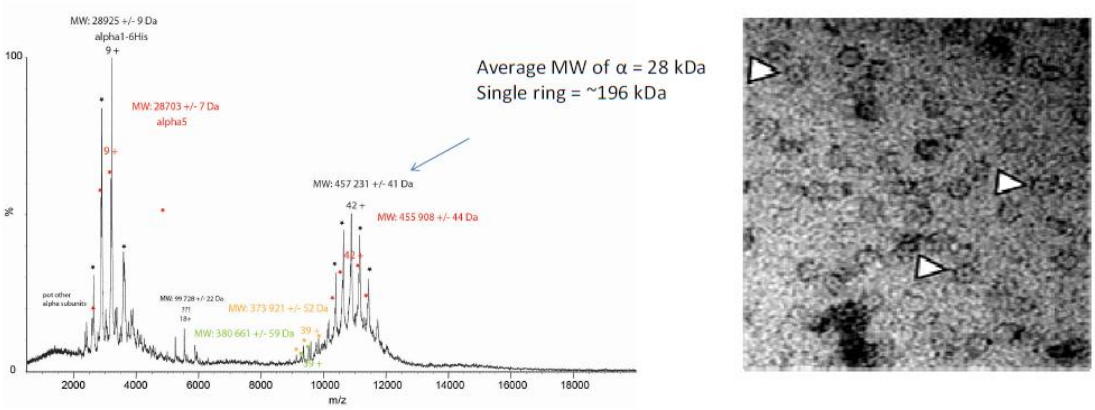

Supplementary Figure 21: Characterization of HMWC by MS and negative stain EM
(a) m/z spectra of α5α6α7α1 HMWC analyzed by mass spectrometry. Arrow points to the expected mass of the complex ~ 457 kDa (Stengel and Kusmierczyk, unpublished) (b) Negative stain EM image of the immobilized cobalt affinity purified (ICAR) α5α6α7α1 complex. White arrowed depicts ringed shaped.

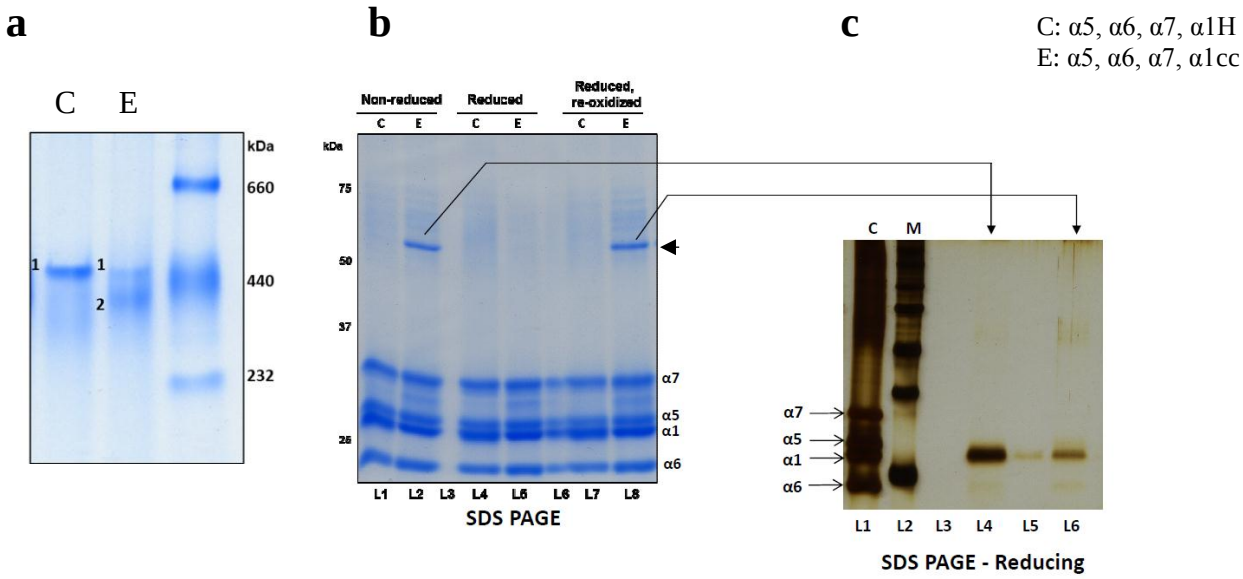

Supplementary Figure 22: The α1 crosslink confirms the DR conformation of HMWC
(a) ICAR purified proteins from the indicated samples were analyzed by Native page. Species of interest, labeled as bands 1 and 2, were excised. (b) Eluted proteins from the excised bands in (a) were analyzed by SDS PAGE under non-reducing (lane 1 and 2) and reducing (lane 2 and 3) conditions. An aliquot from the non-reducing sample was reduced by adding dithiothreitol (lane 3 and 4). An aliquot of the reduced sample was reoxidized by removing dithiothreitol (lane 5 and 6). The α1 dimer band, indicated by an arrowhead, appeared in the crosslinked and reoxidized samples containing the α1cc mutant. (c) The α1 dimer band from (b) was gel excised, the eluted proteins were reduced, followed by SDS PAGE analysis and silver staining. The subunits are indicated by arrows. Molecular size standards (in kDa) are indicated on the right in (a) and left in (b) and (c). Figure source (Ramamurthy, 2014).

a

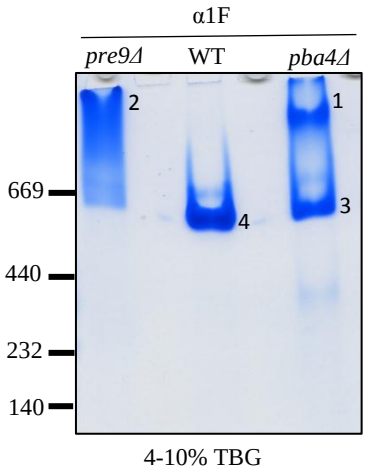

b

	PSMs			
	Band 1	Band 2	Band 3	Band 4
α1	582	505	619	754
α2	202	164	224	299
α3	206	30	318	529
α4	927	853	846	971
α5	318	110	394	666
α6	405	330	383	500
α7	202	169	204	232
β1	185	164	197	362
β2	262	183	256	487
β3	112	61	164	226
β4	139	82	118	216
β5	316	118	330	399
β6	463	252	516	597
β7	847	624	943	1127
Blm10	**83**	**24**	0	0

Supplementary Figure 23: Slower migrating band is CP-bound Blm10 complex
(a) Native PAGE analysis (tris-borate gradient gel) of flag purified proteins from indicated yeast strains shows a slower migrating species when assembly chaperone Pba4 is absent (lane 3). A *pre9Δ* strain was used to compare the migration of α4-α4 proteasome with the slower migrating band in *Pba4Δ* strain. The migration of several molecular size standards (in kDa) is indicated on left. (b) Results of LC-MS/MS analysis of the indicated bands in (a) shows the peptide spectral matches (PSM) for the identified components. The higher PSM for Blm10 in band 1 and band 2 (highlighted in red) and, its absence in band 3 and band 4, indicates that these are CP-bound Blm10 complexes.

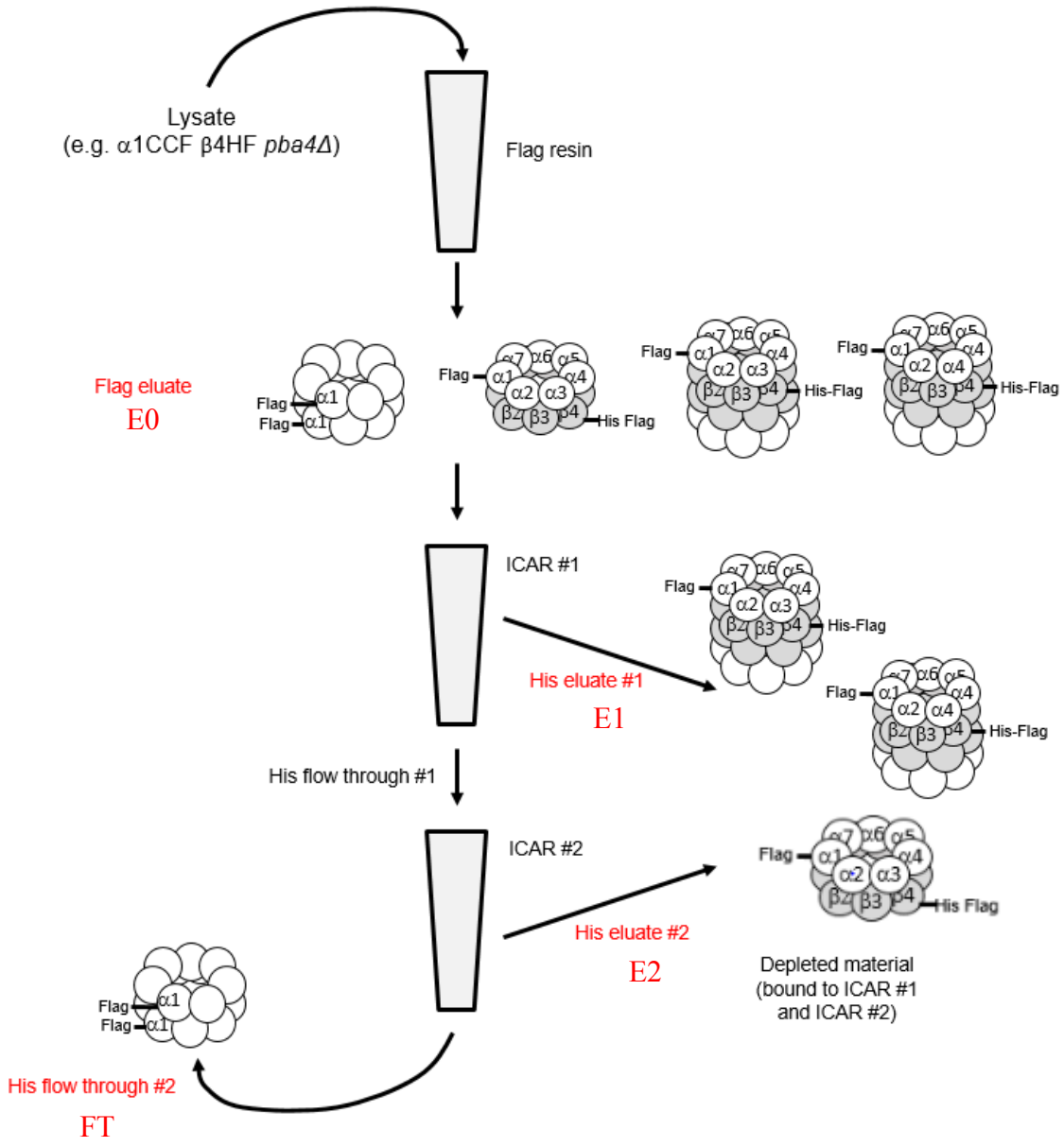

Supplementary Figure 24: Depletion strategy to confirm presence of HMWC
First yeast lysate is bound to Flag resin. The Flag-purified material is subjected to two rounds of ICAR. The assembled CP and intermediates containing the hexahistidine tag on β4 will bind to the TALON resin. Eluted protein fractions bound to TALON resin are designated as E1 and E2. The HMWC lacking the β4 subunit, if formed, will escape the TALON resin binding and remain in the flow through (FT) lane. Results of this strategy are depicted in Fig. 4.4.